NTNU

Norwegian University of
Science and Technology

Area Based Secondary Frequency Control in the Nordic Power System

Katrine Gabrielsen
Andersen

Master of Energy and Environmental Engineering
Submission date: June 2016
Supervisor: Kjetil Uhlen, ELKRAFT
Co-supervisor: Eivind Lindeberg, Statnett SF

Norwegian University of Science and Technology
Department of Electric Power Engineering

Preface

This master's thesis concludes my degree Master of Science at the Norwegian University of Science and Technology (NTNU). The thesis is written in collaboration with Statnett SF.

I would like to thank my supervisor Kjetil Uhlen at the Department of Electrical Power Engineering, NTNU, for his guidance and feedback throughout the work of this thesis. I genuinely appreciate his advice and encouragement to guide me through the challenges of my work. I would also like to thank my co-supervisor Eivind Lindeberg at Statnett SF for his guidance in the software MATLAB® and Simulink®, and for sharing his knowledge about the Nordic power system.

Trondheim, June 10, 2016

Katrine Gabrielsen Andersen

The front page image is from reference [1].

Abstract

In order for a power system to function properly, it is necessary that the power production is equal to the power demand at all times. The next day's power balance is scheduled by the transmission system operators (TSO's) as a result of what the power consumers and producers declare they want to buy and sell. However, unpredictable events are bound to happen. Therefore, there are additional controls using three frequency reserve markets; primary, secondary, and tertiary reserves. The focus in this master's thesis is secondary frequency control, which uses Automatic Frequency Restoration Reserves (aFRR).

Today there is one central proportional–integral controller handling the secondary frequency control of the entire Nordic power system. In this thesis a design and analysis of an alternative control structure is presented. A simplified version of the Nordic synchronous system comprising eleven areas is modeled using Simulink®. The areas consist of one generator in accordance with the installed power generation per area, and one load equal to the value during an actual high load hour. The model uses a combination of the swing equation and DC power flow to do the network calculations. Three Automatic Generation Controllers (AGC's) are included in the system for decentralized secondary frequency control. The input to the controllers is the frequency deviation, and the power flow and capacities in specific tie lines between the areas; while the output is the change in power production.

The AGC's are modeled as classical AGC's with a few modifications. The most important modification of the AGC's is that the tie line power flow is only taken into account when the power flow in the tie lines exceed the capacity limits. In other words, the Area Control Error (ACE) only regards the system frequency and is common for the entire system as long as there are no congestions in the controlled tie lines. The system is split into two or more areas operating with individual ACE's when congestions occur.

The activation of secondary frequency control is based on a merit order list comprised of available volumes and prices of the aFRR in each bidding zone. Hence, the control structure makes sure that when disturbances occur, the cheapest available aFRR is activated. The activation depends on whether there are

any congestions. When the power transfer in any of the tie lines exceed the capacity limits, aFRR is instead activated in areas where the congested line is not a hindrance.

As secondary frequency control is relatively new in the Nordic power system, it is currently paid for by all the Nordic TSO's. By implementing AGC's in all bidding zones, the areas experiencing disturbances will be the ones actually paying for frequency restoration by purchasing the cheapest aFRR available. The Nordic countries and areas would be in control of their own ACE, in addition to cooperating by buying and selling aFRR.

One of the simulated cases in this thesis shows that AGC's in only three areas is not enough because other than the three controlled tie lines may be congested. If the proposed solution is to be implemented in the Nordic power system, an important challenge in the control structure is to control as many tie lines as possible in order to make sure that no grid capacities are exceeded.

Sammendrag

For at et kraftsystem skal fungere ordentlig er det nødvendig at kraftproduksjonen til enhver tid er lik forbruket. Neste dags kraftbalanse blir planlagt av de systemansvarlige basert på hva kraftprodusenter og -forbrukere melder inn. På tross av dette vil det alltid være fare for at uforutsette forstyrrelser skjer. Derfor finnes det ytterligere regulering som bruker tre forskjellige reservemarkeder: primær-, sekundær- og tertiærreserver. Denne masteroppgaven fokuserer på sekundær frekvenskontroll, som bruker automatiske sekundærreserver (aFRR).

I dag brukes én sentral proporsjonal+integral-regulator til å sekundærregulere frekvensen i hele det nordiske kraftsystemet. I denne masteroppgaven blir design og analyser av en alternativ reguleringsstruktur presentert. En forenklet utgave av det nordiske synkronsystemet er modellert i Simulink®. De elleve områdene består hver av en generator som tilsvarer den installerte generatoreffekten per område, og en last i samsvar med forbruket i en faktisk høylasttime. Modellen bruker en kombinasjon av svingeligningen og DC lastflyt for å utføre beregninger for nettverket. Tre automatiske sekundærregulatorer (AGC) er inkludert i systemet for desentralisert sekundær frekvenskontroll. Inngangssignalet til regulatorene er frekvensavviket samt kraftflyt og kapasitetsgrensene i spesifikke linjer som forbinder to områder. Utgangssignalet er endringen i kraftproduksjon.

AGCene er modellert som klassiske AGCer, men med noen få modifikasjoner. Den viktigste modifikasjonen som er gjort i AGCene er at flyten i linjer som forbinder to områder bare betraktes dersom det oppstår en flaskehals i disse linjene. Med andre ord består innstillingsfeilen (ACE) kun av frekvensavviket og er felles for hele systemet så lenge det ikke er noen flaskehalser. Dersom flaskehalser oppstår i de kontrollerte linjene, vil systemet splittes i to eller flere områder som opererer med individuell ACE.

Aktiveringen av sekundær frekvenskontroll er basert på en budliste med tilgjengelig aFRR og prisen på denne i hvert område. Dermed blir billigste tilgjengelige aFRR aktivert når det skjer forstyrrelser. Samtidig er aktiveringen av aFRR avhengig av om det er flaskehalser i systemet. Når det oppstår en flaskehals i en linje som forbinder to områder, vil aFRR i stedet aktiveres i et område der flaskehalsen ikke er et hinder for kraftflyten.

Sekundær frekvenskontroll er relativt nylig innført i det nordiske kraftsystemet, og betales per i dag av alle de nordiske TSOene. Ved å implementere AGC i alle budområdene i Norden, vil det være områdene som faktisk opplever forstyrrelser som betaler for å stabilisere systemfrekvensen ved å kjøpe billigste tilgjengelige aFRR. De nordiske landene og områdene vil i så fall kunne samarbeide ved å selge og kjøpe aFRR til og fra hverandre, og samtidig kontrollere ACE i sitt eget område.

En av simuleringene som ble gjort i denne masteroppgaven viser at AGC i kun tre områder er for lite fordi det kan oppstå flaskehalser i andre linjer enn de som kontrolleres av AGCene. Dersom den foreslåtte løsningen blir implementert i det nordiske synkronsystemet, vil en viktig utfordring i reguleringsstrukturen være å kontrollere så mange linjer som mulig for å forhindre at flaskehalser oppstår.

Abbreviations

ACE	Area Control Error
aFRR	Automatic Frequency Regulating Reserves
AGC	Area Generation Control
DC	Direct Current
DC PF	Direct Current Power Flow
FCR	Frequency Containment Reserves
FCR-D	Frequency Containment Reserves for Disturbances
FCR-N	Frequency Containment Reserves for Normal operation
FRR	Frequency Regulating Reserves
HVDC	High Voltage Direct Current
Hz	Hertz
mFRR	Manual Frequency Regulating Reserves
MVA	Megavolt-ampere
MW	Megawatt
p.u.	Per unit
PI	Proportional–Integral
PID	Proportional–Integral–Derivative
PTDF	Power Transmission Distribution Factor
RP	Regulating Power
s	Seconds
TSO	Transmission System Operator

Contents

List of Figures

List of Tables

Chapter 1

Introduction

Parts of this chapter are redrafts of reference [2].

1.1 Background

In order for a power system to function properly, it is necessary that the power production is equal to power demand at all times. There are several ways to plan and control for so that this is always the case. Statnett is the Norwegian Transmission System Operator (TSO), responsible for ensuring the instant balance between power production, demand, and net export in the Norwegian power system [3] [4]. The next day's power balance is scheduled as a result of what the power consumers and producers declare they want to buy and sell. However, unpredictable events are bound to happen. Therefore there are additional controls using three frequency reserve markets; primary, secondary, and tertiary reserves. These will be further explained in section 2.2.

1.1.1 The Nordic Power System

The Nordic countries have a common synchronous system consisting of eleven bidding zones, or eleven areas, as illustrated in figure 1.1. Areas NO1, NO2, NO3, NO4, and NO5 in Norway, SE1, SE2, SE3, and SE4 in Sweden, FI in Finland, and DK2 in Denmark, are all in the same synchronous area, meaning that they operate with the same frequency. DK1 in Denmark is included in the Nord Pool system, but is not a part of the Nordic synchronous area. Nord Pool is the leading power market in Europe. Trading, clearing, and settlement of day-ahead and intraday markets occur in the Nord Pool system for several countries, including countries in the Nordic power system [5].

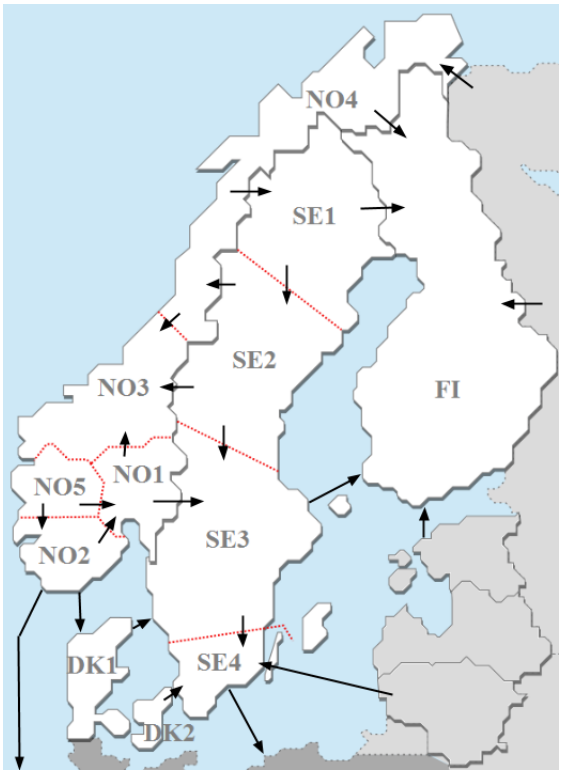

Figure 1.1: The Nordic power system with its bidding zones; NO1, NO2, NO3, NO4, and NO5 in Norway, SE1, SE2, SE3, and SE4 in Sweden, FI in Finland, and DK1 and DK2 in Denmark. DK1 is included in the Nord Pool system, but is not part of the synchronous area. The arrows show the intraconnections and connections with the countries surrounding the Nordic power system. [6]

Currently the dominating frequency reserve controls in the Nordic power market are the primary control, using Frequency Containment Reserves (FCR), and the tertiary control, using Manual Frequency Restoration Reserves (mFRR). The secondary control, using the Automatic Frequency Restoration Reserves (aFRR), is of little use and only serves as a supplement to the FCR and the mFRR [7]. As more and more non-adjustable power sources such as small hydro power, wind, and solar energy become available in Europe, the harder it is to control the frequency. The Nordic countries are working to establish aFRR in the synchronous system, and trial operation started in 2013 [8]. Although there was a temporary stop in the aFRR purchase in the winter 2015/2016 partly due to lack of agreement between the Nordic TSO's, aFRR is expected to be fully implemented in the coming years. Secondary frequency control is activated on a pro-rata basis, i.e. in proportion with how much balancing power is needed, for hours of the day that are especially problematic to balance. Currently, the most

problematic times of day to balance are weekday mornings and afternoons. aFRR is a lot more common in the rest of the European power system, where it is used instead of mFRR [7].

In Norway, NO3 and NO1 are typically deficit areas importing power from other areas, while NO2, NO4, and NO5 are surplus areas exporting power. In Sweden, the power flows southwards because there is a lot of power production in the north while most of the population lives in the southern parts of the country. 99 % of the power in Norway is hydro power [9]; Sweden has some hydro power but also quite a lot of thermal and nuclear power plants, especially in the south [10]. This is also the case in Finland [11]. As the frequency restoration reserves are mostly activated from hydro power, these areas do not contribute much to primary frequency control compared to Norway and the north of Sweden. Denmark does not have any hydro power and is thus not likely to contribute with much aFRR [12].

1.1.2 System Description

The model presented in chapter 4 is a simplification of the Nordic synchronous system. The system was modeled with one generator and one load in each area. Due to the lack of hydro power, DK2 was modeled as a constant value in accordance with power flow in the connection DK2-SE4. The model uses production and consumption data from an actual case; January 6, 2016 during the hour 19:00–20:00. The data was gathered from reference [13]. During this hour there was a power production record in Norway [14]. The data used for the model was slightly adjusted in order to get a suitable load flow. Table A.1 in appendix A.2 lists the values of the system during the specified hour.

1.2 Objective

Today, there is one central Proportional–Integral (PI) controller handling the secondary frequency control of the entire Nordic power system. The objective of the research question at hand is to design and analyze an alternative control structure, where there are controllers in three control areas, i.e. decentralized control. The input to the controllers is the frequency deviation, and the power flow and capacities in specific tie lines between the areas; while the output is the change in power production. An important change in the control structure is that the controllers regulate when there is a deviation in the frequency, but only regard the tie line flow when the flow in these lines exceed the capacity limits. In other words power flow is only adjusted when congestions occur in the system.

Setting of control values will be based on a merit order list of the bids so that the cheapest power available is activated, assuming no line congestion between areas. If

the capacity limits of the tie lines are exceeded, the controllers will activate aFRR in the bidding zones providing the second, third, etc. cheapest bids. This continues until the total power demand is met. Figure 1.2 presents an outline of the control structure. Areas A, B, and C will each have a PI controller for the secondary frequency control. A similar scheme is proposed in reference [15].

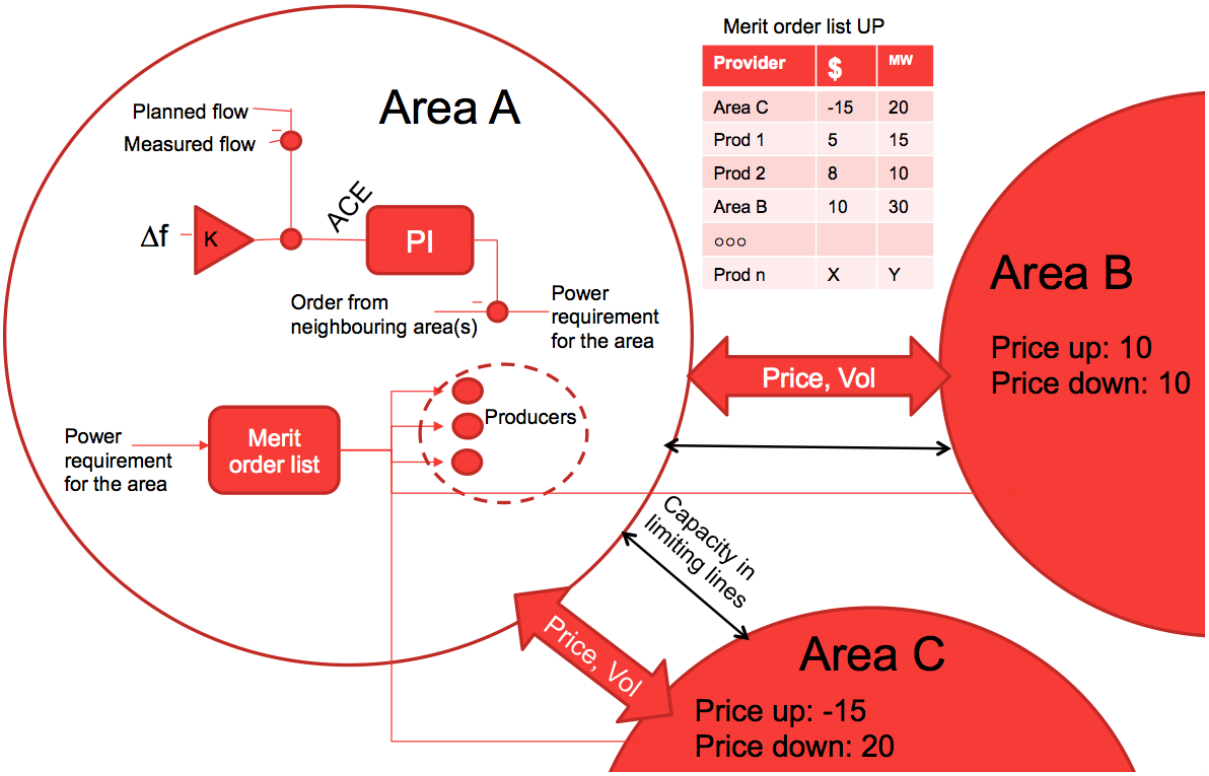

Figure 1.2: An illustration of the idea proposed in the thesis. The areas in the power system interact using a merit order list for the aFRR [7]. As long as there is no tie line congestion, the cheapest aFRR bid will be activated first.

1.3 Scope of Work

The scope of work is divided in three parts: a literary study on congestion handling, frequency control, and linear power flow, developing a model representing the Nordic synchronous system and including three secondary frequency controllers in the system, and analyzing how the system responds when exposed to different disturbances.

1.4 Outline of the Report

The report is organized in eight chapters. Chapter 2 gives an introduction to the theory used for this thesis, including congestion management, frequency stability and control, the swing equation, power system components, DC power flow, power transfer distribution factors, and the per unit system. Chapter 3 describes the software used in the thesis and explains the method used in the modeling, while chapter 4 illustrates the method used on the model representing the Nordic synchronous system. Chapter 5 presents the findings in the various simulations done for the system and a discussion of each. Chapters 6, 7, and 8 hold the conclusions, suggestions for further work, and a list of the references used in the thesis, respectively.

Chapter 2

Theory

Parts of this chapter are redrafts of reference [2]. The chapter describes the theoretical framework needed to understand the study performed in this master's thesis. Firstly, congestion management based on area pricing is explained. The chapter proceeds with a description of frequency stability and control, including primary, secondary, and tertiary control, before the swing equation is derived. Then the power system components turbines, turbine governors, electromechanical dynamics, and automatic generation control are explained. Finally DC power flow, power transfer distribution factors, and the per unit system are presented.

2.1 Congestion Management Based on Area Pricing

In the day-ahead market of Nord Pool, called Elspot, the members place their hour by hour orders, and an equilibrium between the demand and supply curves is established for all the bidding areas. The equilibrium establishes a system price and power flow [16]. As trading capacities between the bidding zones are not taken into account, the system price is an unconstrained market clearing price [17]. Figure 2.1 illustrates this concept. Area A is a surplus area implying an area price, $p_{0,A}$, lower than the system price, while area B is a deficit area with a higher area price, $p_{0,B}$, than the price of the system. The total supply and demand curves in the rightmost plot is found by horizontal addition of the area curves. The system price, p_0, is found for P_0 amount of power. The system price gives the highest social surplus for all participating areas [18].

If congestions in the grid are discovered, the Nordic area is divided into several price areas. This is called market splitting. On each side of the congestion the bids in the bidding areas are aggregated into total demand and supply curves in the same way as in the system price calculation, resulting in area prices [17].

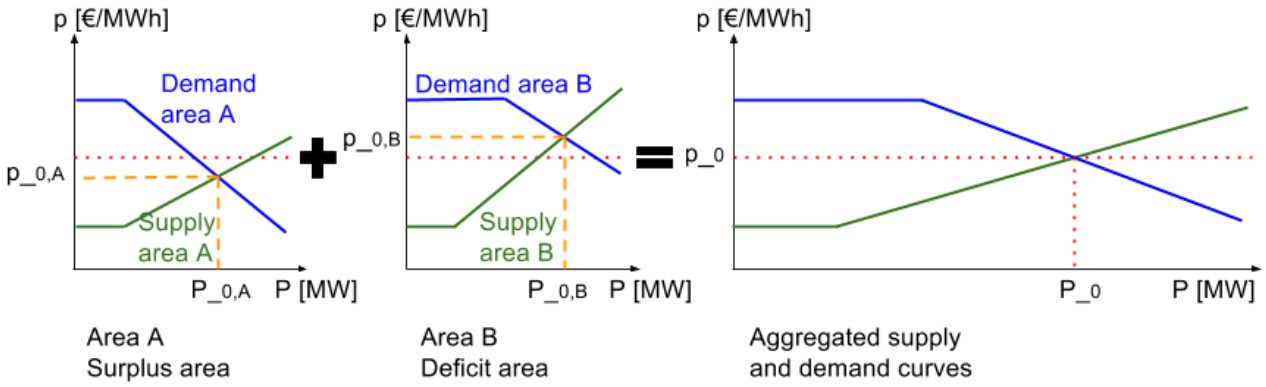

Figure 2.1: Finding the system power price from horizontally adding the area supply and demand curves.

2.2 Frequency Stability and Control

The reference frequency of the Nordic power system is 50.00 Hz. The frequency is continuously monitored in order to maintain a stable power system and make sure there is enough supply. When a power system is exposed to a power imbalance caused by e.g. connection of a large load, disconnection of such, or tripping of a generator unit, there will be a long-term distortion in the power balance between delivered and consumed power. The response of the power system to the power imbalance can be divided into four stages, depending on the duration of the dynamics and controls involved [7] [19]:

Stage I	Rotor swings in the generators (the first few seconds)
Stage II	Frequency change (a few to several seconds)
Stage III	Primary control by the turbine governing systems (several (5–60) seconds)
Stage IV	Secondary control by the central regulators (several seconds to a few minutes (30–300 seconds))

Stages III and IV in addition to tertiary control, which is activated after the secondary control, are represented graphically in figure 2.2:

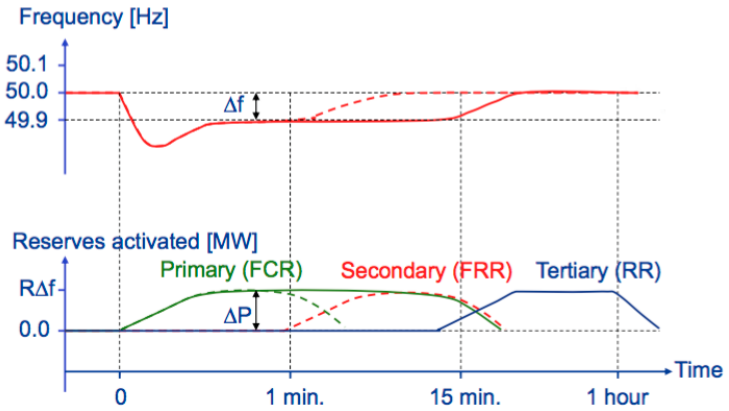

Figure 2.2: Control stages in power system operation after a drop in frequency [20]. The combination of primary and tertiary controls give the solid line for the frequency change, whereas the combination of primary and secondary controls give the dotted line.

The Nordic power system consists of primary, secondary, and tertiary frequency controls [21], and this thesis deals with the secondary frequency control structure. Figure 2.2 shows how the primary, secondary, and tertiary controls react to a dip in frequency. If a generating unit is disconnected due to for instance a fault, neighbouring generating units will experience large rotor swings, while units further away will experience smaller swings. This is stage I of the power system response. In the upper curve of figure 2.2, stage II is a drop in frequency. The slope of the curve depends on the amount of inertia in the system, i.e. the curve will be less steep for a system with a considerable amount of inertia. When the frequency starts to drop, the primary control is activated in stage III to stabilize the frequency. As figure 2.2 illustrates, the primary control can be relieved after approximately a minute by the secondary control, or not be relieved before tertiary control is initiated after approximately 15 minutes. Stage IV is the secondary control, which restores the frequency at the initial value; for the Nordic power system the initial value is 50.00 Hz.

Although these sections explain the frequency controls in terms of a large disturbance, the three frequency reserves are continuously active throughout the day. Frequency reserves are mainly used to correct the frequency when there is a mismatch between the power supply and demand, which happens often. A more thorough explanation of the controls is presented in the following subsections.

2.2.1 Primary Frequency Control

The primary frequency control, which uses Frequency Containment Reserves (FCR), is activated when there is a change in frequency. The primary control happens within a few seconds of the frequency variation, but it takes up to 60 seconds before full

activation is reached. The turbine governors execute the primary control [19]. They control the flow rate of water to the hydro power turbines, steam into a steam power turbine, etc., so as to maintain a constant rotational speed. The objective of a turbine governor is to re-establish the balance between the generated power and power demanded, thus stabilizing the system frequency. The primary control is a fully automatic regulation.

The speed-droop coefficient, or droop, is noted by ρ. The reciprocal of the droop, $R = \frac{1}{\rho}$, is the effective gain of the turbine governing system, or system frequency response, and has the denomination MW/Hz. The requirement for the system frequency response is 6000 MW/Hz in the Nordic power system [7]. Droop can be interpreted as how much the frequency has to change for the turbine valves to move from fully open to fully closed. There are requirements established in order to secure enough inertia and FCR to support the entire system, even if there are tie line outages. None of the generating units need to have the same speed-droop coefficient, but in the Norwegian power system the TSO requires the droop to be a maximum of 12 % for generating units above a certain rated power. Going beyond this limit means that a small load fluctuation would lead to a larger rotational speed change than what is expected of a good control system. The current practice of setting a maximum limit for the droop may be revised soon [7].

In the Nordic power system the FCR is divided in two; FCR in Normal operation (FCR-N) for frequencies between 49.90 and 50.10 Hz, and FCR in Disturbed operation (FCR-D) [22]. The goal is that the frequency should not drop below 49.00 Hz [23], and FCR-D is used for handling incidents where this is about to happen. The FCR-D volume should be at a level where it can handle the largest single incident that may occur; usually the outage of a large power station or an HVDC interconnector [7].

In order to ensure sufficient FCR in the system, there is a separate power market for these reserves. The primary frequency control continuously regulates the power production to stabilize the frequency. However, it does not restore the frequency to its nominal value, meaning that a stationary error in the frequency remains. In order to restore the frequency to 50.00 Hz, the secondary frequency control is necessary.

2.2.2 Secondary Frequency Control

If the distortion that has occurred turns out to be long-term, the primary frequency control will be relieved by the secondary frequency control within a minute. The secondary control is the main focus of this thesis, and has two main objectives; the secondary frequency control has to bring the frequency back to 50.00 Hz, so that the primary reserves can be freed up to deal with any other imbalances that may occur [8]. At the same time it is important that the primary regulation is not prevented from functioning normally when secondary frequency control is implemented in a

power system. Due to this, the secondary control reacts slower to changes compared to the primary control [24].

The secondary control uses Automatic Frequency Restoration Reserves (aFRR), and is accordingly an automatic control function. The way it works is that a signal is sent from the TSO to the control system of a power supplier, which automatically changes the production or the consumption of the plant. The secondary frequency control is handled by Automatic Generation Controllers (AGC), which is further explained in subsection 2.4.3.

aFRR is greatly prevalent in the rest of Europe, where it is used to handle deviations in both frequency and scheduled tie line power flow [8]. The Nordic countries are working to establish aFRR in the synchronous system, and trial operation started in 2013. For the time being it is only a supplement to the primary and tertiary control. Currently, the aFRR is only in operation during certain hours of the day when the frequency is hard to regulate, i.e. weekday mornings and evenings. Although there was a temporary halt in the aFRR purchase during the winter 2015/2016 partly due to a lack of agreement between the Nordic TSO's, aFRR is expected to be fully implemented in the coming years [7].

The secondary control will mainly be used for managing frequency deviations. When it is implemented in the Nordic power system, the aFRR will be required to be fully activated within 120 seconds. In the rest of Europe the requirement for activation is 15 minutes [7]. Hydro power is a very convenient power reserve to use for aFRR, as it is easily stored in power basins and can be turned on and off within a few minutes. Hence, the Norwegian hydro power is likely to play a big role in aFRR when it is implemented.

2.2.3 Tertiary Frequency Control

The tertiary frequency control is used for relieving the primary and secondary reserves in frequency control, and to secure exchange of power between areas [25]. The tertiary control uses Manual Frequency Restoration Reserves (mFRR), which has an activation time of up to 15 minutes.

All the Nordic countries are required to have tertiary control reserves equal to the dimensioning fault of the subsystem. There is also a separate market for mFRR, called the Regulating Power (RP) market. The RP market is the common market in the Nordic power system. The power producers and consumers bid a certain amount of power to a specified price in the RP market. For example, a system consisting of two areas activates the cheapest bids first in any of the two areas if there is a need for tertiary control. If there is a congestion in the transmission lines between the areas, the activation has to happen in the same area as the imbalance, which causes the price to be different in the two areas [25]. This is known as market splitting.

The RP market is operated by a system that takes into account a merit order price list and tie line congestion, which is part of the idea behind the research question at hand. In Europe, where aFRR is more prevalent than in the Nordic countries, there is little use of tertiary control, and this may end up being the case in the Nordic power system when aFRR is successfully implemented. Thus, the RP market could be transferred from mFRR to aFRR. The obvious difference and challenge is that aFRR activates automatically, whereas the TSO's examine the tie lines for congestions before activating mFRR.

2.3 The Swing Equation

When studying frequency and power balance of a power system, the swing equation is an important balance equation. The swing equation defines the relationship between electrical and mechanical power of a machine, the frequency change, and the inertia of the machine [19]. Newton's second law is the basis of the swing equation. Equation 2.1 presents Newton's second law on the form that is used to derive the swing equation:

$$J\dot{\omega}_m + D_m\omega_m = \tau_m - \tau_e \tag{2.1}$$

J is the total moment of inertia, ω_m is the speed of the rotor shaft, D_m is the damping torque, τ_m and τ_e are the mechanical turbine torque and electrical torque produced by the generator, respectively. The mechanical rotational loss due to windage and fricition in the generator are accounted for in the damping torque [19]. The equation takes SI units.

Using the relation $J = \frac{2HS_N}{\omega_s^2}$, the swing equation becomes:

$$\frac{2HS_N}{\omega_s^2}\dot{\omega}_m + D_m\omega_m = \tau_m - \tau_e \tag{2.2}$$

H is the normalized inertia constant and S_N is the rated power of the machine. ω_s is the synchronous speed of the generator, defined as $2\pi f_N$, where f_N is the nominal frequency.

The relation $\omega = \frac{\omega_m}{\omega_s}$, where ω is the per unit (p.u.) speed, gives:

$$\frac{2HS_N}{\omega_s}\dot{\omega} + D_m\omega\omega_s = \tau_m - \tau_e \tag{2.3}$$

All parts of the equation should be in p.u.; therefore the equation is divided by the system basis of the torque, $\tau_{base} = \frac{S_N}{\omega_s}$:

$$2H\dot{\omega} + \frac{D_m\omega\omega_s^2}{S_N} = \tau_m - \tau_e \tag{2.4}$$

Defining $D = \frac{D_m \omega_s^2}{S_N}$ and inserting D into the equation:

$$2H\dot{\omega} + D\omega = \tau_m - \tau_e \tag{2.5}$$

Active power is equal to the speed of the generator times torque, i.e. $P = \omega\tau$. When linearizing around ω equal to 1.0, the approximation $P \approx \tau$ becomes true. This and the relation $\dot{\delta} = \omega_s\omega$ is used to get the final version of the swing equation:

$$\frac{2H}{\omega_s}\ddot{\delta} + \frac{D}{\omega_s}\dot{\delta} = P_m - P_e \tag{2.6}$$

δ is the voltage angle, defined as the angle between the rotor and the stator's magnetic field in the synchronous generators, while P_m and P_e are the mechanical and electrical active powers, respectively.

2.4 Power System Components

The following subsections explain the functionality of the turbines and turbine governors, electromechanical dynamics, and conventional automatic generation control in a power system.

2.4.1 Turbine and Turbine Governor

The primary control of a power system is handled by the turbine governors. Figure 2.3 shows the block diagram of the turbine and turbine governor used in this thesis. The governing systems are modeled using Proportional–Integral–Derivative (PID) controllers, seen in figure 2.3. The input to the controller is the difference in reference speed, ω_{ref}, the actual speed of the system, $\Delta\omega$, and the change in speed set point provided by the AGC, ΔP_{ref}. The signal for the valve position of the turbine, Δc, is controlled by the proportional gain, K_p, and the integral time constant, T_i [26]. In the proportional term, the gain is multiplied by the magnitude of the error, whereas the integral term gives an integral of the error multiplied by the proportional gain as output. The derivative constant, K_D, represents the derivative part of the PID controller, while K_f is the constant of the low-pass filter in the same part. In the modeling done for this thesis, K_D was set equal to zero; that is the controller was in reality a PI controller. The derivative part controls transient faults, and was included in the model in order to have as an option for further modeling.

Through a feedback loop, the deviation in the mechanical power, ΔP_m, is multiplied by the steady state feedback, or the droop, ρ. The lower left summation block calculates the deviation from the planned power, which is given as input to the integrator. When a disturbance occurs, resulting in power deviation, the

controller integrates to ensure that the power production is equal to the power demand after the disturbance. As system frequency is not amongst the inputs to the turbine governor, the integrator does not get the frequency back to the reference value. However, the frequency will reach a new value when steady state is restored. The droop feedback loop also prevents the generators in the system from working against each other. Finally, the T_w is the water starting time of the turbine.

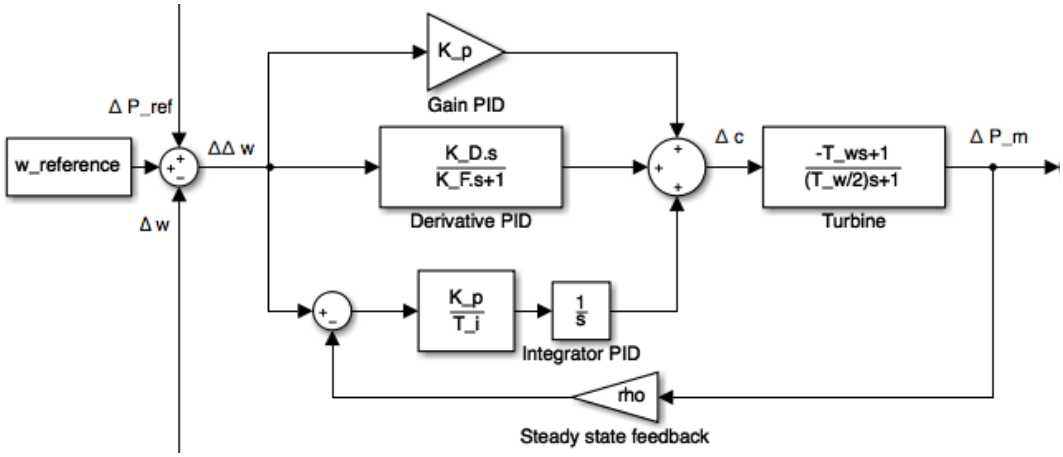

Figure 2.3: Block diagram of the turbine and the turbine governor.

2.4.2 Electromechanical Dynamics

Figure 2.4 shows the block diagram of the synchronous generators used in this thesis. These execute the electromechanical dynamics in the model, and take the change in mechanical power, electrical power, and the frequency dependent load, ΔP_m, ΔP_e, and ΔP_d, respectively, as input. The final output is the difference in voltage angles, $\Delta\delta$. The block diagram consists of two integrators. The first one takes the difference in power multiplied by the inverse of two times the normalized inertia constant, H, and gives the difference in the generator's speed, $\Delta\omega$, as output. The second one takes the change in speed times the standard formulation of the electrical frequency, $2\pi f_N$, as input, and gives the change in voltage angles, $\Delta\delta$, as output. This is used as input to the MATLAB® Function blocks which are further described in sections 3.2 and 4.2.4.1. When studying the generator modeling it is clear that the block diagram of the synchronous generators is based on the swing equation described in section 2.3.

The change in electrical frequency, ω_N, is subtracted from the change in speed and used in the feedback loop for the frequency dependent load. The reason for this is further explained in section 3.2. D is the damping coefficient of the frequency

dependent load in the generators. In steady state, the electrical power is equal to the mechanical power, and the frequency dependent load makes no contribution.

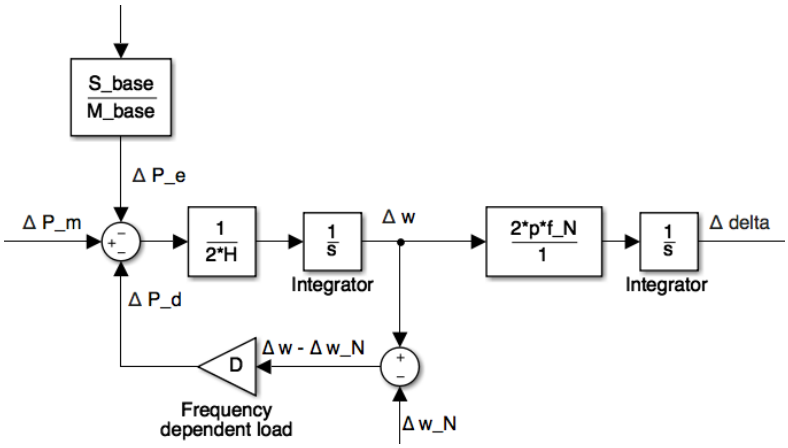

Figure 2.4: Block diagram of the generator.

In a power system with generators of different sizes, the power base values are dissimilar. Thus, the local bases of each generator, $M_{base,i}$, where i represents the ith generator, will have different values. Additionally, a global base value, S_{base}, for the entire system must be specified. When calculating the electrical power output needed from each generator, the values need to be converted from global to local by multiplying the calculated values by S_{base} and dividing by $M_{base,i}$. This is done to attain the electrical powers, $\Delta P_{e,i}$, required from each generator.

2.4.3 Automatic Generation Control

This section describes a conventional Automatic Generation Control (AGC) which is used to achieve the secondary frequency control. In order to regain the initial operation frequency, 50.00 Hz in the Nordic power system, the speed-droop curve must be shifted. This is done by changing the reference point of the produced power, P_{ref}, for the generating units' governing systems [19], as illustrated in figure 2.5.

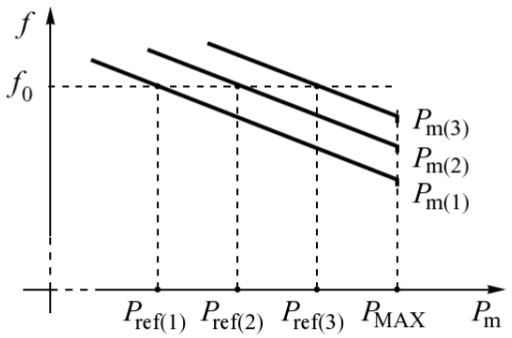

Figure 2.5: Speed-droop characteristic for different values of P_{ref} [19, p. 341]. f_0 is the frequency reference value.

The main purpose of AGC is to:

- Restore the system frequency to the nominal value after a disturbance.
- Free the primary reserves to make them available to deal with any future imbalances.
- Maintain the scheduled flow of power exchanged between different control areas, known as tie-line control. This only applies to certain power systems.

For cases where multiple power systems are interconnected, AGC is implemented separately for each area. If the AGC is not implemented separately, the result would be undesired changes of the scheduled power flow in the tie lines, causing violations of contracts between the cooperating systems. Each area regulator is therefore individually responsible for regaining frequency and maintaining net tie-line interchanges for their respective area. This approach is called the non-intervention rule [19].

When an area experiences a deficit in power generation, e.g. as a result of a power load increase, the other generating units in the area must increase the production in order to cover the loss. The change of generation power, ΔP_f, can be expressed by the following equation:

$$\Delta P_f = \lambda_R \Delta f \tag{2.7}$$

where λ_R [MW/Hz] is the frequency bias factor of each area and Δf denotes the frequency deviation following the power imbalance. This power change is added to the deviation in power interchange in the tie lines, ΔP_{tie}, to obtain the Area Control Error (ACE). Thus, the ACE is defined as:

$$ACE = \lambda_R \Delta f + \Delta P_{tie} \tag{2.8}$$

Figure 2.6 illustrates the concept of the AGC. The ACE is sent as input to a PI controller. $K_{i,agc}$ denotes the proportional gain while $T_{i,agc}$ is the integral time constant of the PI controller. If a disturbance results in a frequency change, the controllers will integrate until the frequency is back to the reference value.

The PI controller determines the change of the total P_{ref} that is needed, which is then allocated between the generators in the affected area or areas. The contribution from each generating unit is decided by the participation factors $\alpha_1, ..., \alpha_i, ..., \alpha_n$ related to generators $1, ..., i, ..., n$ in the area. Therefore, the necessary ΔP_{ref} for each generating unit is found individually, and the information for the new set points are fed to the governing systems of the generators. This is the classical way to determine the change in power output from the generators.

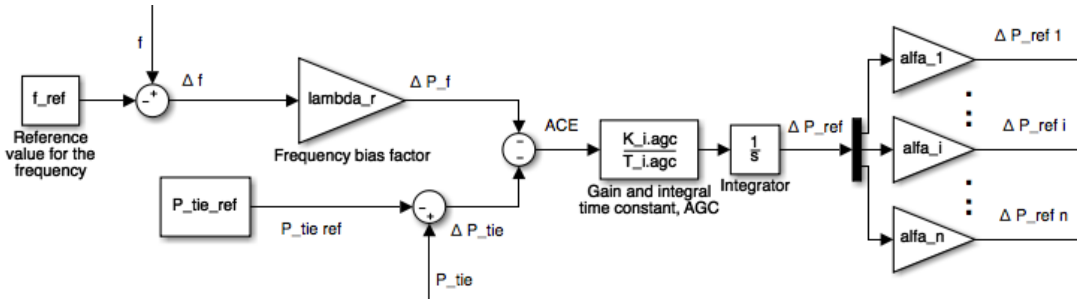

Figure 2.6: Block diagram of the AGC.

2.4.4 Automatic Generation Control Schemes

When a single controller, like the one described in section 2.4.3, is responsible for controlling the ACE of a whole country, it is called centralized AGC control scheme. This type of controller has been operating the aFRR in the Nordic power system since 2013.

In addition to the centralized AGC control scheme, there is also the hierarchical AGC. In this type of control scheme, the areas have their own controllers that are secondary to a supervisory national controller. The controllers of each area are responsible for handling deviations in frequency and tie line power flow in their own area, whereas the national controller regulates interchange with neighbouring countries [27]. This hierarchical design is suitable for e.g. central Europe, where there are AC transmission lines and corridors to neighbouring countries. In the Nordic power system however, there are mostly HVDC connections to surrounding countries, which have their own transmission plans and do not respond to frequency variations.

This thesis proposes a new AGC scheme for the Nordic synchronous system. In this solution there are AGC's in all areas, but only the frequency and not the

scheduled power flow is of importance. However, congestions and system security still needs to be taken into account. The idea is that when the system is operated without congestions, the ACE is common for the entire system. Whenever any congestions occur, the system is split into two or more areas, giving local ACE's. In other words, the Nordic countries are regarded as one area unless grid capacities force smaller areas. This is similar to market splitting, explained in section 2.1.

2.5 DC Power Flow

The voltage regulation and reactive power flow is of little interest when studying the frequency. Hence, DC Power Flow (DC PF) was a useful tool in this thesis. DC PF is a linear method used to solve power flow problems in large AC systems. It is an approximation to the full AC power flow solution, but the calculations are faster, less time consuming, and less costly.

For a system with n busbars, where i and j are the ith and jth busbars, the ordinary AC power flow solution for a given state of operation is obtained by solving the following set of load flow equations:

$$Y = \begin{bmatrix} y_{11} & \cdots & -y_{1j} & \cdots & -y_{1n} \\ \vdots & \ddots & & & \vdots \\ -y_{i1} & \cdots & y_{ij} & \cdots & -y_{in} \\ \vdots & & & \ddots & \vdots \\ -y_{n1} & \cdots & -y_{nj} & \cdots & y_{nn} \end{bmatrix} \tag{2.9}$$

$$y_{ij} = |y_{ij}|\angle\theta_{ij} \tag{2.10}$$

$$V_i = |V_i|e^{j\delta_i} = |V_i|\angle\delta_i \tag{2.11}$$

$$V_j = |V_j|e^{j\delta_j} = |V_j|\angle\delta_j \tag{2.12}$$

$$P_i = \sum_{j=1}^{n} |V_i||V_j||y_{ij}|\cos(\delta_i - \delta_j - \theta_{ij}) \tag{2.13}$$

$$Q_i = \sum_{j=1}^{n} |V_i||V_j||y_{ij}|\sin(\delta_i - \delta_j - \theta_{ij}) \tag{2.14}$$

Y is the system admittance matrix, the $|y_{ij}|$'s are the magnitudes of the Y matrix elements, the θ_{ij}'s represent the angles of the admittance matrix elements, and V_i and V_j are the voltages at the ith and jth busbars. δ_i and δ_j are the voltage angles at the ith and jth busbars. P_i and Q_i are the active and reactive powers at the ith busbar, respectively.

Below are the two main simplifications when deriving DC PF equations:

- The voltage profile in the grid is assumed to be uniform and such that all voltages are close to nominal, i.e. all V_i's are assumed to be 1.0 p.u.
- All grid losses can be neglected or incorporated e.g. in the loads. This assumption can usually only be applied in the high voltage transmission grid where the reactances are much larger than the transformer and line resistances. When the resistances are neglected, all transformer and line impedances can be modeled as $Z_i = jX_i$. This also means that the angles of the admittance matrix elements will be $\pm 90°$, i.e. $\theta_{ij} = -\frac{\pi}{2}$ for all diagonal elements and $+\frac{\pi}{2}$ for all non-diagonal elements.

DC PF can be used in any power system. When applying the simplifications above in addition to the relation $\cos(x - \frac{\pi}{2}) = \sin(x)$, equation 2.13 becomes:

$$P_i = \sum_{j=1}^{n} |y_{ij}| \sin(\delta_i - \delta_j) \tag{2.15}$$

Finally, the approximation that for small angle differences, $\Delta\delta$, the sine function can be linearized such that $\sin(\delta) = \delta$, is applied:

$$P_i = \sum_{j=1}^{n} |y_{ij}|(\delta_i - \delta_j) \tag{2.16}$$

Similar simplifications can be done for the reactive power. The focus of this thesis is not on the reactive power, and therefore it is disregarded in this context.

When calculating the active power flow in the transmission lines, P_{i-j}, in the system, the following equation is used:

$$P_{i-j} = |y_{ij}|(\delta_i - \delta_j) \tag{2.17}$$

P_{i-j} is the active power flow in the lines between busbars i and j [28].

2.6 Power Transfer Distribution Factor

Power Transfer Distribution Factor (PTDF) is an alternative approach when performing power flow calculations, and are becoming more common in the day ahead power markets. PTDF's can be used to calculate the incremental impact a power change in a node has on a specific transmission line. Nodes can be defined in several ways; for instance areas, zones, single busbars, etc. can constitute nodes. The PTDF's provide a linear approximation between how the flows in transmission lines change when power demand or supply is increased or decreased in a node. When resolving congestions in a power system, the nodes that affect the congested

lines the most are known from the PTDF's of the system, and the PTDF display is hence a convenient tool in congestion handling [29].

Calculation of the PTDF's of a power system is done with equation 2.18, which is derived by using the DC PF equations.

$$PTDF_{ij,n} = y_{ij}(z_{in} - z_{jn}) \tag{2.18}$$

The equation shows the change of active power flow, i.e. the PTDF value, in the transmission line between nodes i and j due to a power injection in node n. y_{ij} is the admittance in the line between nodes i and j. z_{in} and z_{jn} are the impedances in the lines between nodes i and n, and j and n. By repeating the same procedure for all nodes and lines in a power system, the nodal transfer PTDF matrix for the system can be computed [30].

Calculating the PTDF matrix is illustrated by an example from reference [30]. Figure 2.7 shows a power system consisting of three nodes. Node 3 is the slack node in this example. In accordance with the DC PF approximation the line resistances are neglected and only the reactances are regarded.

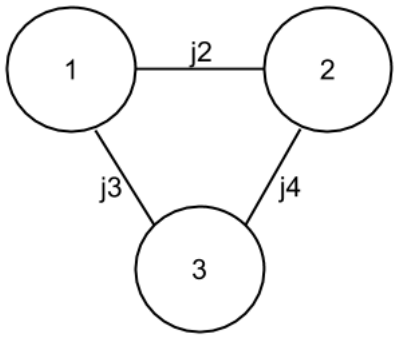

Figure 2.7: Three node system for illustration of PTDF calculation. $j2$, $j3$, and $j4$ are the reactances of lines 1–2, 1–3, and 2–3, respectively.

The admittance matrix, Y, for the system is given by equation 2.19.

$$Y = \begin{bmatrix} \frac{1}{2}+\frac{1}{3} & -\frac{1}{2} & -\frac{1}{3} \\ -\frac{1}{2} & \frac{1}{2}+\frac{1}{4} & -\frac{1}{4} \\ -\frac{1}{3} & -\frac{1}{4} & \frac{1}{3}+\frac{1}{4} \end{bmatrix} \tag{2.19}$$

The impedance matrix, Z, for the system is composed by adding +1 to the diagonal element of the admittance matrix corresponding to the slack node, node 3. Equation 2.20 shows how this is done.

$$Z = \begin{bmatrix} \frac{1}{2}+\frac{1}{3} & -\frac{1}{2} & -\frac{1}{3} \\ -\frac{1}{2} & \frac{1}{2}+\frac{1}{4} & -\frac{1}{4} \\ -\frac{1}{3} & -\frac{1}{4} & \frac{1}{3}+\frac{1}{4}+1 \end{bmatrix}^{-1} = \begin{bmatrix} 3.00 & 2.33 & 1.00 \\ 2.33 & 3.22 & 1.00 \\ 1.00 & 1.00 & 1.00 \end{bmatrix} \tag{2.20}$$

Using equation 2.18, the PTDF values of the example system can be calculated. Equation 2.21 shows how the PTDF value from node 1 to the transmission line between nodes 1 and 2 is calculated.

$$PTDF_{12,1} = y_{12}(z_{bus,11} - z_{bus,21}) = \frac{1}{2}(3.00 - 2.33) = 0.33 = 33\% \tag{2.21}$$

33% of the power will flow in the line between nodes 1 and 2 for production in node 1. The power flow will be reversed for consumption in node 1, i.e. the power will flow from 2 to 1. The PTDF values of the other nodes are calculated similarly, and the result can be seen in equation 2.22. The rows represent the lines, ij, while the columns represent the nodes, n.

$$PTDF = \begin{array}{c} \\ \textbf{1–2} \\ \textbf{1–3} \\ \textbf{2–3} \end{array} \begin{array}{c} \begin{array}{ccc} \textbf{1} & \textbf{2} & \textbf{3} \end{array} \\ \begin{bmatrix} 0.33 & -0.44 & 0 \\ 0.67 & 0.44 & 0 \\ 0.33 & 0.56 & 0 \end{bmatrix} \end{array} \tag{2.22}$$

2.7 Per Unit System

The principle of the per unit (p.u.) system is to express quantities of an electric power system as fractions of a pre-defined base quantity. Since the magnitudes are relative, they can be directly compared, and manual calculations are greatly simplified. Normally the nominal apparent power of the system, S_{base}, is used as the base for the active and reactive powers, and the nominal voltage, V_{base}, is used as the base for the voltage. Other base quantities, such as current and impedance, can be derived by calculation from the S_{base} and the V_{base} [31]. Equation 2.23 shows how the p.u. value of active power is calculated. By modifying the equation the MW value can be found from the p.u. value of the active power.

$$P_{p.u.} = \frac{P_{MW}}{S_{base}} \tag{2.23}$$

Chapter 3

Method

Parts of this chapter are redrafts of reference [2]. The software that was utilized to do the modeling and simulations in this thesis is described first. Then the method used in the modeling is explained. The method that is put forward is utilized in the model described in chapter 4.

3.1 Software – MATLAB® and Simulink®

The software used for the simulations was MATLAB® and Simulink®, both developed by MathWorks®. MATLAB® (Matrix Laboratory) is an extensive mathematics program, and is one of the most commonly used mathematics software among engineers and scientists [32]. In this thesis, MATLAB® was used as a tool to set values and do calculations for the model that was constructed in Simulink®. Simulink® is a graphical block diagram environment for modeling and simulating dynamic systems. Simulink® is widely used in automatic control [33], making it a useful tool for this thesis. Simulink® is tightly integrated with MATLAB®, which can be run from Simulink® or vice versa. The graphical editor has a large block diagram library which can be customized by adding or removing various tool extensions.

The model described in this thesis used blocks from the standard library, which included transfer function blocks, constants, gains, integrators, steps, muxes and demuxes, sums, switches, clocks, a lookup table, a math function, and MATLAB® Function blocks. Additionally, scopes were used to study responses in the different parts of the model, and 'to file' blocks were used to export data from the model to various MATLAB® scripts.

3.2 Method of Modeling

The control structure in the model described in chapter 4 uses a method based on a combination of the swing equation and DC Power Flow (PF). This makes it fairly simple to expand the system to any arbitrarily sized system. Each area in a power system comprises a specific amount of generating units and power loads. The generating units are modeled as synchronous generators connected to hydro power turbines and turbine governors. Power loads are modeled as unit step blocks or ramps, which step or ramp the loads up or down to a specified value at a specified time.

The method uses per unit values, and is referred to a system frequency of 50.00 Hz. This means that when the speed is zero, the system frequency is 50.00 Hz and the system is operating in steady state. The base value for the apparent power of the system, the global base value, S_{base}, is 1000 MVA, while the generators have local bases, $M_{base,i}$'s, related to each generator's capacity. The base values for the specific model used in this thesis are listed in chapter 4.

The final output from the power plant model is the generator voltage angles. These are, together with the loads and the admittance matrix of the system, used as input to a MATLAB® Function block in the Simulink® model. The function block uses the input to calculate what the electrical power output, ΔP_e, should be from the generators. This is then used in a feedback loop from the function block back to the generators.

For a system with n generating units, the swing equations can be represented by equation 3.1:

$$\begin{aligned} \frac{2H_1}{\omega_s}\ddot{\delta_1} + \frac{D_1}{\omega_s}\dot{\delta_1} &= P_{m,1} - P_{e,1}, \\ \frac{2H_2}{\omega_s}\ddot{\delta_2} + \frac{D_2}{\omega_s}\dot{\delta_2} &= P_{m,2} - P_{e,2}, \\ &\vdots \\ \frac{2H_n}{\omega_s}\ddot{\delta_n} + \frac{D_n}{\omega_s}\dot{\delta_n} &= P_{m,n} - P_{e,n} \end{aligned} \tag{3.1}$$

The expression $P_e = Y\delta$ from DC PF can be expressed in matrix form. In a system with n generating units and m power loads, the expression looks like the following:

$$\begin{bmatrix} \Delta P_{e,1} \\ \vdots \\ \Delta P_{e,n} \\ -\Delta P_{l,1} \\ \vdots \\ -\Delta P_{l,m} \end{bmatrix} = \begin{bmatrix} Y_{11} & Y_{12} \\ Y_{21} & Y_{22} \end{bmatrix} \begin{bmatrix} \Delta\delta_{g,1} \\ \vdots \\ \Delta\delta_{g,n} \\ \Delta\delta_{l,1} \\ \vdots \\ \Delta\delta_{l,m} \end{bmatrix} \tag{3.2}$$

The ΔP_e's represent the change in the power generating units; the ΔP_l's represent the change in power loads; Y_{11}, Y_{12}, Y_{21}, and Y_{22} are submatrices of the admittance matrix, Y; the $\Delta\delta_g$'s are the change in the inner voltage angles of the generators, while the $\Delta\delta_l$'s are the change in voltage angles between the busbars. The power loads are represented with a minus in order to distinguish between the generating units and the loads. Equation 3.2 can be written more concisely as:

$$\begin{bmatrix} \Delta P_e \\ \Delta P_l \end{bmatrix} = \begin{bmatrix} Y_{11} & Y_{12} \\ Y_{21} & Y_{22} \end{bmatrix} \begin{bmatrix} \Delta\delta_g \\ \Delta\delta_l \end{bmatrix} \tag{3.3}$$

ΔP_e and ΔP_l represent the change in power generation and load, respectively; the $\Delta\delta_g$ and $\Delta\delta_l$ represent the change in voltage angles for the generating unit and load busbars, respectively. The ΔP_l submatrix is defined such that the various power loads are written with a minus, like $\begin{bmatrix} -\Delta P_{l,1} & -\Delta P_{l,2} & \cdots \end{bmatrix}^T$. The admittance submatrices are divided according to the amount of generation and load units in the system. For empty busbars with no generating unit or load connected, the P matrix will have as many extra null elements added as there are empty busbars. The null elements are put in the ΔP_l submatrix. The admittance and voltage angle matrices will be expanded correspondingly, but these new elements will not necessarily be zeros.

The admittance matrix elements and the power loads are known values. The voltage angles of the generators are also known, as they are the output from the power plant model. From equation 3.3, the remaining voltage angles and thus the electrical powers are calculated as follows:

$$\Delta\delta_l = Y_{22}^{-1} \left(\Delta P_l - Y_{21} \Delta\delta_g \right) \tag{3.4}$$

$$\Delta P_e = Y_{11} \Delta\delta_g + Y_{12} \Delta\delta_l \tag{3.5}$$

The output from the function block is ΔP_e. This submatrix represents the electrical power needed from all the generating units in the system. The calculated change in electrical power is, through feedback loops, used as input to the generators. The ΔP_e's are multiplied by the global S_{base} and divided by the local $M_{base,i}$ in order to get the correct value of the ΔP_e's to the generators.

Some of the areas have AGC's to handle the secondary frequency control. Inputs to the AGC's is the deviation in frequency, Δf, and change in the tie line power transmission, ΔP_{tie}. The AGC's are modeled as regular AGC's, but with switches that connect the ΔP_{tie}'s only if these exceed their reference values. The power flow in all the transmission lines and corridors of the modeled system are calculated based on equation 2.17 in chapter 2 in a separate MATLAB® Function block. For any system, equation 2.17 can be represented on matrix form so as to calculate several line power flows at the same time. Equation 3.6 shows the matrices of an example system with four busbars and five transmission lines. There are lines between all the busbars except busbars 1 and 4.

$$\begin{bmatrix} \Delta P_{1-2} \\ \Delta P_{1-3} \\ \Delta P_{2-3} \\ \Delta P_{2-4} \\ \Delta P_{3-4} \end{bmatrix} = \begin{bmatrix} y_{12} & -y_{12} & 0 & 0 \\ y_{13} & 0 & -y_{13} & 0 \\ 0 & y_{23} & -y_{23} & 0 \\ 0 & y_{24} & 0 & -y_{24} \\ 0 & 0 & y_{34} & -y_{34} \end{bmatrix} \begin{bmatrix} \Delta\delta_1 \\ \Delta\delta_2 \\ \Delta\delta_3 \\ \Delta\delta_4 \end{bmatrix} \tag{3.6}$$

The method does not explicitly take into account the voltages and currents in the system, thus the electrical frequency, usually known as $\omega_{el} = 2\pi f_N$, is not defined. But as this is a synchronous system, the generator speeds define the frequency. Hence, the electrical frequency is defined as a nominal speed, ω_N. For a system with n generators, ω_N is defined as the scaled mean value of the sum of the generator speeds in the system:

$$w_N = \frac{\sum_{i=1}^{n} H_i \omega_i}{\sum_{i=1}^{n} H_i} \tag{3.7}$$

In a large power system the speed of generating units with large inertia will have more significance than that of smaller units. After a change in load or similar disturbances, the generator speeds will even out and attain the same value. Furthermore, ω_N is, together with the individual generator speeds, ω_i, given as input to the frequency dependent load of each generator. This is done so that the frequency dependent load does not contribute when the system is in steady state.

The advantage of using the described method in power system models is that the models can be easily expanded without too many adjustments. The next chapter describes a model representing the Nordic power system where this method is applied.

Chapter 4

Model

Parts of this chapter are redrafts of reference [2]. A model representing the Nordic power system was put together in Simulink® in order to illustrate the proposed solution to the research question. The modeled power system and the different parts of the model are described in the following sections. A detailed block diagram of the model can be found in appendix A.1.

4.1 Description of the Modeled System

The model is a simplified representation of the Nordic power system, illustrated in figure 1.1 in chapter 1. Figure 4.1 shows a single line diagram of the modeled system. Bidding zones NO1, NO2, NO3, NO4, and NO5 in Norway, SE1, SE2, SE3, and SE4 in Sweden, and FI in Finland are all represented by one generator and one load each. Due to the lack of hydro power in Denmark, area DK2 is represented by a load of a constant value in accordance with the flow in the corridor between Denmark and the southern part of Sweden, DK2-SE4, during the hour 19:00–20:00 January 6, 2016.

In reality the connection between southern Sweden and Finland, SE3-FI, is an HVDC link. In this model it was designed as a variable AC connection. Hence, this connection is not modeled correctly. However, the SE3-FI link did not vary considerably when the model was exposed to different disturbances, with the exception of a load increase in Finland, described in section 5.6.

As the model is not a fully detailed representation of the Nordic power system, the reactances of the transmission lines were chosen as the inverse of the maximum transfer capacity in the connections between the areas. This data was gathered from reference [34]. The reactance values of the system can be found in appendix A.2. The reactances of lines NO4-FI and SE1-FI were adjusted in order to get an appropriate power flow.

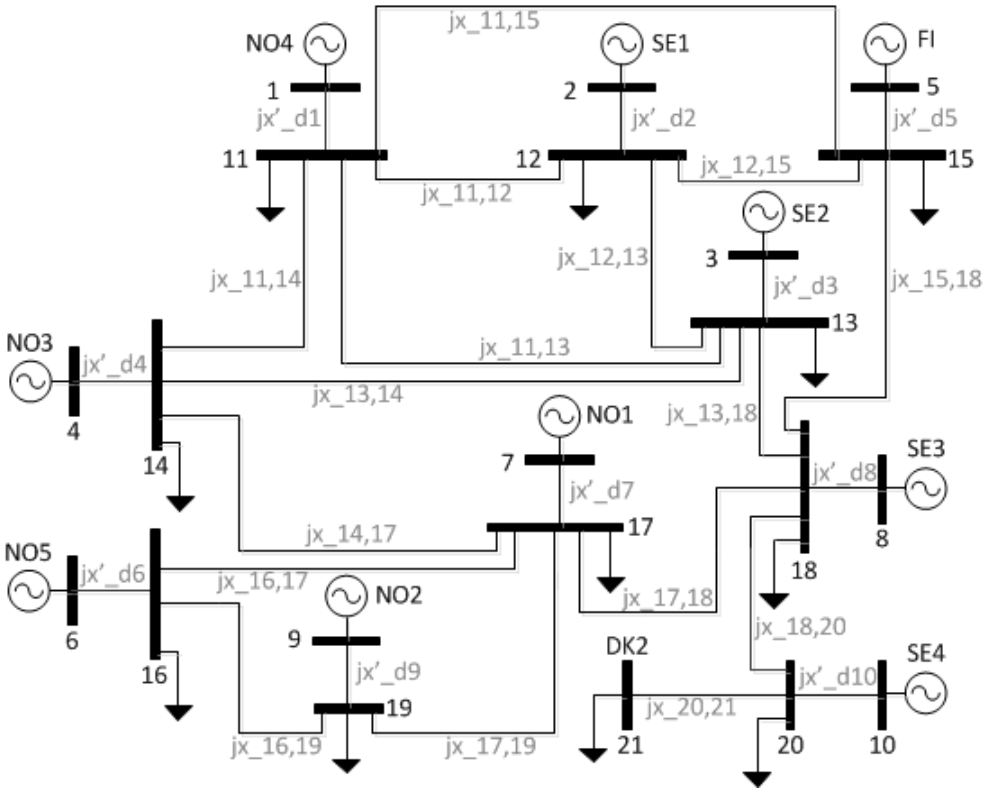

Figure 4.1: Single line diagram of the modeled power system. There are eleven areas in the system, all of which comprise a generator and a power load, except area DK2 which consists of only a load. The generator transient direct axis reactances, $jx'_{d,i}$, are shown for each generator; in addition to the line reactances of each transmission line, $jx_{i,j}$. The values of these parameters can be found in appendix A.2.

During the development of the model, different layouts were tested. To start with there was no secondary frequency control in the system, only the primary control. The model was then expanded to include three AGC's. The AGC approach is further described in section 4.2.3.

4.1.1 System Frequency Response

The system in the model uses data from the hour of 19:00–20:00 January 6, 2016, when a production record was set in Norway. During a high load hour, as the one modeled, the system frequency response in the Nordic synchronous area is usually larger than the requirement of 6000 MW/Hz. The system frequency response used in this model was 9592 MW/Hz. Detailed calculations of the system frequency response can be found in appendix B.

4.1.2 Base Values of the System

Table 4.1 shows the per unit base values used in the model. The values are not exactly the same values as in the actual Nordic power system, but a good enough approximation for the model used in this thesis.

Table 4.1: Base values of the system.

Parameter	Value
f	50.00 Hz
S_{base}	1000 MVA
$M_{base,NO1}$	2650 MVA
$M_{base,NO2}$	11000 MVA
$M_{base,NO3}$	4400 MVA
$M_{base,NO4}$	5000 MVA
$M_{base,NO5}$	8000 MVA
$M_{base,SE1}$	6000 MVA
$M_{base,SE2}$	8000 MVA
$M_{base,SE3}$	15300 MVA
$M_{base,SE4}$	7800 MVA
$M_{base,FI}$	14502 MVA

The reference frequency of the system was 50.00 Hz. However, the speed represented the frequency in the model, and a speed of 0.00 p.u. implied a frequency of 50.00 Hz. The global power base, S_{base}, was used for the overall system, including the transmission in the power lines and corridors, the loads, and the calculations in the MATLAB® Function blocks. All the generating units had different local power bases, $M_{base,i}$, in accordance with the installed power generation per area.

4.1.3 aFRR Merit Order Lists

The aFRR merit order lists that were used as basis for the simulations are listed in tables 4.2 and 4.3. The lists were inspired by an actual hour in the RK market, and are for the purpose of the thesis a satisfactory approach to real aFRR bidding lists [7]. Table 4.2 displays the total amount of aFRR available in each area for up regulation, and the price in € per 5 MW activated. The bids for down regulation are listed in table 4.3. In reality, the aFRR would have different prices depending on how much the buyer wants activated, i.e. the first 5 MW of up regulation in an area would be cheaper than the last 5 MW available. However, the lists have been simplified in this thesis so that the total aFRR available in each area has the same

price. Although the lists show how much aFRR was available in each area, these numbers were only used as a relative guidance and not strictly followed. Only hydro power reserves made available as aFRR were taken into account when the bidding lists were created.

NO1, NO3, and NO4 are not in any of the control areas (more details on this in section 4.2.3), hence the aFRR in these areas are not included in the lists. SE4 does not usually provide any aFRR and was therefore not included in the lists.

Table 4.2: Merit order list of aFRR bids for up regulation, sorted from cheapest to most expensive.

Bidding zone	**Price [€/5 MW]**	**Total volume of aFRR [MW]**
NO5	33.09	290
SE2	33.95	70
NO2	34.27	295
SE1	36.22	160
SE3	44.40	75
FI	59.00	180

Table 4.3: Merit order list of aFRR bids for down regulation, sorted from cheapest to most expensive.

Bidding zone	**Price [€/5 MW]**	**Total volume of aFRR [MW]**
NO5	23.63	440
NO2	28.36	475
SE3	28.8	90
SE1	30.56	95
SE2	32.2	450
FI	35	150

4.2 Description of the Model

The following sections provide explanations of the different parts of the model.

4.2.1 Turbine and Turbine Governor

The primary control of the system is handled by the turbine governors. The operation of the turbine governors is explained in section 2.4.1, and the modeling of the turbine and turbine governor of the modeled system was done exactly as in figure 2.3 in chapter 2. Areas SE3, SE4, and FI contribute minimally to the primary frequency control; therefore, their droop values are higher compared to the other areas. The specific parameter values can be found in appendix A.2.

4.2.2 Synchronous Generator

The generators of the system are modeled as synchronous generators. The block diagram of the generators can be found in figure 2.4 in chapter 2.

The power base values of the system are listed in table 4.1. As previously stated, all the generators have their own local power base values. The normalized inertia constants, H_i, of the generators and the turbine and turbine governor parameters are set based on the size of the generators, and are listed in appendix A.2. The normalized inertia constants were calculated as weighted sums based on the number and sizes of the generators in each area.

In the modeling method presented in this thesis, the output from the network calculations block in the model is the change in electrical power for the generators, $\Delta P_{e,i}$. These are calculated based on the global base. In order to convert the electrical power to values complying with the local base of the generators, the output from the network calculations block is multiplied by S_{base} and divided by $M_{base,i}$. This gives the resulting change in electrical power which is the input for the generators. Figure 2.4 in chapter 2 shows how the recalculation is done in the block diagram.

4.2.3 Automatic Generation Control

The AGC's are modeled as ordinary AGC's with a few modifications. Figure 4.2 shows the AGC used in the control area Sweden and Finland; the two other AGC's are similar but have different parameter values and different amounts of participation factors, α_i's. As explained in chapter 3, the frequency is defined as the nominal speed, ω_N. In combination with the reference value of the frequency, $f_{ref} = 0$, the nominal speed is the input to the frequency part of the ACE. The product of the change in frequency multiplied by the frequency bias factor, λ_R, is the change in generation power necessary to keep a constant system frequency. The reference value of the tie line power, $P_{tie,ref}$, is subtracted from the actual tie line power; the change in tie line power flow, ΔP_{tie}, is used as input to the second part of the ACE.

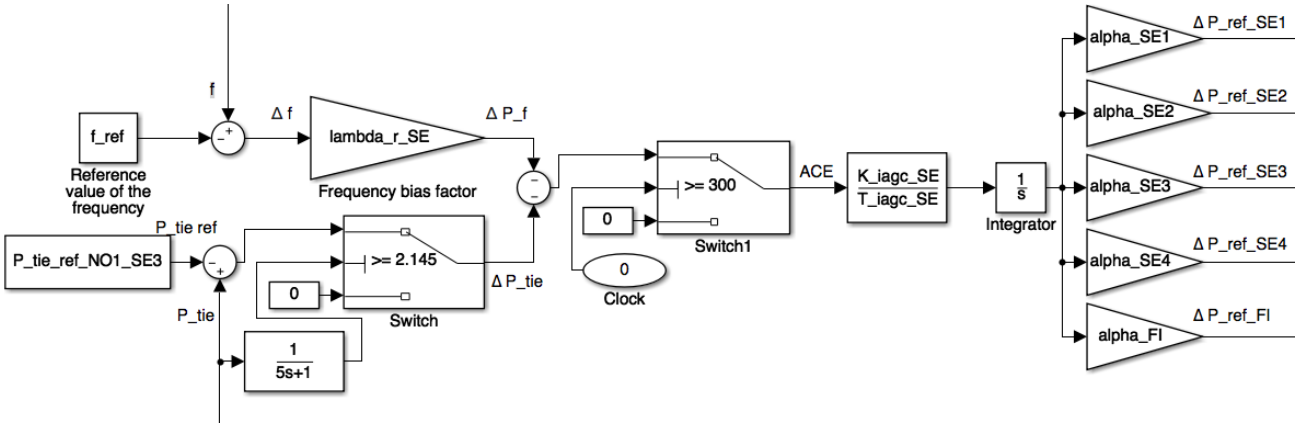

Figure 4.2: Block diagram of the modified AGC with parameter values of the AGC in control area Sweden and Finland.

There are two switches included in the AGC. The system uses tens of seconds to stabilize to the initial values. Therefore, the right switch is included to add the AGC's to the model after the system has reached steady state. The switch takes the signal from a clock as input, and switches from the constant value of zero to the ACE signal after a specified amount of time; 300 seconds in figure 4.2. The simulations in chapter 4 were all run after the system stabilized. The left switch is an important element of the model. It takes the value of the tie line power flow as input, and is only switched on if the tie line power transmission exceeds the reference value. The reference value in the figure is 2.145 p.u., which is the maximum capacity in the NO1-SE3 corridor. Thus, the AGC's only regulate when the frequency deviates from the initial value when the tie lines are not congested. When congestions occur, the AGC's also regulate for this. There is a low pass filter, $\frac{1}{1+5s}$, between the line flow and the switch; this makes sure that the switch does not consider the brief but large swings directly after a disturbance.

The proportional gain, $K_{i,agc}$, of the PI controller of the AGC is set equal to one, hence the controller is a pure integrator with integral time $T_{i,agc}$. The output from the AGC, ΔP_{ref}, is multiplied by the participation factors, α_i.

The three chosen control areas were NO2 by itself, NO5 by itself, and Sweden and Finland together. Since the connection between the south and north of Norway is fairly weak, the aFRR in NO3 and NO4 is disregarded in this model. The AGC's were tested in two different situations; first $ACE = \lambda_R \Delta f$, followed by $ACE = \lambda_R \Delta f + \Delta P_{tie}$. In the latter situation the ΔP_{tie} part of the ACE was only taken into account when a congestion occurred. Finally, the three AGC's control three different tie line connections; the NO1-SE3, NO2-NO1, and the NO5-NO1 corridors. In reality these corridors are named Hasle, Flesaker, and Hallingdal, respectively. It was possible that congestions could occur in these corridors when the modeled

system was exposed to disturbances. NO2 and NO5 provide cheap aFRR, making a high power transfer in the NO2-NO1 and NO5-NO1 corridors likely, while NO1-SE3 is an important connection for power transfer between Norway and Sweden. An increase in power transfer in corridor NO1-SE3 is not necessarily an indication of power production increase in either of these two areas, but rather a power increase in e.g. NO2 or NO5 being transferred from Norway to Sweden.

The participation factors in this model were not used exactly as in conventional AGC's. Before running each case described in chapter 5, the aFRR merit order lists were studied in order to find the cheapest bids and available aFRR in each area. Based on the load change, it was decided how much aFRR should be activated in each area. The planned activated aFRR per AGC was summed up, and the participation factors per area were calculated.

As an example a 700 MW load increase in e.g. NO1 would activate 290 MW in NO5, this being the cheapest aFRR, 70 MW in SE2 - the second cheapest aFRR, 295 MW in NO2, and 45 MW in SE1. The participation factor of the NO2 AGC would be set equal to 1.0; the same in NO5. In Sweden a total of 115 MW would be activated. Hence, the participation factor of SE1 would be set to 0.39, and 0.61 in SE2. Although the participation factors are set in accordance with the aFRR merit order lists, any congestions in the grid may cause the activation to exceed the listed values of available aFRR in some areas. That is why the aFRR bidding lists are only used as guidance to the planned activation in the model and not followed strictly.

Table 4.4 lists the values used for the $P_{tie,ref}$'s of each AGC. In reality the $P_{tie,ref}$ is likely changed on an hour to hour basis in accordance with the planned power flow in the system. To simplify, the $P_{tie,ref}$'s were in this model kept constant at the maximum transfer capacity.

Table 4.4: $P_{tie,ref}$'s of the AGC's.

Parameter	**Value [MW]**	**Value [p.u.]**
$P_{tie,ref}$, NO1-SE3	2145	2.145
$P_{tie,ref}$, NO2-NO1	3500	3.5
$P_{tie,ref}$, NO5-NO1	3900	3.9

4.2.4 MATLAB® Function Blocks

The MATLAB® Function blocks play important parts in the model. Figure 4.3 summarizes the inputs and outputs of the blocks, which are further described in the following paragraphs.

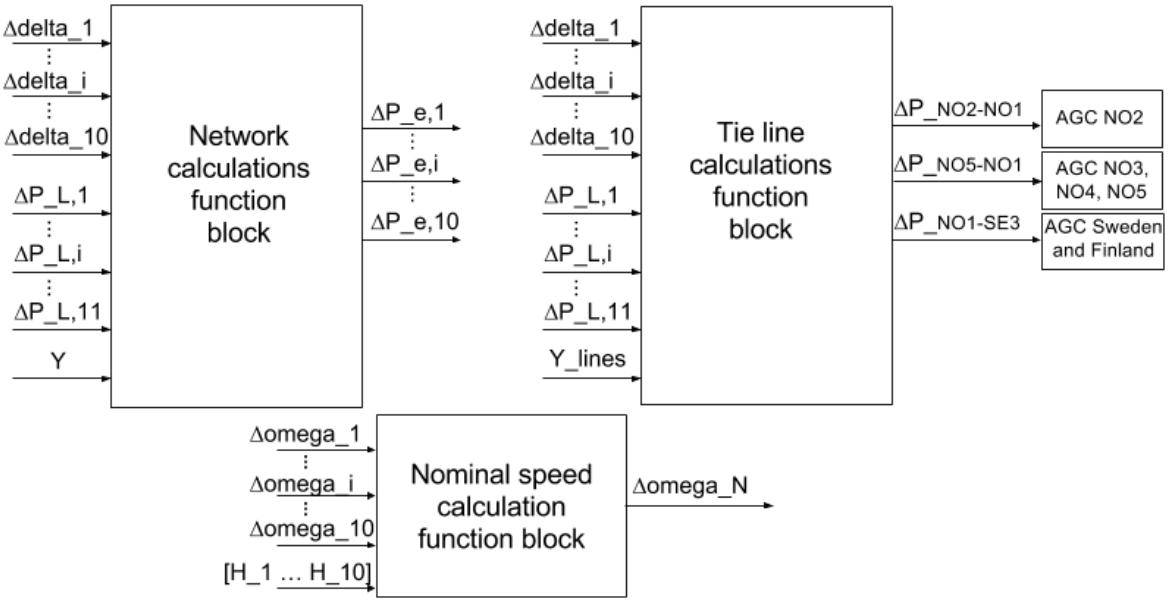

Figure 4.3: The MATLAB® Function blocks used in the model. The $\Delta delta$'s indicate the voltage angles of the generators; the ΔP_L's are the loads in the system; the $\Delta omega$'s indicate the speeds of the generators. Y is the admittance matrix, Y_{lines} is the line flow matrix of the system, and $[H_1 ... H_{10}]$ indicate the normalized inertia constants of the generators. $\Delta P_{NO2-NO1}$, $\Delta P_{NO5-NO1}$, and $\Delta P_{NO1-SE3}$ are the power transmissions in the specific corridors.

4.2.4.1 Network Calculations Function Block

The model uses a decoupled linear power flow calculation, where voltage angles and active powers are represented. The network calculations block as described in chapter 3 is an important part of the model. It takes the difference in voltage angles from the generators, the change in the loads, and the system admittance matrix as inputs. The inputs are used in the matrix calculations in the function block. The output from the block is the difference in electrical power, which is used as the input to the generators.

When defining the power and voltage angle submatrices as in equation 3.3 in chapter 3, the electrical power is in the network calculations function block calculated as follows for the modeled system:

$$\begin{bmatrix}\Delta\delta_{11}\\ \Delta\delta_{12}\\ \Delta\delta_{13}\\ \Delta\delta_{14}\\ \Delta\delta_{15}\\ \Delta\delta_{16}\\ \Delta\delta_{17}\\ \Delta\delta_{18}\\ \Delta\delta_{19}\\ \Delta\delta_{20}\\ \Delta\delta_{21}\end{bmatrix} = {Y_{22}}^{-1}\left(\begin{bmatrix}-\Delta P_{l,11}\\ -\Delta P_{l,12}\\ -\Delta P_{l,13}\\ -\Delta P_{l,14}\\ -\Delta P_{l,15}\\ -\Delta P_{l,16}\\ -\Delta P_{l,17}\\ -\Delta P_{l,18}\\ -\Delta P_{l,19}\\ -\Delta P_{l,20}\\ -\Delta P_{l,21}\end{bmatrix} - Y_{21}\begin{bmatrix}\Delta\delta_{1}\\ \Delta\delta_{2}\\ \Delta\delta_{3}\\ \Delta\delta_{4}\\ \Delta\delta_{5}\\ \Delta\delta_{6}\\ \Delta\delta_{7}\\ \Delta\delta_{8}\\ \Delta\delta_{9}\\ \Delta\delta_{10}\end{bmatrix}\right) \tag{4.1}$$

$$\begin{bmatrix}\Delta P_{e,1}\\ \Delta P_{e,2}\\ \Delta P_{e,3}\\ \Delta P_{e,4}\\ \Delta P_{e,5}\\ \Delta P_{e,6}\\ \Delta P_{e,7}\\ \Delta P_{e,8}\\ \Delta P_{e,9}\\ \Delta P_{e,10}\end{bmatrix} = Y_{11}\begin{bmatrix}\Delta\delta_{1}\\ \Delta\delta_{2}\\ \Delta\delta_{3}\\ \Delta\delta_{4}\\ \Delta\delta_{5}\\ \Delta\delta_{6}\\ \Delta\delta_{7}\\ \Delta\delta_{8}\\ \Delta\delta_{9}\\ \Delta\delta_{10}\end{bmatrix} + Y_{12}\begin{bmatrix}\Delta\delta_{11}\\ \Delta\delta_{12}\\ \Delta\delta_{13}\\ \Delta\delta_{14}\\ \Delta\delta_{15}\\ \Delta\delta_{16}\\ \Delta\delta_{17}\\ \Delta\delta_{18}\\ \Delta\delta_{19}\\ \Delta\delta_{20}\\ \Delta\delta_{21}\end{bmatrix} \tag{4.2}$$

The electrical power, the $\Delta P_{e,i}$'s, are fed back to the generators. The detailed admittance matrix for the modeled system can be found in appendix C.

4.2.4.2 Nominal Speed Calculation Function Block

The nominal speed calculation block takes the speeds, ω_i, and the normalized inertia constants, H_i, of all ten generators as inputs and gives ω_N as output. Since the generators in the various areas have unequal parameter settings, the ω_N is calculated as in equation 4.3.

$$\omega_N = \frac{\sum_{i=1}^{n} H_i\omega_i}{\sum_{i=1}^{n} H_i} \tag{4.3}$$

4.2.4.3 Tie Line Calculations Function Block

The final function block in the model, the block for tie line calculations, calculates the flow in the power lines of the system, as shown in equation 4.4:

$$\begin{bmatrix} \Delta P_{11-13} \\ \Delta P_{11-14} \\ \Delta P_{11-15} \\ \Delta P_{12-11} \\ \Delta P_{12-13} \\ \Delta P_{12-15} \\ \Delta P_{13-14} \\ \Delta P_{13-18} \\ \Delta P_{16-17} \\ \Delta P_{17-14} \\ \Delta P_{17-18} \\ \Delta P_{18-15} \\ \Delta P_{18-20} \\ \Delta P_{19-16} \\ \Delta P_{19-17} \\ \Delta P_{21-20} \end{bmatrix} = Y_{lines} \begin{bmatrix} \Delta\delta_{11} \\ \Delta\delta_{12} \\ \Delta\delta_{13} \\ \Delta\delta_{14} \\ \Delta\delta_{15} \\ \Delta\delta_{16} \\ \Delta\delta_{17} \\ \Delta\delta_{18} \\ \Delta\delta_{19} \\ \Delta\delta_{20} \\ \Delta\delta_{21} \end{bmatrix} \tag{4.4}$$

The flow in lines NO1-SE3, NO2-NO1, and NO5-NO1 are sent to the AGC's as input to the ΔP_{tie} part of the ACE's. The detailed line flow matrix of the modeled system, Y_{lines}, can be found in appendix D.

Chapter 5

Results and Discussion

This chapter presents a variety of cases where the system in figure 4.1 in chapter 4 is exposed to different disturbances. Most of the cases are transient disturbances in the form of load step ups and step downs, while case 2 is a ramped load increase; more similar to a real hour shift. The cases presented were chosen because they are relevant situations in the Nordic power system. The parameter values for the model that were kept constant are listed in appendix A.2. All the disturbances happened after 50 seconds.

The cases were modeled in three different situations. Situation 1 had no AGC's included. Situation 2 was with AGC's, where ACE $= \lambda_R \Delta f$. Finally, situation 3 was with AGC's included, where ACE $= \lambda_R \Delta f$ for no congestions and ACE $= \lambda_R \Delta f + \Delta P_{tie}$ when any of the tie lines were congested. The reference values of the tie line powers of the AGC's, the $P_{tie,ref}$'s, were kept constant at the values listed in table 4.4 in chapter 4 throughout each case.

The participation factors of each case were calculated based on the aFRR merit order lists described in section 4.1.3. The aFRR available in each area and the participation factors of the AGC's are listed in tables for each case. As explained in section 4.2.3 the merit order lists were only used as guidance to the calculation of the participation factors, and the aFRR activated per area may in some cases exceed the listed available power.

5.1 Initial Power Flow

Initially, the system frequency was at 50.00 Hz, indicating a balanced power flow. The initial transmission in the transmission lines and corridors can be seen in figure 5.1.

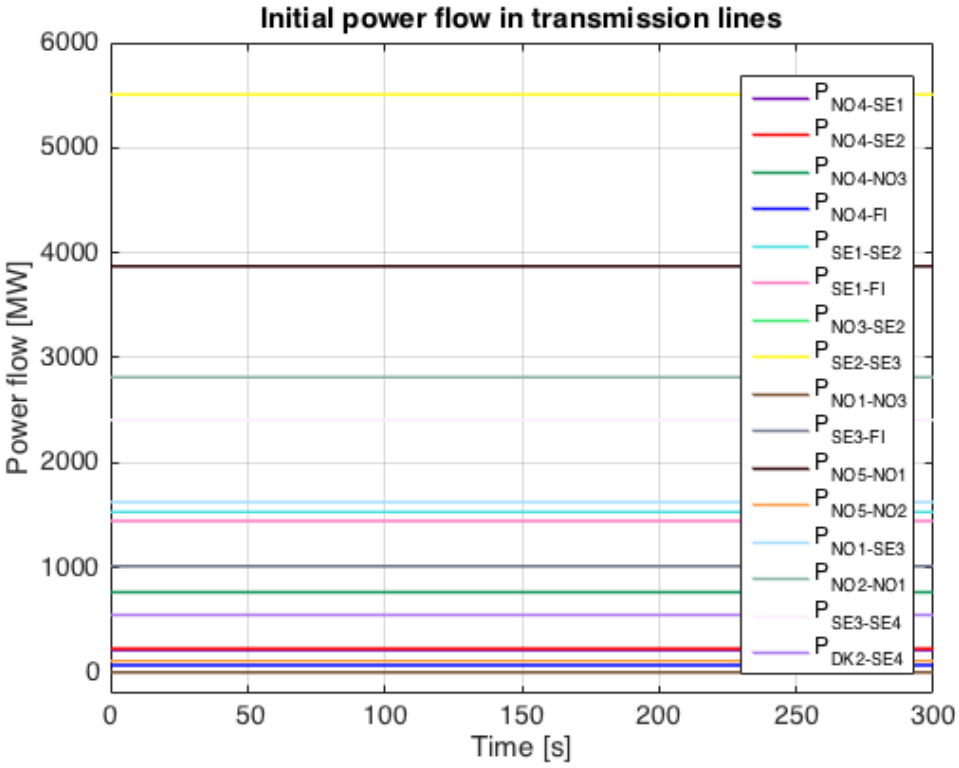

Figure 5.1: Initial power flow in the transmission corridors and lines of the system.

The following sections present the different cases that the system was exposed to. In many of the transmission lines and corridors, only small power flow changes occurred. Hence, only the lines and corridors with interesting flow changes are presented.

5.2 Case 1: Load Increase in NO1

Case 1 is a transient disturbance in the form of a load increase of 700 MW in area NO1. The aFRR that were supposed to be activated per area and the participation factors of the AGC's in this case are listed in table 5.1.

Table 5.1: aFRR activation per area and participation factors of the AGC's, case 1.

Area	**aFRR per area [MW]**	**Participation factor**	**Participation factor value [-]**
NO2	295	α_{NO2}	1.0
NO5	290	α_{NO5}	1.0
SE1	45	α_{SE1}	0.39
SE2	70	α_{SE2}	0.61

Figure 5.2 shows the system's frequency response to the disturbance. The model's immediate response to the disturbance was a drastic drop in the frequency. This is due to the load increase being modeled as an instant step up. A similar response can be seen in all cases except for in case 2, where the load was ramped up. The line power flows, the power generation, and the ACE's responded with the same spiked curves immediately after the disturbance happened, before stabilizing at new values.

After the immediate response, the frequency in case 1 was rapidly lifted by the primary frequency control. Without AGC's the system frequency stabilized at 0.07298 Hz below the initial value, giving a system frequency response of 9592 MW/Hz. With AGC's the frequency was fully restored to 50.00 Hz after a few hundred seconds. The frequency was restored faster in situation 2, while it took longer in situation 3 due to congestion.

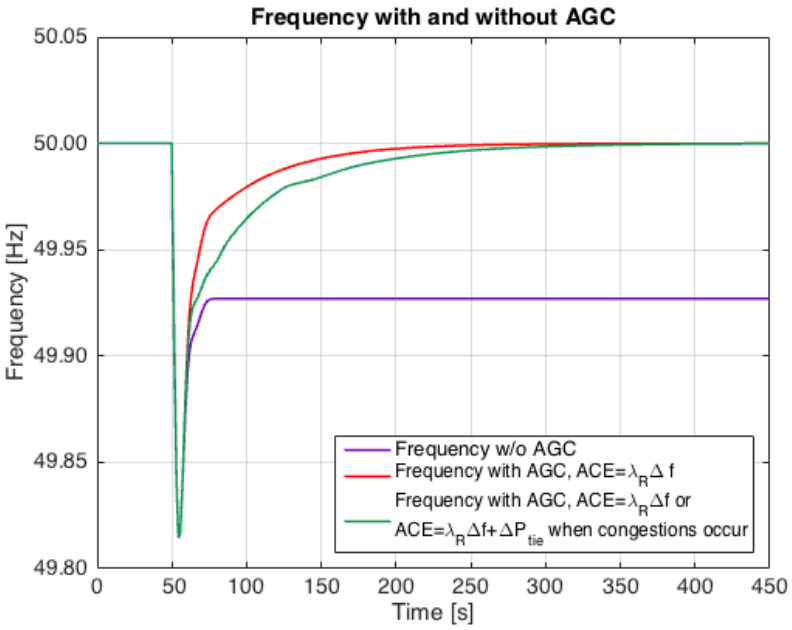

Figure 5.2: Frequency of the system in case 1. The load increase happened after 50 seconds.

The reason for the different regulation of the frequency is found in figure 5.3. In situations 1 and 2, the power transfer in the NO5-NO1 corridor exceeded the transfer capacity limit of 3900 MW. In situation 3 the power transfer was reduced to and stabilized at 3900 MW. Hence, the flow from NO2 to NO1, shown in figure 5.4, increased in order to supply the power that was removed from the NO5-NO1 corridor. In addition, the flow in corridor NO1-SE3, see figure 5.5, was reduced as a consequence of the power increase in NO1. In all corridors the power transfer was greater when AGC's were included because the aFRR activated in order to restore the frequency at 50.00 Hz.

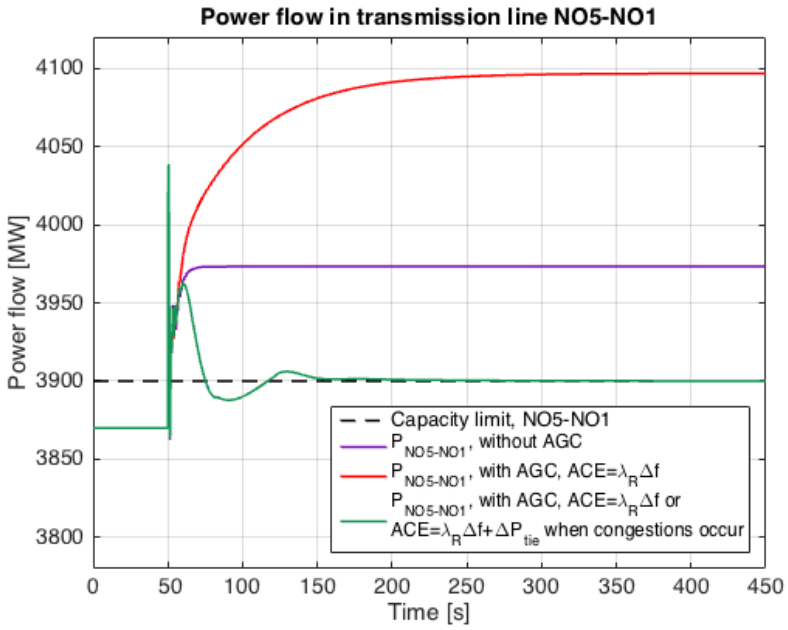

Figure 5.3: Power flow in the NO5-NO1 corridor in case 1. The load increase happened after 50 seconds.

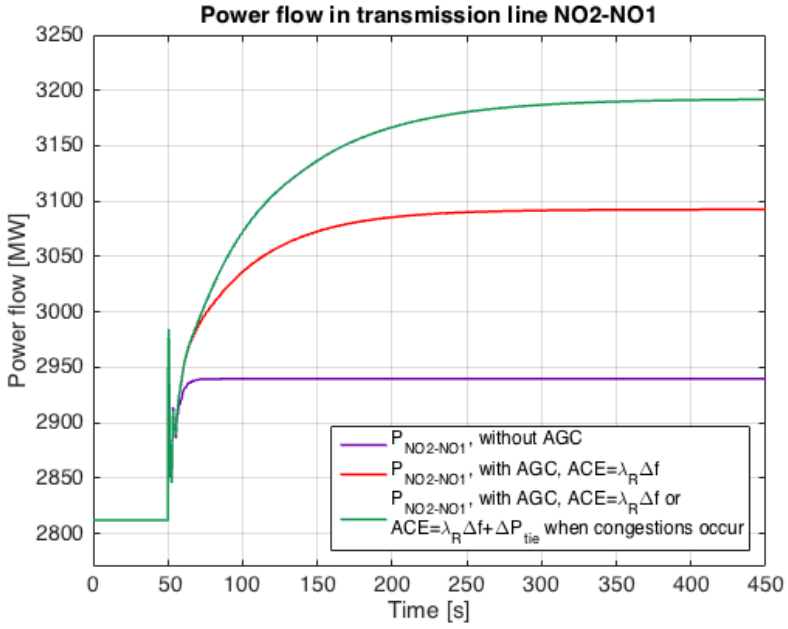

Figure 5.4: Power flow in the NO2-NO1 corridor in case 1. The load increase happened after 50 seconds.

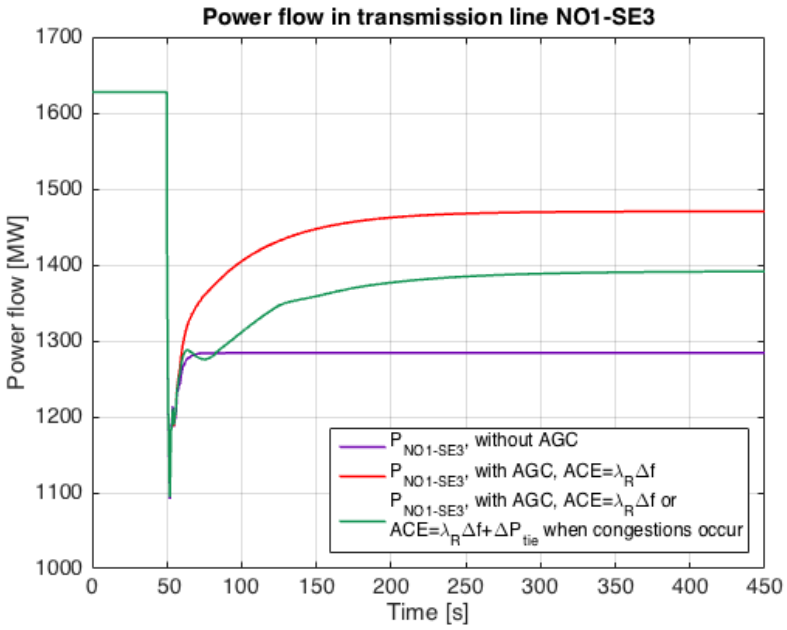

Figure 5.5: Power flow in the NO1-SE3 corridor in case 1. The load increase happened after 50 seconds.

Figure 5.6 shows the change in power production in the areas where aFRR were activated in situation 3. NO5 had the cheapest aFRR but due to the congestion in the NO5-NO1 corridor no aFRR were activated here. In SE2 approximately 200 MW were activated, in SE1 approximately 100 MW, while the production was reduced by a few MW in NO5. The third cheapest bid was in NO2, where approximately 430 MW were activated. In total, the load increase of 700 MW was compensated for.

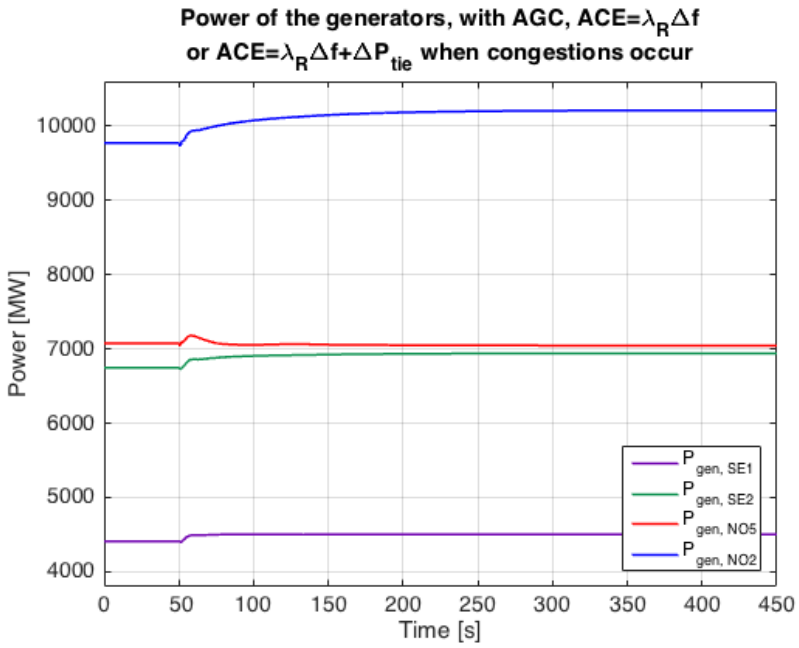

Figure 5.6: Power production of the generators in the areas where aFRR were activated in case 1. The load increase happened after 50 seconds.

Figure 5.7 shows an overview of how the flow in the power system changed in situation 3, case 1. The aFRR activation in NO5 increased until the capacity limit in the NO5-NO1 corridor was reached. The activation of aFRR in NO2 increased and so did the transfer between NO2 and NO1, while the transmission in the NO1-SE3 corridor decreased as a consequence of the load increase in NO1.

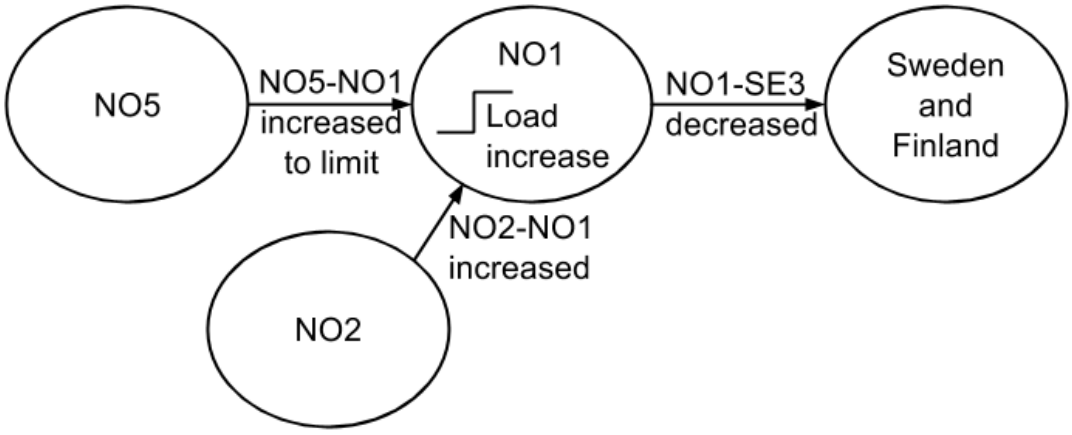

Figure 5.7: Overview of the power flow in situation 3, case 1.

The results are reflected in the ACE's of the AGC's, seen in figures 5.8 and 5.9.

The ACE in NO2 and Sweden were the same as there were no congestions in the tie lines controlled by these AGC's. The ACE increased when the disturbance occurred, but was restored to zero at the same time that the frequency went back to 50.00 Hz. The ACE in NO5 increased as the disturbance occurred, but rapidly decreased when the NO5-NO1 corridor was congested. Additionally, there were a few smaller swings as the power flow in the corridor NO5-NO1 stabilized at 3900 MW.

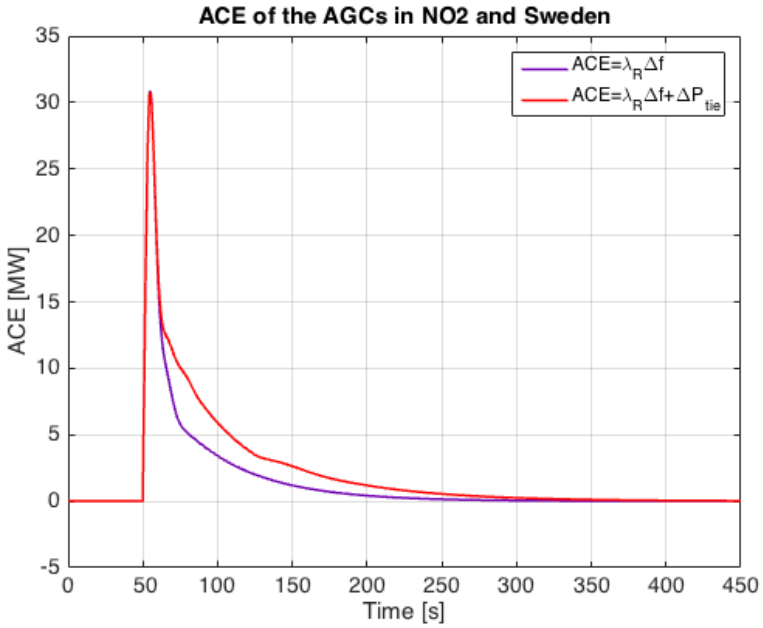

Figure 5.8: ACE of the AGC's in NO2 and Sweden in case 1. The load increase happened after 50 seconds.

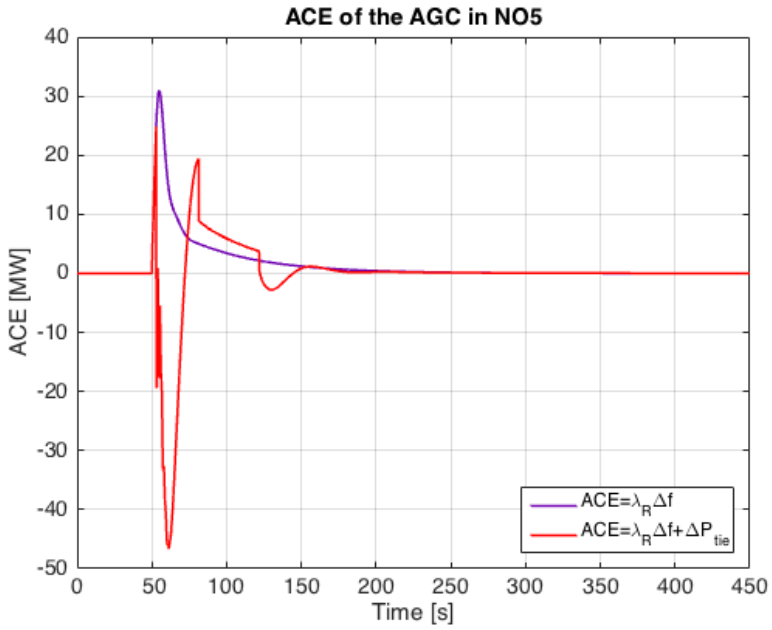

Figure 5.9: ACE of the AGC in NO5 in case 1. The load increase happened after 50 seconds.

5.3 Case 2: Ramped Load Increase in NO1

Case 2 is a ramped load increase in NO1 of 700 MW. The blocks used in the model for ramping the load is shown in appendix A.1. The load was ramped up after 50 seconds, then down to the initial value after 750 seconds, and finally up yet again after 1050 seconds. The purpose of this case is to illustrate the imbalance that occurs during a real hour shift. In reality a load increase happens gradually during an hour, while the power generation is mostly only increased when there is an hour shift. When the hour shift occurs more power supply is added from the suppliers, such that the sign of the imbalance changes, before increasing yet again. Figure 5.10 shows how the load increase happened.

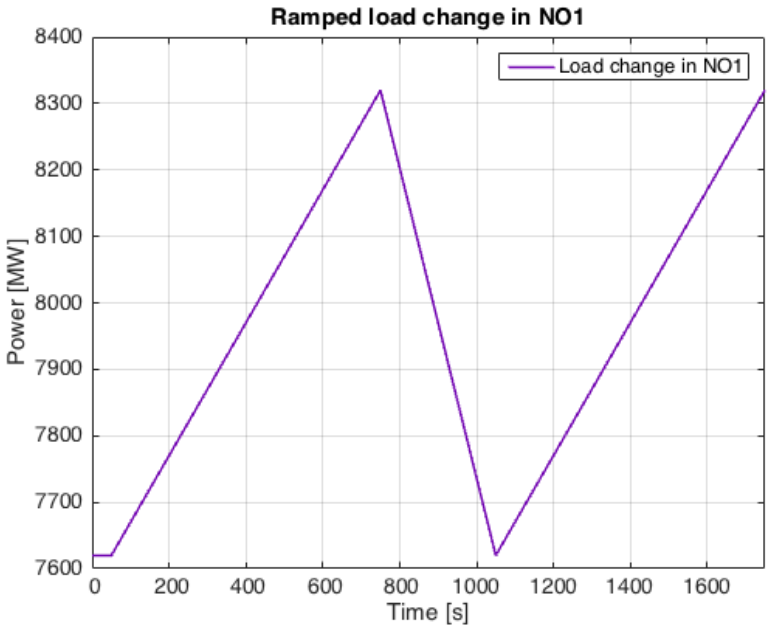

Figure 5.10: Ramped load change in case 2. The load ramping happened after 50, 750, and 1050 seconds.

The aFRR that were supposed to be activated per area and participation factors of the AGC's were the same in this case as in case 1, and are listed in table 5.2.

Table 5.2: aFRR activation per area and participation factors of the AGC's, case 2.

Area	**aFRR per area [MW]**	**Participation factor**	**Participation factor value [-]**
NO2	295	α_{NO2}	1.0
NO5	290	α_{NO5}	1.0
SE1	45	α_{SE1}	0.39
SE2	70	α_{SE2}	0.61

The frequency deviation in this case can be seen in figure 5.11. In situation 1 the frequency deviation was sawtooth shaped, and the frequency was 0.07298 Hz below the initial value when the load had increased by 700 MW. Hence, the system frequency response was the same as in case 1; 9592 MW/Hz. In situations 2 and 3 there was a stationary deviation while the first load ramp up took place. Due to a congestion in the NO5-NO1 corridor, there was a slight difference in the frequency for situations 2 and 3. When the load was ramped down to the initial value, the frequency rose above the reference value of 50.00 Hz because of the response of the

primary frequency control. However, the secondary frequency control stabilized the frequency after a few hundred seconds. When the load was ramped up the second time the primary frequency control regulated the frequency below the initial value, before the secondary frequency control stabilized the frequency.

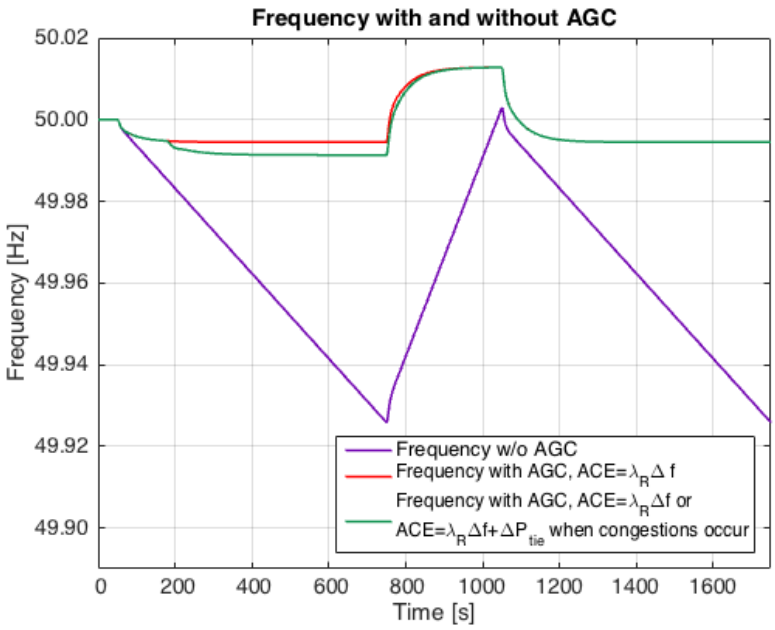

Figure 5.11: Frequency of the system in case 2. The load ramping happened after 50, 750, and 1050 seconds.

As seen in figure 5.12 the power flow increased in the NO5-NO1 corridor as the load was ramped up both with and without AGC's. There was a congestion in this corridor, which was handled by the AGC in NO5 in situation 3. Figures 5.13 and 5.14 display the power transmission in corridors NO2-NO1 and NO1-SE3, respectively. Neither of these experienced congestions. The transmission increase in NO2-NO1 was greater when the NO5-NO1 congestion was handled; the power production in NO2 was amplified due to the reduction in NO5. For the same reason there was not the same amount of power transmission from Norway to Sweden through the NO1-SE3 corridor, and as a result the transmission here was reduced more in situation 3. In accordance with the primary and secondary frequency controls, the power flow in all three corridors was decreased when the load was ramped down, before rising when the load ramped up again.

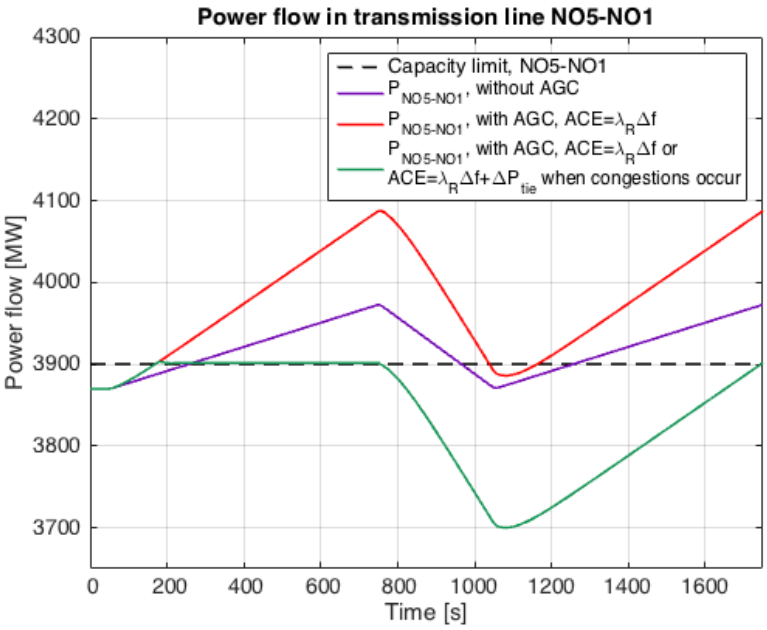

Figure 5.12: Power flow in the NO5-NO1 corridor in case 2. The load ramping happened after 50, 750, and 1050 seconds.

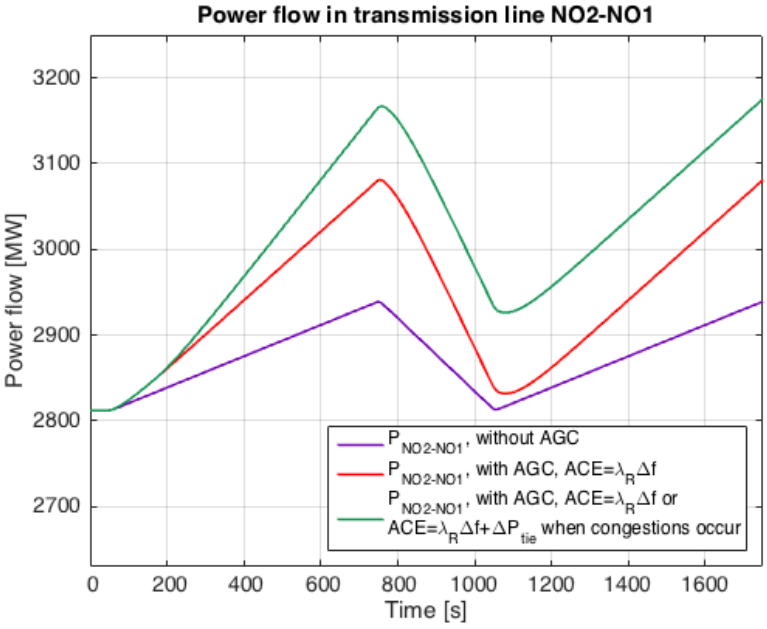

Figure 5.13: Power flow in the NO2-NO1 corridor in case 2. The load ramping happened after 50, 750, and 1050 seconds.

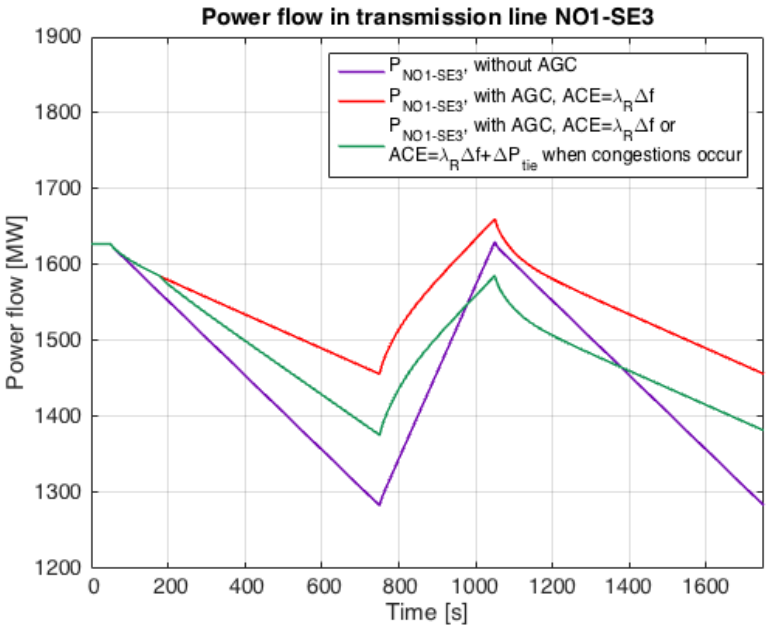

Figure 5.14: Power flow in the NO1-SE3 corridor in case 2. The load ramping happened after 50, 750, and 1050 seconds.

The aFRR activation in situation 3 was similar to case 1; the same amount of aFRR was activated in the same areas, resulting in a full compensation for the final 700 MW load increase. The power production followed the load ramping. Figure 5.15 shows the results.

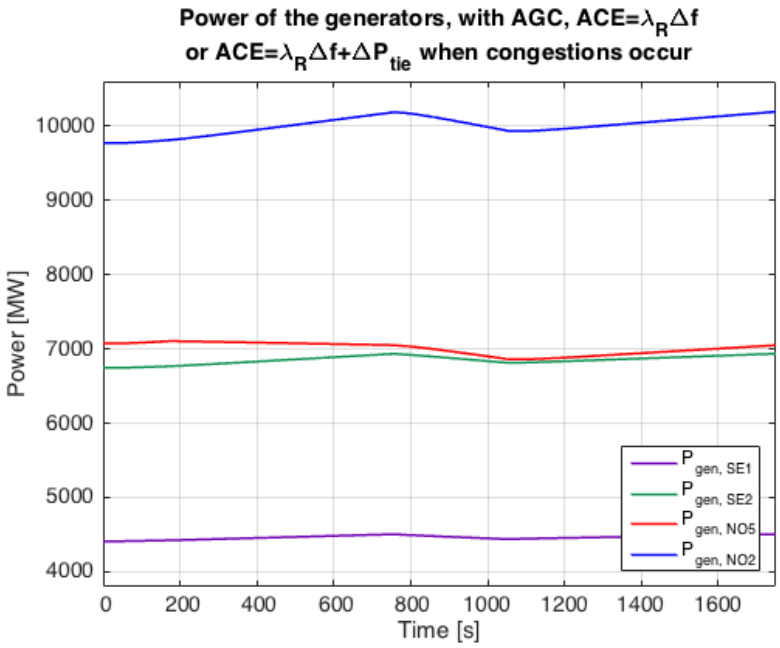

Figure 5.15: Power production of the generators in the areas where aFRR were activated in case 2. The load ramping happened after 50, 750, and 1050 seconds.

Figure 5.16 shows an overview of how the flow in the power system changed in situation 3, case 2. The flow was similar to case 1 overall, with the exception of changing flow instead of the more instant flow in case 1. The aFRR activation in NO5 increased until the capacity limit in the NO5-NO1 corridor was reached. The activation of aFRR in NO2 increased and so did the transfer between NO2 and NO1, while the transmission in the NO1-SE3 corridor decreased as a consequence of the load increase in NO1.

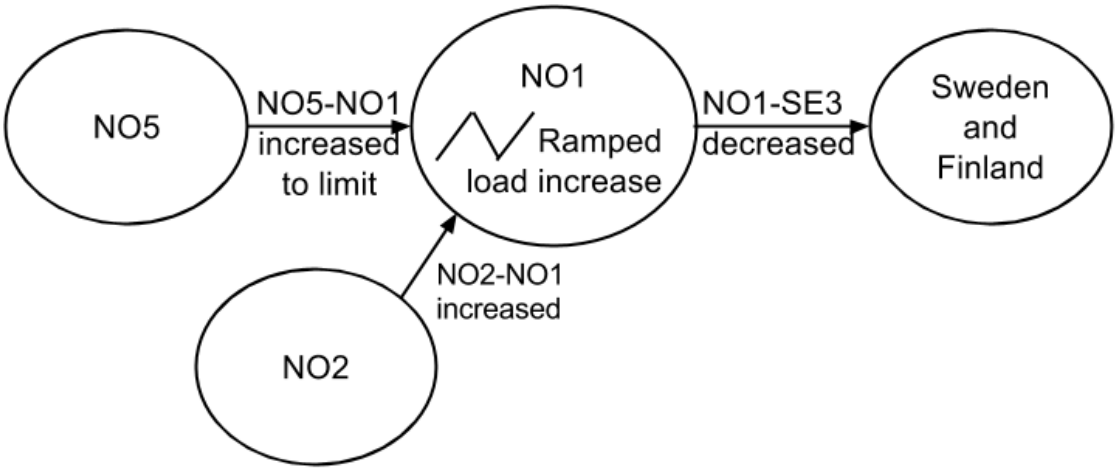

Figure 5.16: Overview of the power flow in situation 3, case 2.

The results are reflected in the ACE's, seen in figures 5.17 and 5.18. For NO2 and Sweden the ACE increased when the load ramping started. In situation 3 the ACE increased further when the congestion in corridor NO5-NO1 occurred, just like the frequency decreased further. The ACE of the NO5 AGC was stationary during the first load ramping in situation 2, but decreased in situation 3. When the load was ramped down to the initial value after 750 seconds all ACE's dropped and were stabilized simultaneously with the frequency. When the load was ramped up again the ACE's increased and were stabilized together with the frequency.

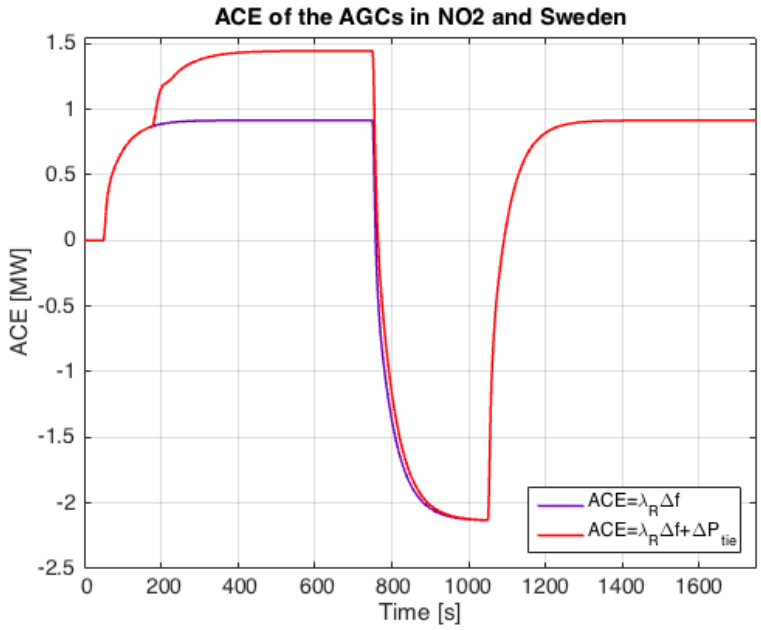

Figure 5.17: ACE of the AGC's in NO2 and Sweden in case 2. The load ramping happened after 50, 750, and 1050 seconds.

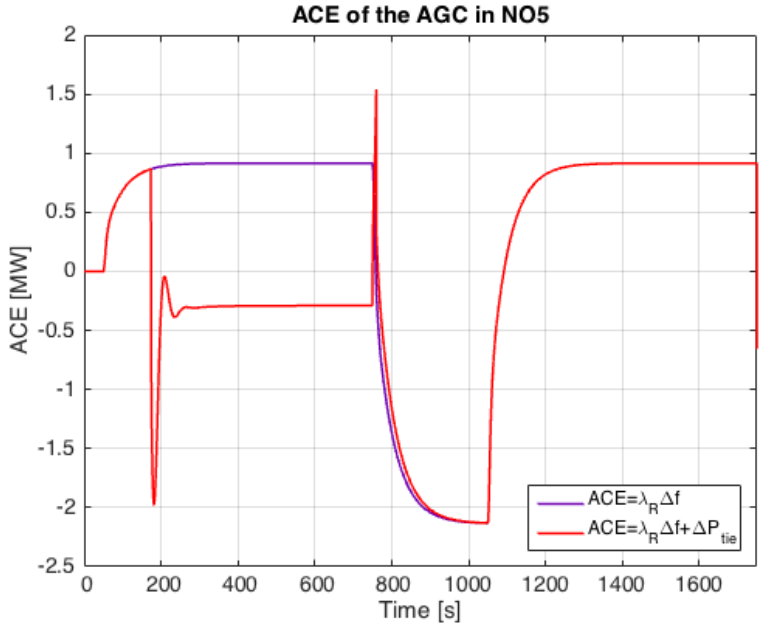

Figure 5.18: ACE of the AGC in NO5 in case 2. The load ramping happened after 50, 750, and 1050 seconds.

5.4 Case 3: Load Increase in NO5

In case 3, where the load in NO5 was stepped up 600 MW, no line congestions occurred. Hence, situations 2 and 3 were identical. The aFRR that were supposed to be activated per area and the participation factors of the AGC's in this case are listed in table 5.3.

Table 5.3: aFRR activation per area and participation factors of the AGC's, case 3.

Area	aFRR per area [MW]	Participation factor	Participation factor value [-]
NO2	240	α_{NO2}	1.0
NO5	290	α_{NO5}	1.0
SE2	70	α_{SE2}	1.0

The frequency, illustrated in figure 5.19, dropped rapidly when the disturbance happened, but was increased by the primary frequency control within the first few seconds. Without AGC's the frequency stabilized 0.06255 Hz below the initial value, implying a system frequency response of 9592 MW/Hz. With AGC's the frequency was restored to 50.00 Hz after a few hundred seconds.

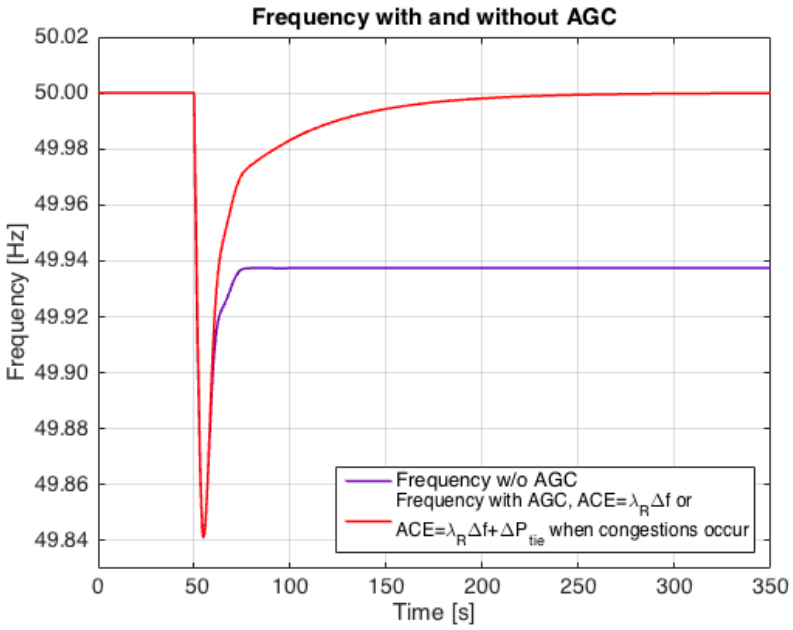

Figure 5.19: Frequency of the system in case 3. The load increase happened after 50 seconds.

Figures 5.20, 5.21, and 5.22 show how the power transmission of the system slightly turned when there was a load step up in NO5. The power export from NO5 decreased, as did the transmission from Norway to Sweden in the NO1-SE3 corridor. The power transmission from NO2 to NO1 increased in order to compensate for less power from NO5 to NO1. The power transmission was greater in all corridors in situations 2 and 3 compared to situation 1 because aFRR were activated in order to restore the frequency.

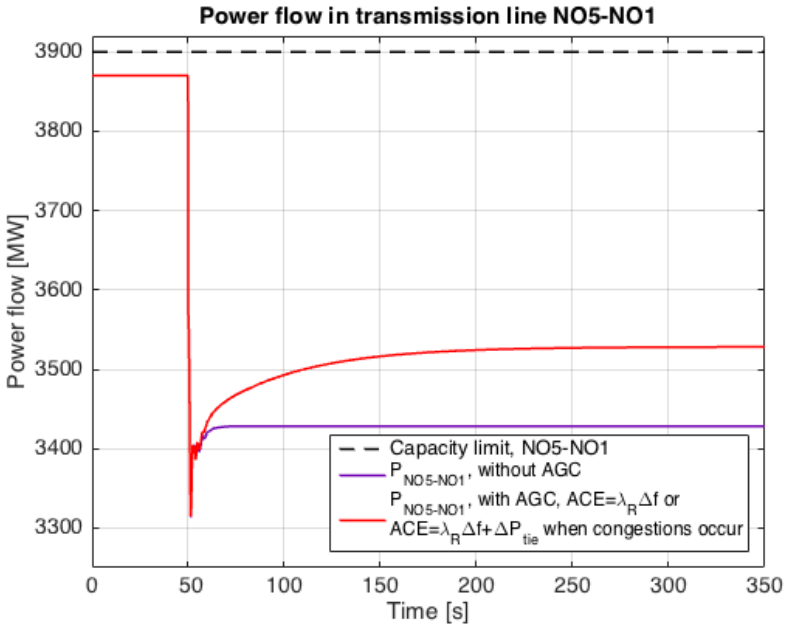

Figure 5.20: Power flow in the NO5-NO1 corridor in case 3. The load increase happened after 50 seconds.

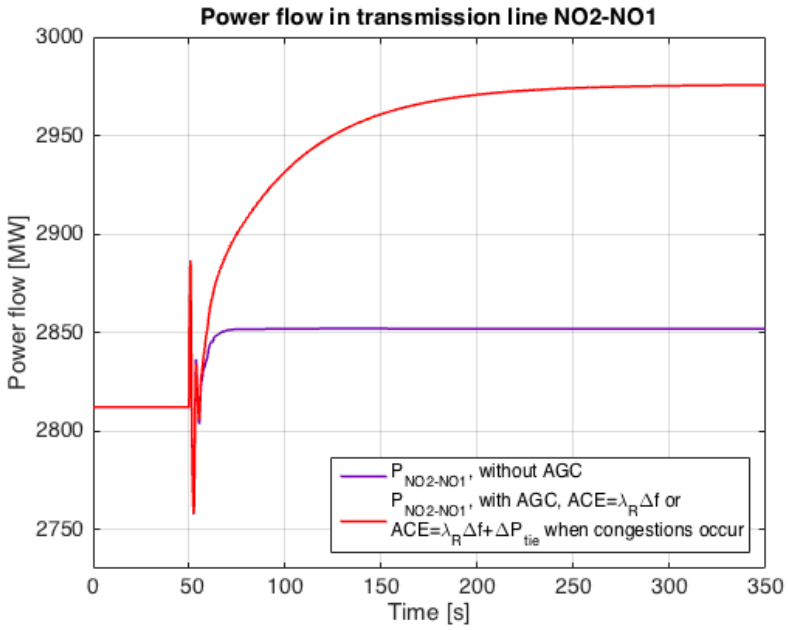

Figure 5.21: Power flow in the NO2-NO1 corridor in case 3. The load increase happened after 50 seconds.

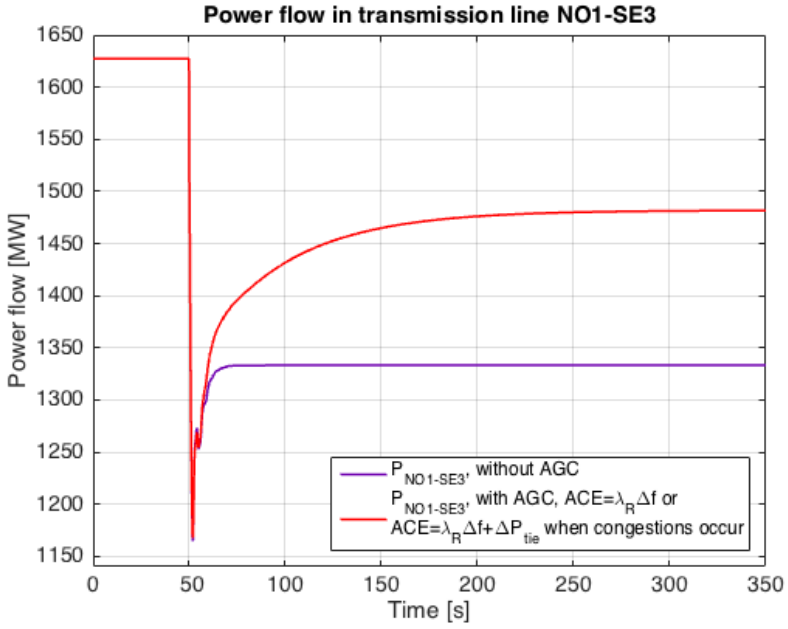

Figure 5.22: Power flow in the NO1-SE3 corridor in case 3. The load increase happened after 50 seconds.

The power production in the areas where aFRR were activated in situation 3 is shown in figure 5.23. NO5 had the cheapest aFRR and as there was no congestion, about 180 MW were activated in this area. In NO2 approximately 250 MW of aFRR were activated and in SE2 about 170 MW, making the total aFRR activated equal to the load step up.

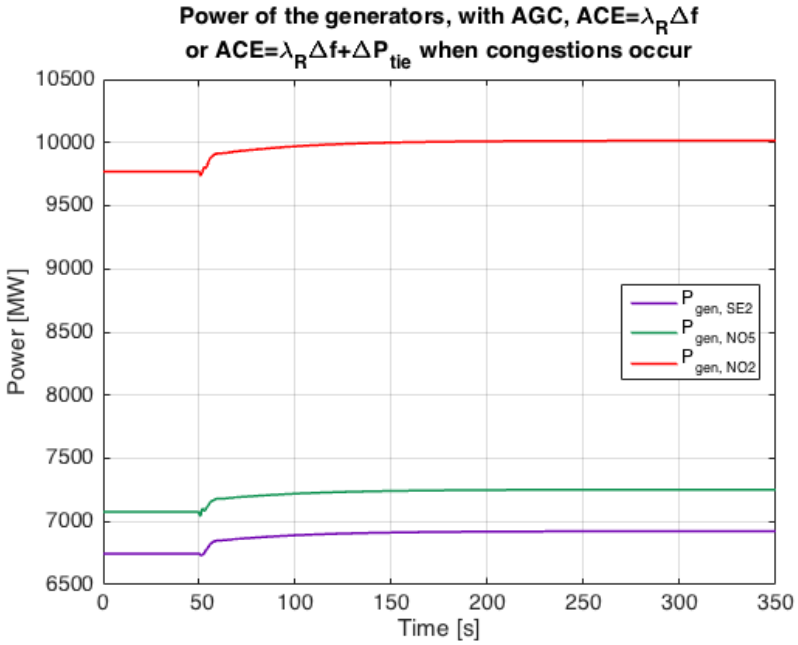

Figure 5.23: Power production of the generators in the areas where aFRR were activated in case 3. The load increase happened after 50 seconds.

Figure 5.24 shows an overview of how the power flow changed in situation 3, case 3. The power flow from NO5 to NO1 decreased as there was a load increase in NO5. This caused the power flow from NO2 to NO1 to increase in order to compensate for the lost power from NO5. The power transmission in the corridor NO1-SE3 also decreased due to less power being transferred from Norway to Sweden.

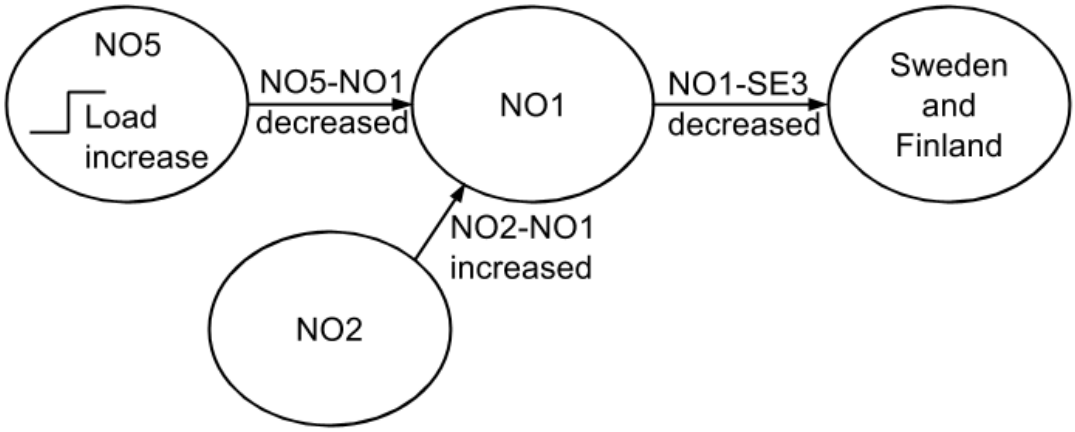

Figure 5.24: Overview of the power flow in situation 3, case 3.

As mentioned there were no congestions in this case, meaning that the ACE $= \lambda_R \Delta f$ in both situations 2 and 3. All the AGC's experienced the same ACE, shown in figure 5.25. When the load step up occurred the ACE, like the frequency, increased drastically, after which the AGC's worked to restore the ACE to zero.

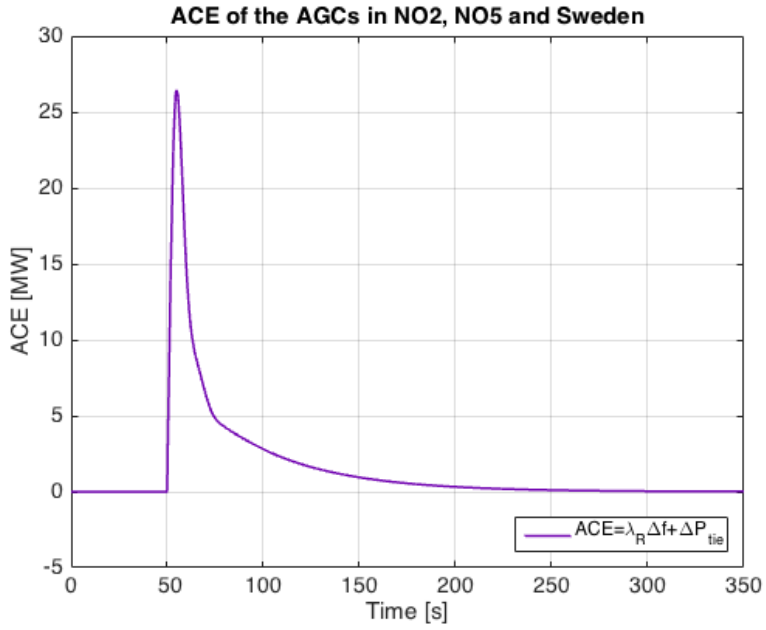

Figure 5.25: ACE of the AGC's in NO2, NO5, and Sweden in case 3. The load increase happened after 50 seconds.

5.5 Case 4: Load Increase in SE4

A load step up of 1000 MW in SE4 happened in case 4. The aFRR that were supposed to be activated per area and the participation factors of the AGC's in this case are listed in table 5.4.

Table 5.4: aFRR activation per area and participation factors of the AGC's, case 4.

Area	**aFRR per area [MW]**	**Participation factor**	**Participation factor value [-]**
NO2	295	α_{NO2}	1.0
NO5	290	α_{NO5}	1.0
SE1	160	α_{SE1}	0.39
SE2	70	α_{SE2}	0.17
SE3	75	α_{SE1}	0.18
FI	110	α_{SE2}	0.27

When the load was stepped up the frequency dropped drastically but was increased by the primary frequency control after a few seconds. Without AGC's the frequency dropped approximately 0.10425 Hz, exceeding the limit of 50.00 ± 0.1 Hz that is reckoned as frequency deviation in the Nordic power system [23]. The system frequency response was 9592 MW/Hz in this case too. With AGC's included, the frequency was restored to 50.00 Hz faster in situation 2 compared to in situation 3. After a few hundred seconds the frequency was back at the initial value.

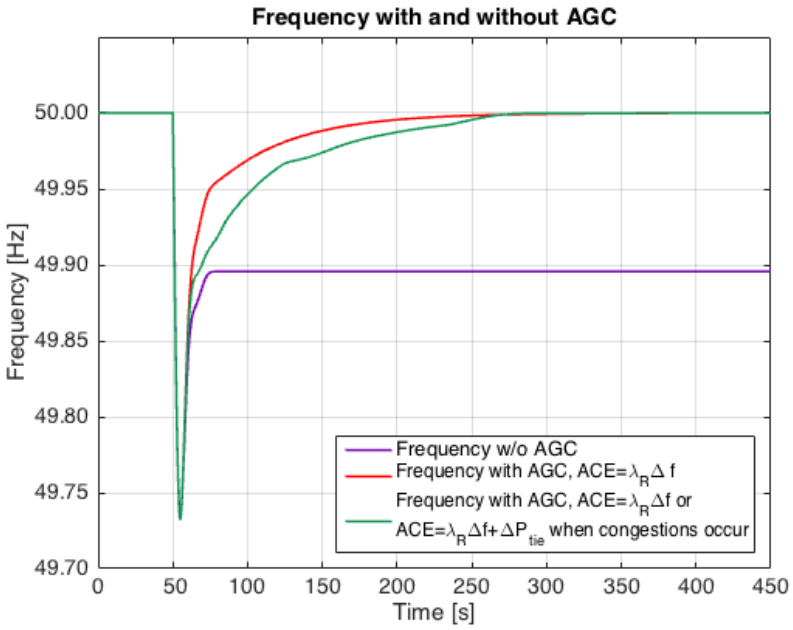

Figure 5.26: Frequency of the system in case 4. The load increase happened after 50 seconds.

The power transmission in corridors NO1-NO5, see figure 5.27, NO2-NO1, shown in figure 5.28, and NO1-SE3, see figure 5.29, increased both with and without AGC's in the system, giving congestions in the NO5-NO1 and NO1-SE3 corridors. In situation 3 the power transmission in NO5-NO1 was by the AGC in NO5 decreased to the reference value of 3900 MW. Hence, the flow in NO2-NO1 increased in order to compensate for the power reduction from NO5 to NO1. The power transmission in corridor NO1-SE3 increased as the power from NO2 increased. After approximately 240 seconds the transmission in the NO1-SE3 corridor exceeded the reference value of 2145 MW, and was then stabilized at this value by the AGC in Sweden.

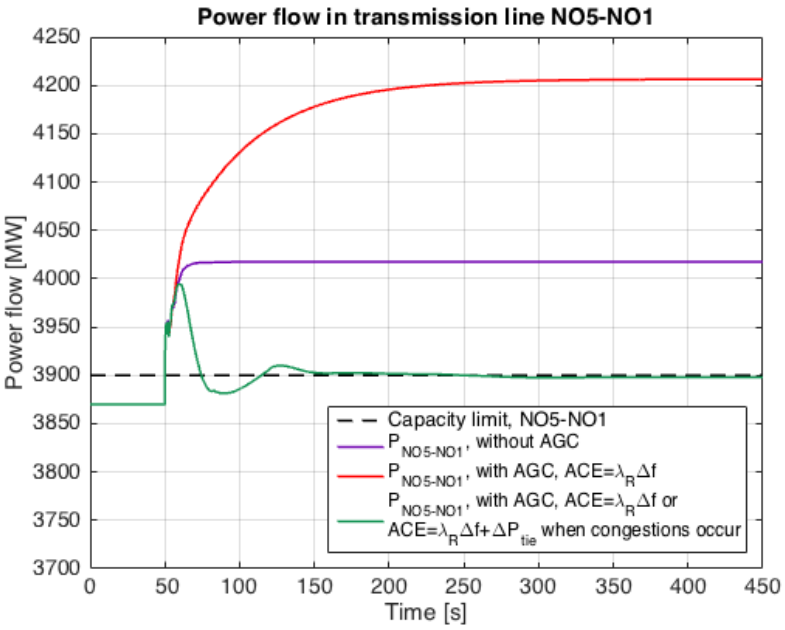

Figure 5.27: Power flow in the NO5-NO1 corridor in case 4. The load increase happened after 50 seconds.

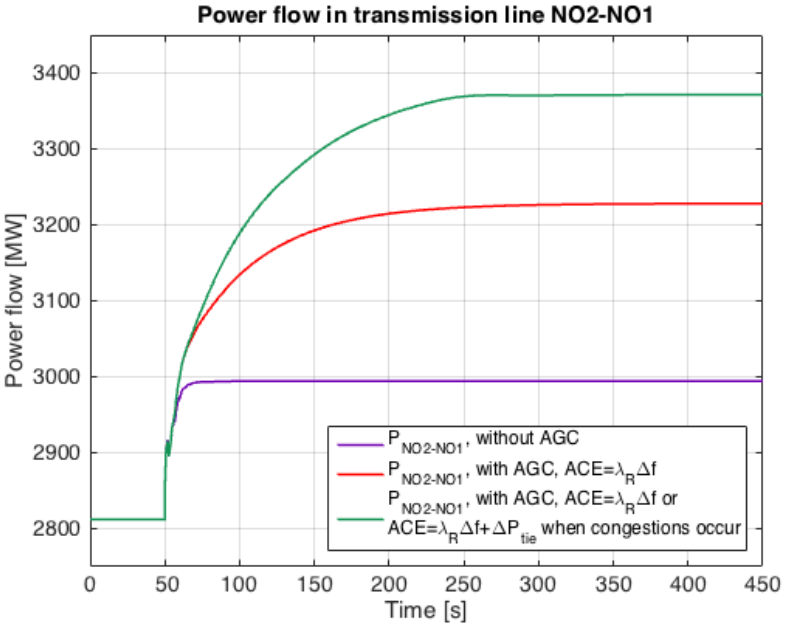

Figure 5.28: Power flow in the NO2-NO1 corridor in case 4. The load increase happened after 50 seconds.

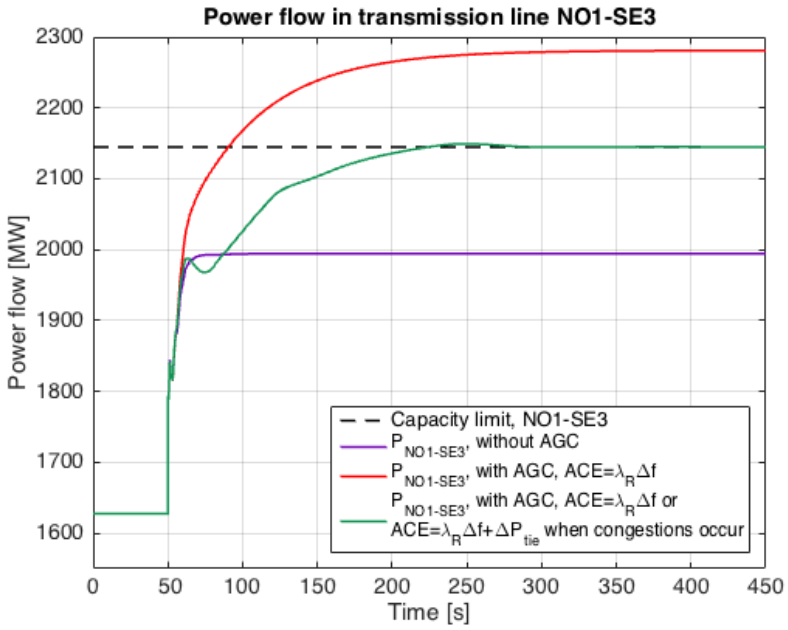

Figure 5.29: Power flow in the NO1-SE3 corridor in case 4. The load increase happened after 50 seconds.

The transmission in SE2-SE3, shown in figure 5.30, increased immediately after the load step up, but the transmission was slightly reduced in situations 2 and 3 compared to situation 1 due to the increased flow from Norway to Sweden in the NO1-SE3 corridor.

Figure 5.31 shows the power flow in the SE3-SE4 corridor. Without AGC's, the power production in SE4 slightly increased, giving a small contribution to the compensation for the power imbalance in the area. As there was no available aFRR in SE4 the total 1000 MW went through the transmission corridor SE3-SE4 in situation 2 and 3.

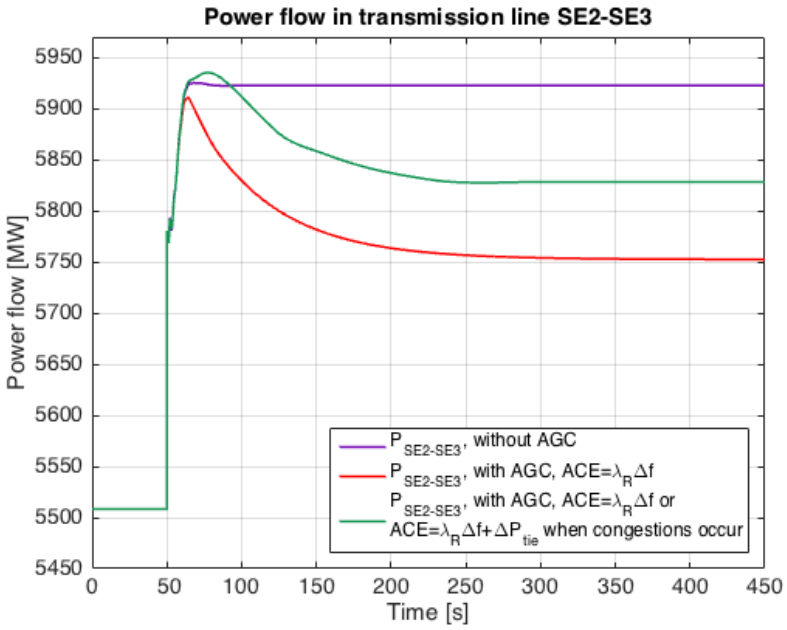

Figure 5.30: Power flow in the SE2-SE3 corridor in case 4. The load increase happened after 50 seconds.

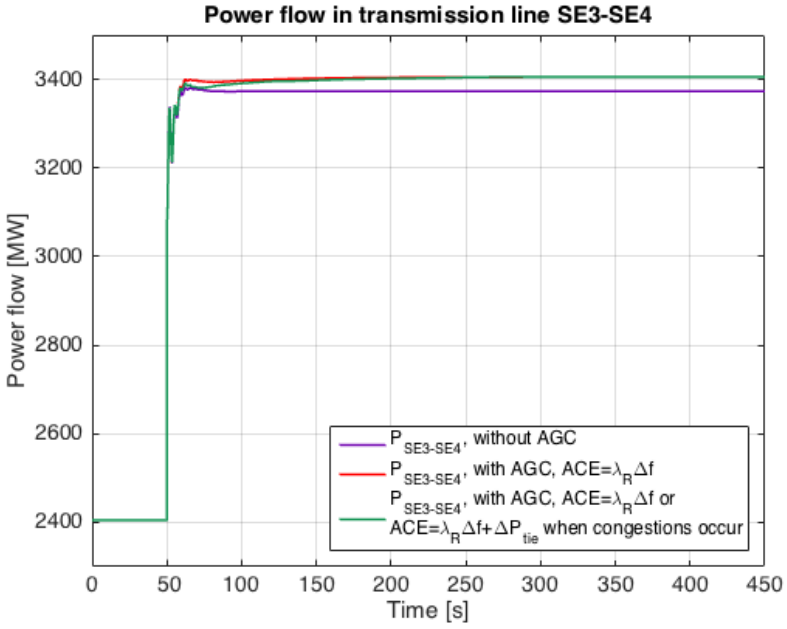

Figure 5.31: Power flow in the SE3-SE4 corridor in case 4. The load increase happened after 50 seconds.

To compensate for the 1000 MW load step up, available aFRR in six areas had to be activated in situation 3. Figure 5.32 shows the power increase in the areas where aFRR were activated. NO5 had the cheapest bid, but due to the capacity limit the power production in this area decreased by a few tens of MW. Some aFRR were activated in areas SE1, SE2, SE3, and FI, while the largest activation happened in NO2 with around 660 MW. In total the activated aFRR were equal to the load increase of 1000 MW.

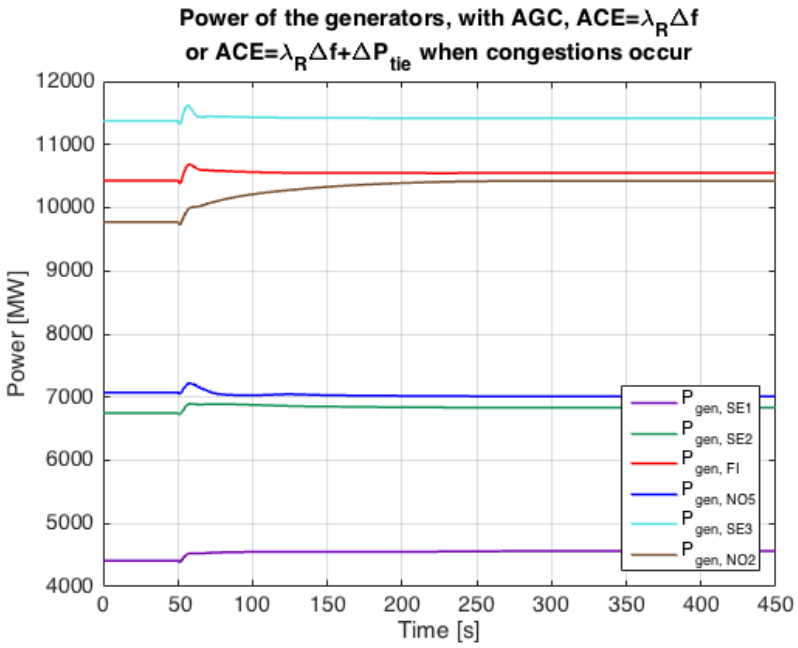

Figure 5.32: Power production of the generators in the areas where aFRR were activated in case 4. The load increase happened after 50 seconds.

Figure 5.33 shows an overview of how the power flow changed in situation 3, case 4. The power flow in NO5-NO1 increased to the transfer capacity limit, causing the power flow in NO2-NO1 to increase. The flow in NO1-SE3 increased until the power transfer was stabilized at the reference value. The power flow also increased from SE2 to SE3 and from SE3 to SE4 due to activation of aFRR in areas SE1, SE2, SE3, and FI.

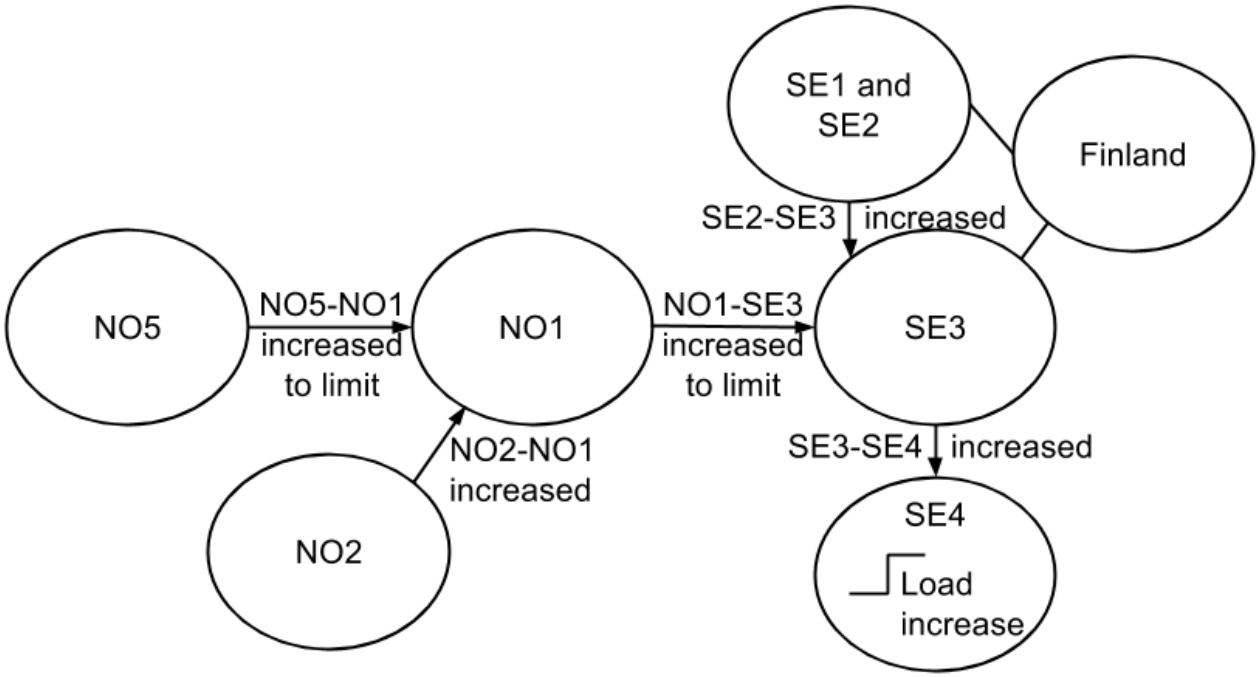

Figure 5.33: Overview of the power flow in situation 3, case 4.

The results are recognizable in the ACE's of the AGC's. For NO2 the ACE, visible in figure 5.34, increased but was restored to zero in both situation 2 and 3 after a few hundred seconds. The small bumps after approximately 130 and 240 seconds in situation 3 were caused by the bumps in the frequency at the same points in time, which happened due to congestions in the NO5-NO1 and NO1-SE3 corridors. The ACE of the AGC in NO5, seen in figure 5.35, initially increased, but dropped when the power transmission in NO5-NO1 exceeded the reference value of 3900 MW. The ACE proceeded to follow the frequency oscillations and the power transmission in NO5-NO1 as these stabilized. The ACE of Sweden's AGC, seen in figure 5.36, followed a similar course as the NO2 ACE. After approximately 240 seconds, the power transmission in corridor NO1-SE3 exceeded the reference value of 2145 MW, making the ACE increase some, before stabilizing at zero.

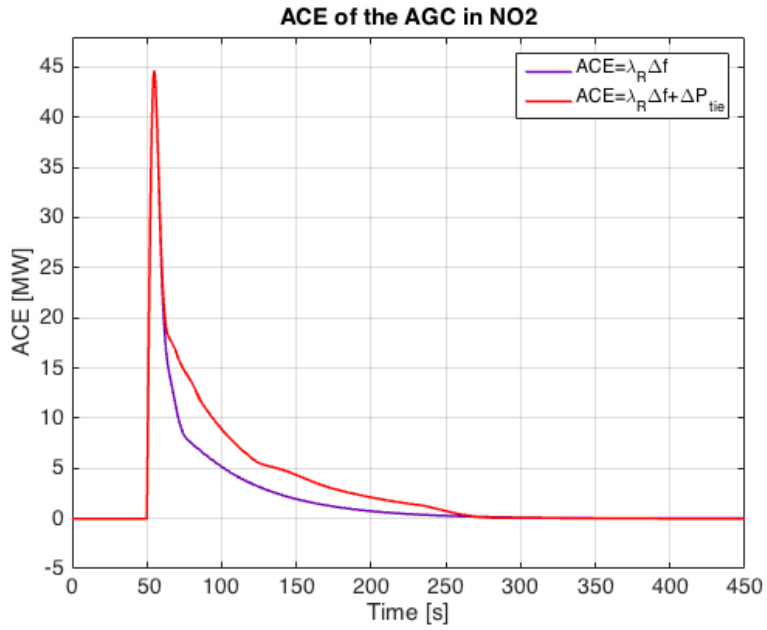

Figure 5.34: ACE of the AGC in NO2 in case 4. The load increase happened after 50 seconds.

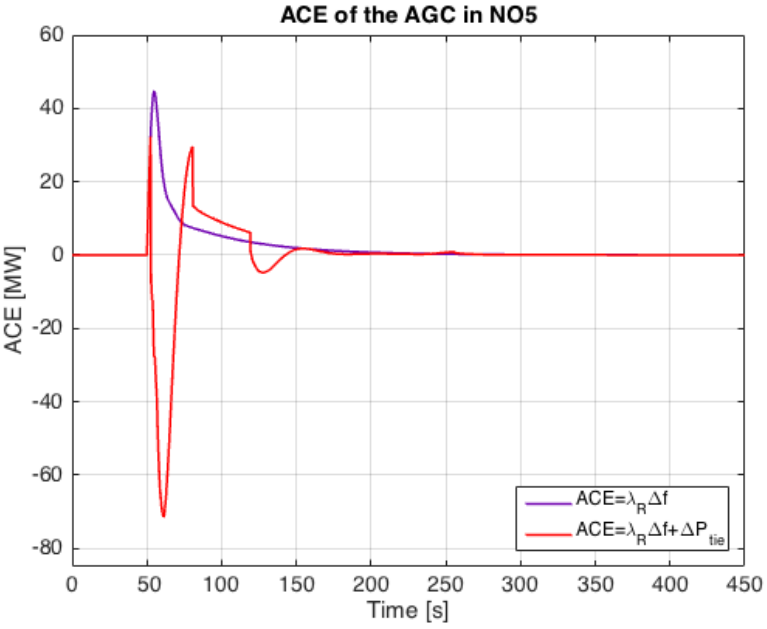

Figure 5.35: ACE of the AGC in NO5 in case 4. The load increase happened after 50 seconds.

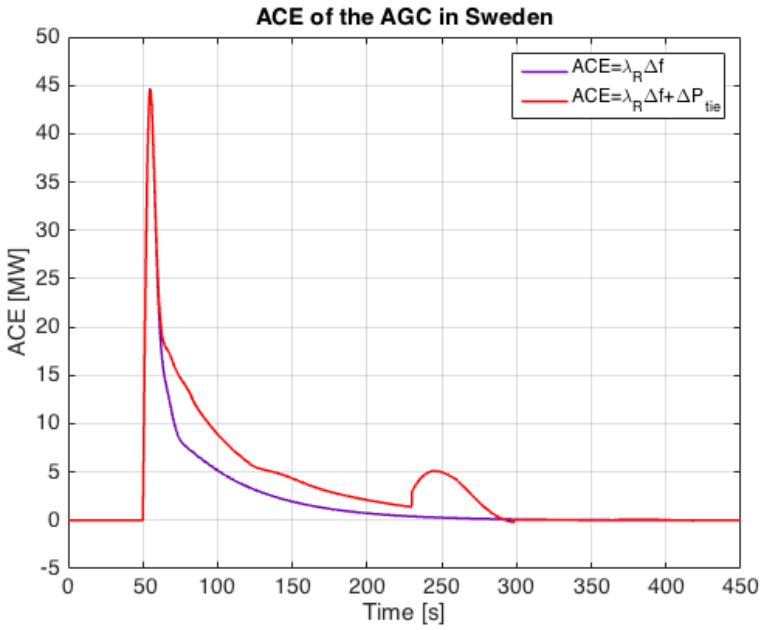

Figure 5.36: ACE of the AGC in Sweden in case 4. The load increase happened after 50 seconds.

5.6 Case 5: Load Increase in FI

Case 5 is a load increase of 800 MW in Finland. The aFRR that were supposed to be activated per area and the participation factors of the AGC's in this case are listed in table 5.5.

Table 5.5: aFRR activation per area and participation factors of the AGC's, case 5.

Area	aFRR per area [MW]	Participation factor	Participation factor value [-]
NO2	295	α_{NO2}	1.0
NO5	290	α_{NO5}	1.0
SE1	145	α_{SE1}	0.67
SE2	70	α_{SE2}	0.33

The frequency dropped as the load stepped up, but was increased by the primary frequency control and stabilized 0.0834 Hz below the initial value when there were no AGC's in the system. The system frequency response was 9592 MW/Hz. With AGC's the frequency was restored to 50.00 Hz within a few hundred seconds; it was

somewhat slower in situation 3 than situation 2. The frequency restoration curves were somewhat irregular because of the congestion described below.

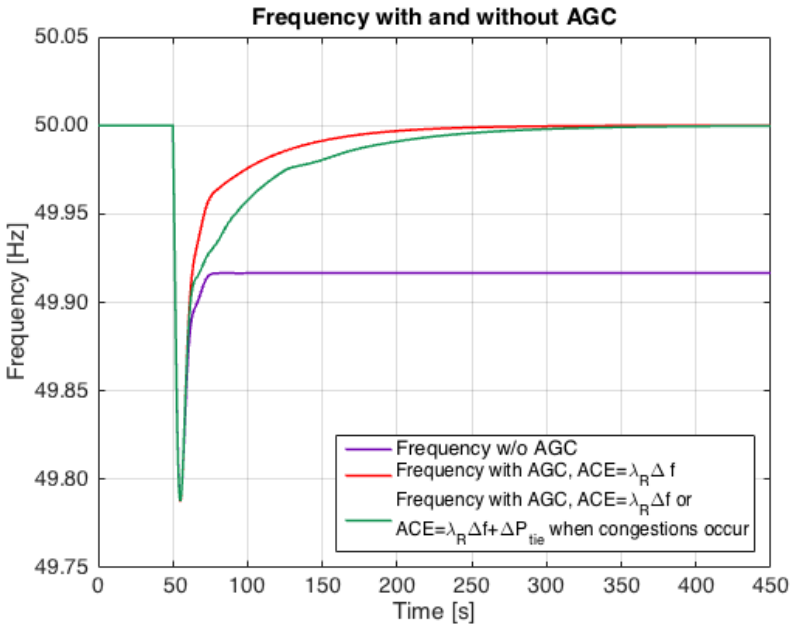

Figure 5.37: Frequency of the system in case 5. The load increase happened after 50 seconds.

The flow in the NO5-NO1 corridor, see figure 5.38, increased both with and without AGC's installed. Similarly to previous cases, the power flow in that corridor exceeded the reference value in situation 1 and 2. In situation 3, the AGC stabilized the transmission at 3900 MW. The flow in corridor NO2-NO1, see figure 5.39, increased in all situations, but the most in situation 3. The reduction in power transmission from NO5 to NO1 in situation 3 caused the power in NO2, and hence the transmission in the NO2-NO1 corridor, to increase. Figure 5.40 shows the flow in corridor NO1-SE3. The flow was the largest in situation 2 due to the larger power transmission from NO5 in this situation.

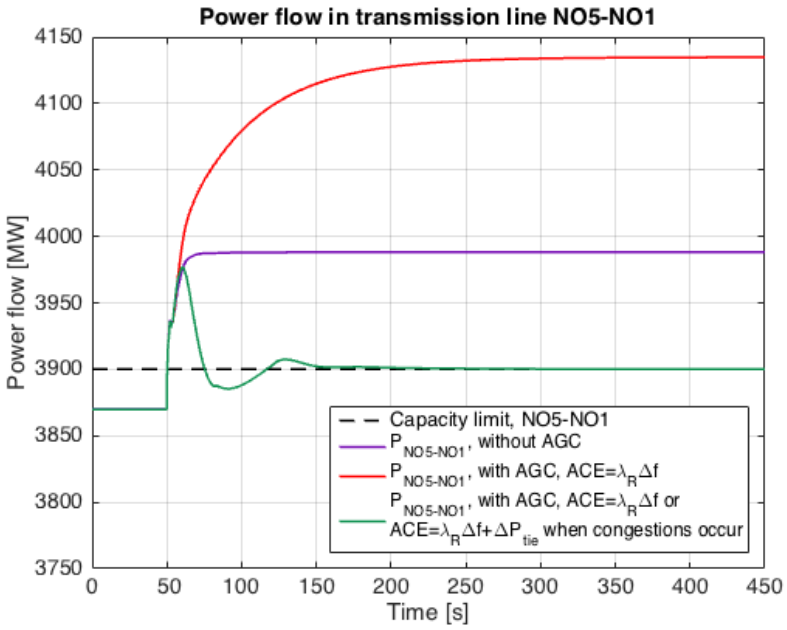

Figure 5.38: Power flow in the NO5-NO1 corridor in case 5. The load increase happened after 50 seconds.

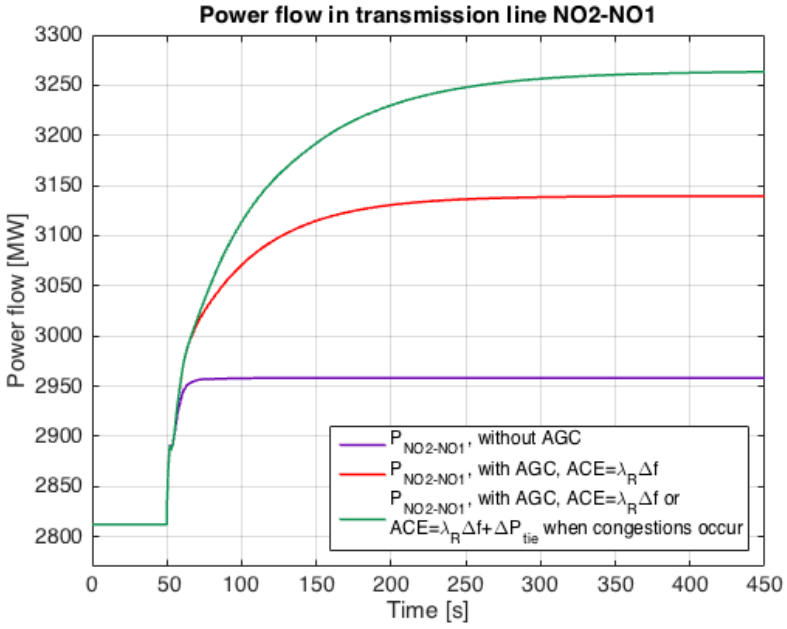

Figure 5.39: Power flow in the NO2-NO1 corridor in case 5. The load increase happened after 50 seconds.

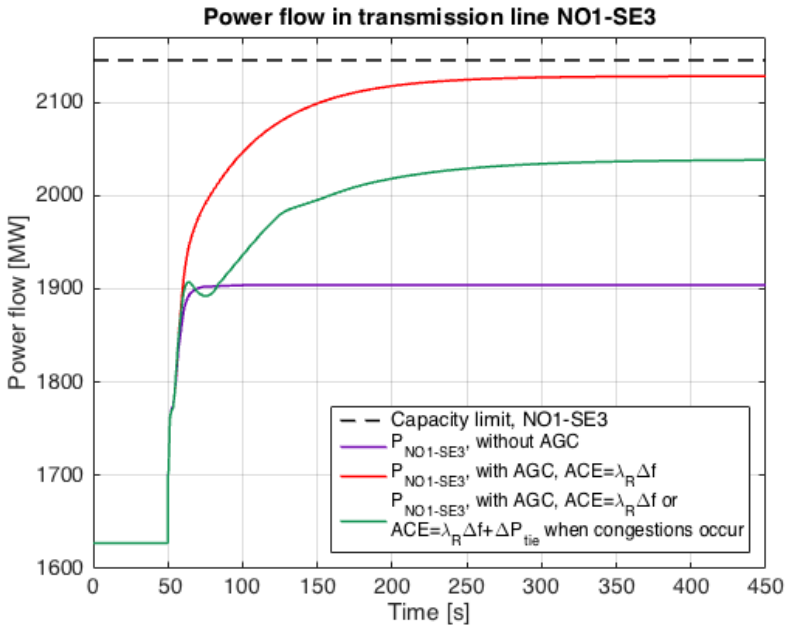

Figure 5.40: Power flow in the NO1-SE3 corridor in case 5. The load increase happened after 50 seconds.

In figures 5.41 and 5.42, the power transmission from SE1 and SE3 to Finland, respectively, are shown. As the load increase occurred in Finland and no aFRR were activated there, the power had to be transferred from Norway and Sweden to stabilize the system after the disturbance. The maximum capacities of the transmission corridors SE1-FI and SE3-FI were 1500 and 1200 MW, respectively. These limits were exceeded in this case. As described in chapter 4 the SE3-FI connection is in reality an HVDC link which does not respond to a disturbance but follows its own transmission plan. However, because it was considered a transmission line in this model, the congestions in this and the SE1-FI corridor illustrate that in order to avoid excess of the grid capacities there should be more AGC's in the system to control the rest of the tie lines.

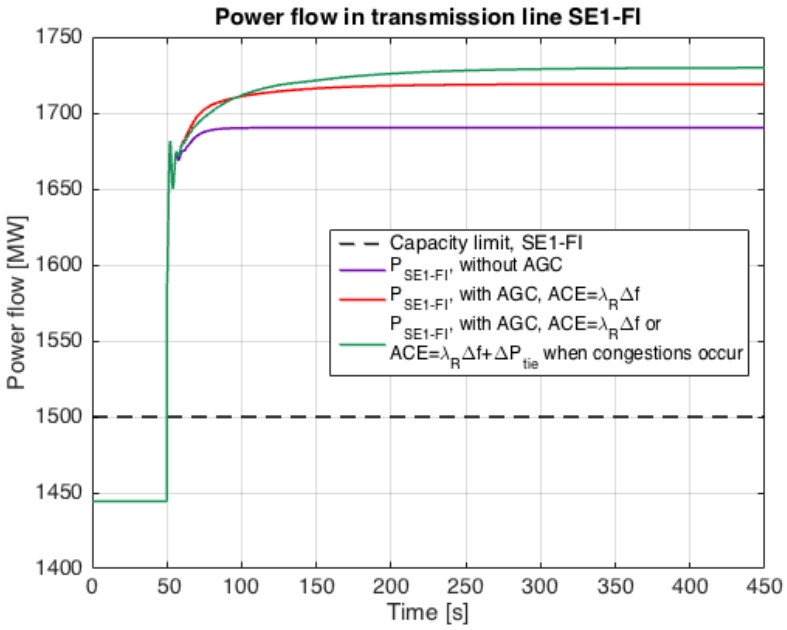

Figure 5.41: Power flow in the SE1-FI corridor in case 5. The load increase happened after 50 seconds.

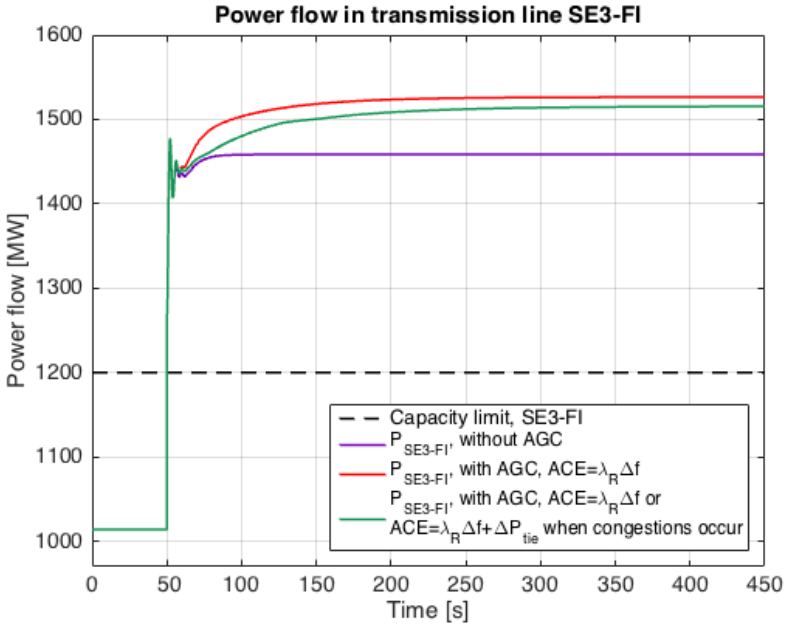

Figure 5.42: Power flow in the SE3-FI corridor in case 5. The load increase happened after 50 seconds.

aFRR in four areas were activated in situation 3 to compensate for the load step up. The result can be seen in figure 5.43. As in several other cases the power production in NO5 somewhat decreased by a few tens of MW, due to the congestion in the NO5-NO1 corridor. In SE1 almost 200 MW and in SE2 about 150 MW of aFRR were activated, while NO2 contributed about 520 MW of aFRR. In total the full load change of 800 MW was compensated for.

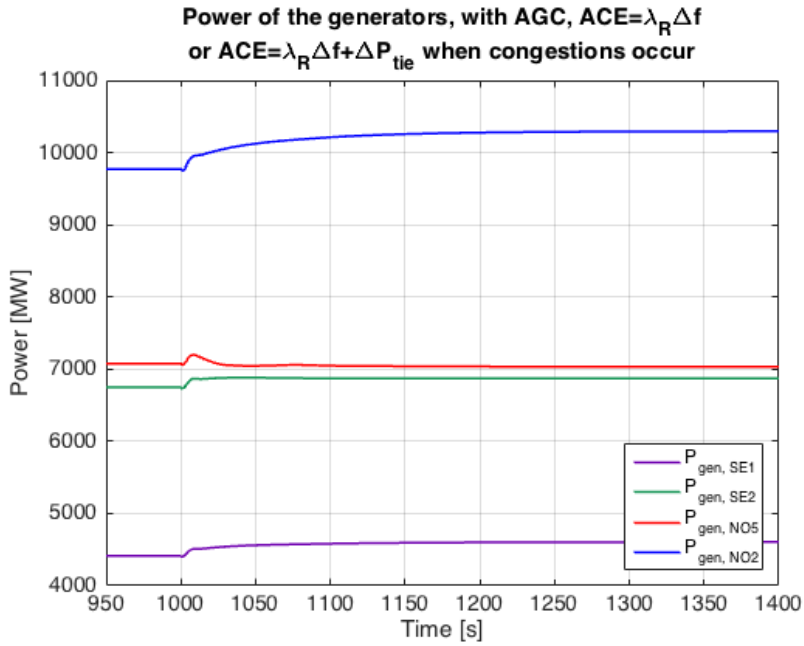

Figure 5.43: Power production of the generators in the areas where aFRR were activated in case 5. The load increase happened after 50 seconds.

Figure 5.44 shows an overview of how the power flow changed in situation 3, case 5. The power flow in NO5-NO1 increased to the transfer capacity limit, causing the power flow in NO2-NO1 to increase. The flow in NO1-SE3 increased in order to transfer power from Norway to Sweden and further to Finland. The power flow from SE1 and SE3 to FI increased greatly in order to compensate for the load step up, and the capacity limits of these tie lines were exceeded.

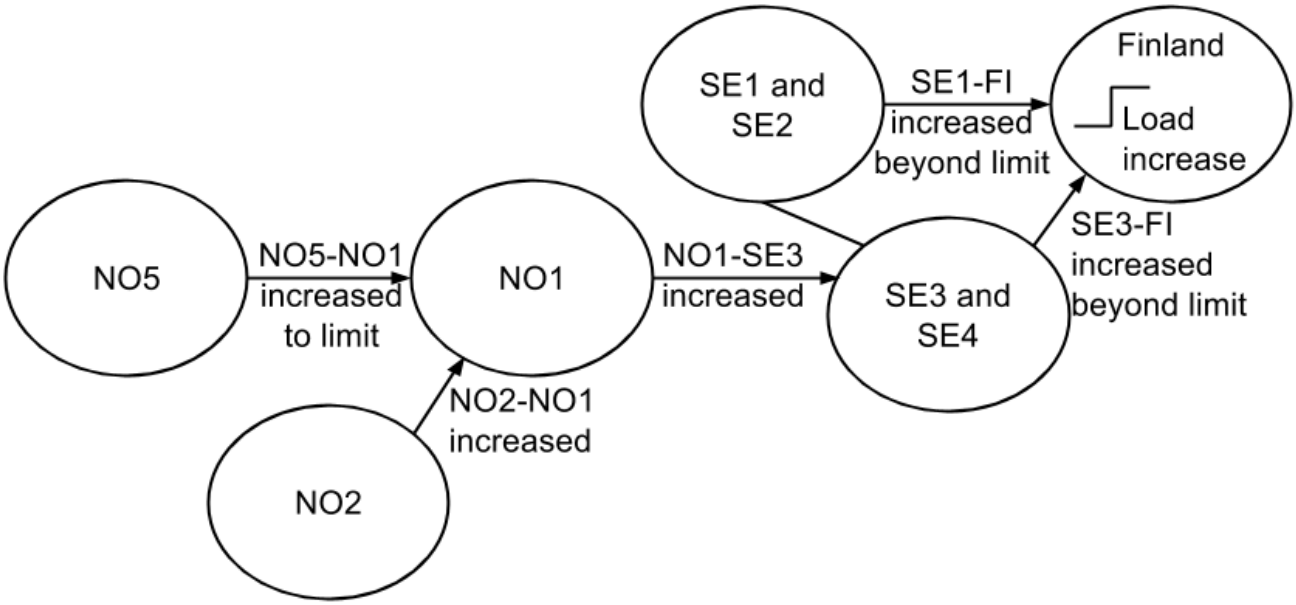

Figure 5.44: Overview of the power flow in situation 3, case 5.

As the only congested corridor of the controlled tie lines was the NO5-NO1 corridor, the ACE's of the AGC's in NO2 and Sweden, see figure 5.45, were the same. The ACE in these areas increased as the load step up occurred, and was stabilized at zero at the same time as the frequency was restored. The ACE in NO5, shown in figure 5.46, increased, dropped as the power flow in the NO5-NO1 transmission corridor exceeded the tie line reference value, and was restored to zero as the frequency was restored and the power flow in the NO5-NO1 line stabilized at 3900 MW.

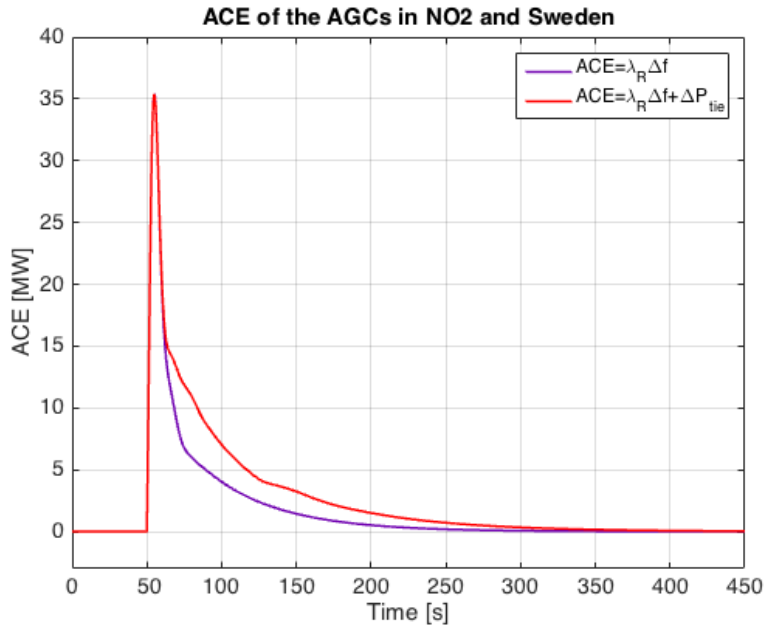

Figure 5.45: ACE of the AGC's in NO2 and Sweden in case 5. The load increase happened after 50 seconds.

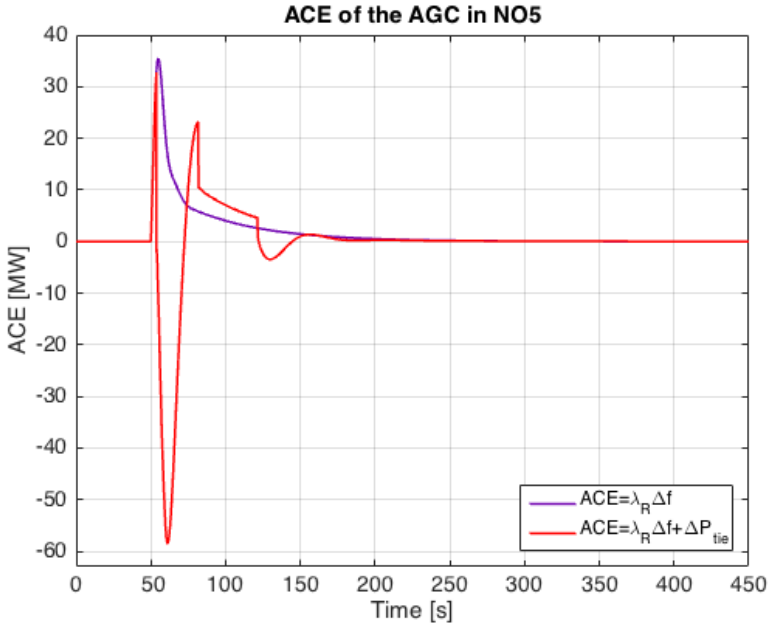

Figure 5.46: ACE of the AGC in NO5 in case 5. The load increase happened after 50 seconds.

5.7 Case 6: Load Increase in SE4, Simultaneous Load Decrease in NO2

To demonstrate a case with system power balance with shifts in the power transmission, case 6 was run. The load in SE4 was stepped up by 800 MW and the load in NO2 was simultaneously decreased by the same value. The available aFRR for activation per area and the participation factors of the AGC's in this case are listed in table 5.6. As there was power balance in the system throughout the disturbance, the net aFRR activation was zero, but the AGC's had to be operational in order to be able to control the frequency and the tie lines. Hence, the cheapest aFRR in each of the control areas were set available.

Table 5.6: aFRR activation per area and participation factors of the AGC's, case 6.

Area	**aFRR per area [MW]**	**Participation factor**	**Participation factor value [-]**
NO2	295	α_{NO2}	1.0
NO5	290	α_{NO5}	1.0
SE2	70	α_{SE2}	1.0

In situation 1 and 2 the system experienced a disturbance at first, but the frequency evened out after a few seconds. In situation 3 it took a few hundred seconds to stabilize the frequency. Regardless, the frequency deviation was minimal during the instability, see figure 5.47.

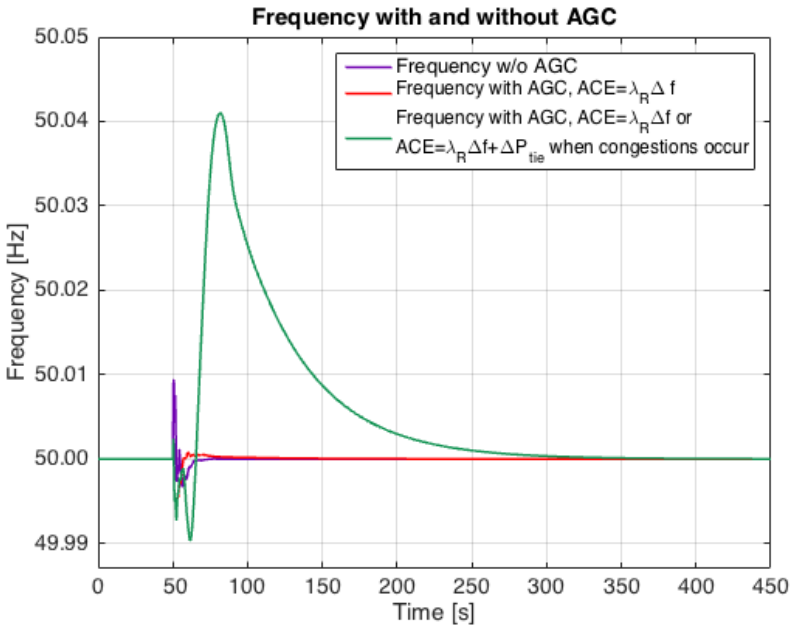

Figure 5.47: Frequency of the system in case 6. The load increase happened after 50 seconds.

Figure 5.48 shows the transmission in the NO5-NO1 corridor. The flow exceeded the tie line reference value in situation 1 and 2. In situation 3 the transmission was reduced to a value below the initial power flow. Figures 5.49 and 5.50 show that the same happened in the NO2-NO1 and NO1-SE3 corridors; the capacity limits were exceeded in situation 1 and 2, while the power flow was reduced to a value below the limits in situation 3.

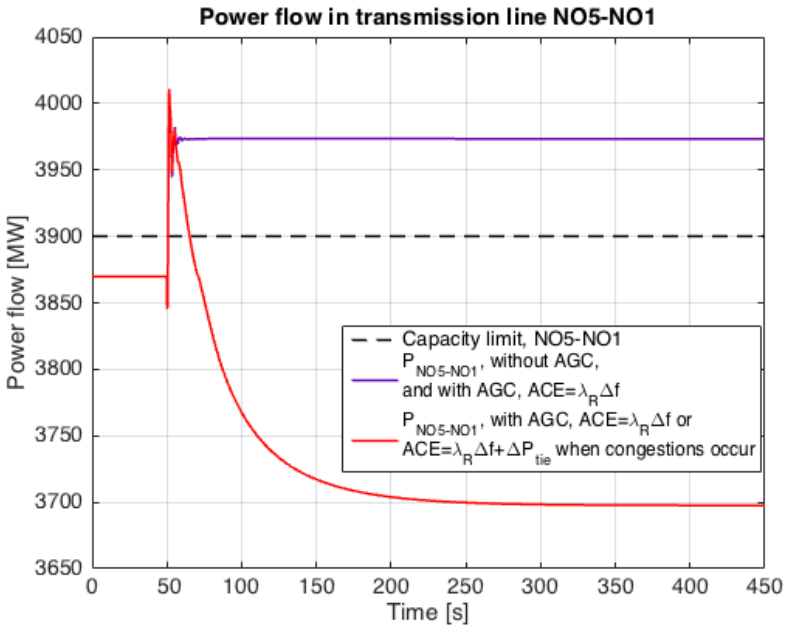

Figure 5.48: Power flow in the NO5-NO1 corridor in case 6. The load increase happened after 50 seconds.

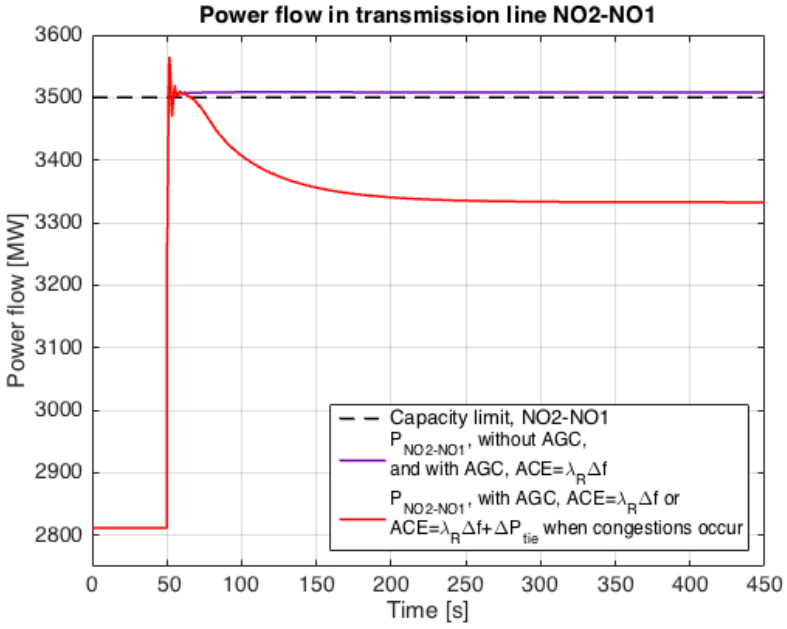

Figure 5.49: Power flow in the NO2-NO1 corridor in case 6. The load increase happened after 50 seconds.

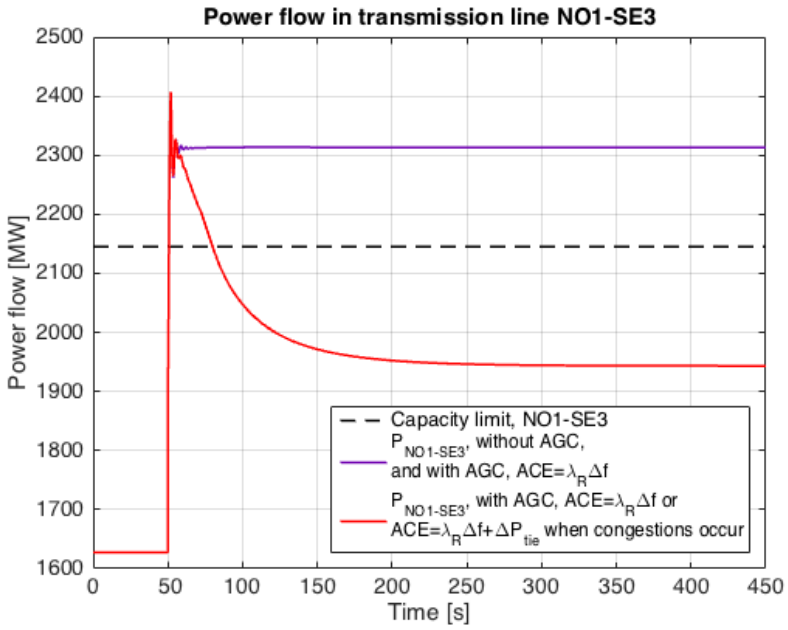

Figure 5.50: Power flow in the NO1-SE3 corridor in case 6. The load increase happened after 50 seconds.

As a consequence of the decreased power flow from Norway to Sweden in situation 3, the power flow from SE2 to SE3 increased by several hundred MW compared to situation 1 and 2. The result can be seen in figure 5.51. The power flow from SE3 to SE4 was increased by 800 MW for all three situations, illustrated in figure 5.52.

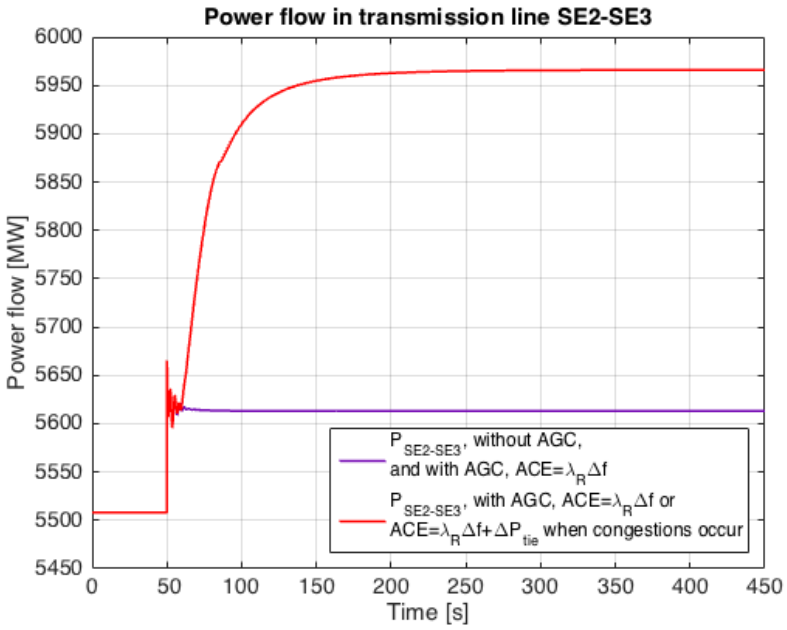

Figure 5.51: Power flow in the SE2-SE3 corridor in case 6. The load increase happened after 50 seconds.

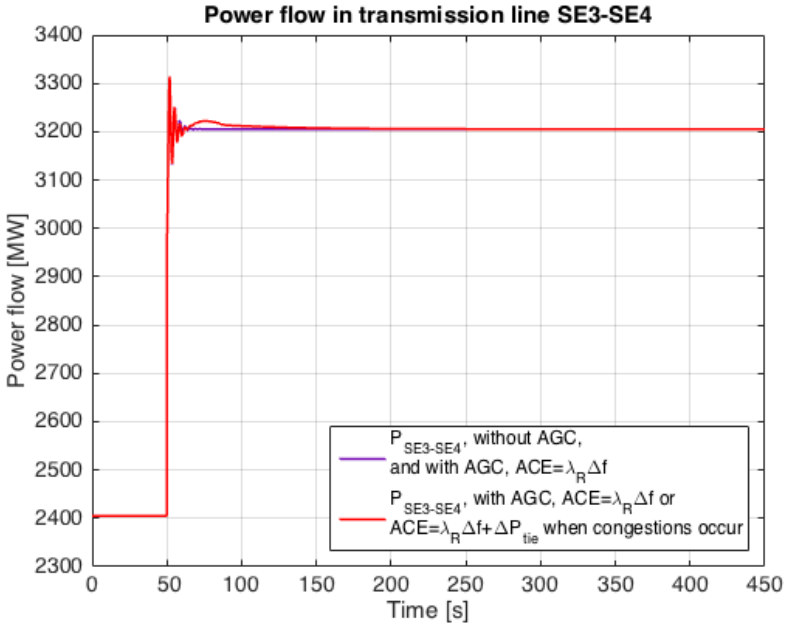

Figure 5.52: Power flow in the SE3-SE4 corridor in case 6. The load increase happened after 50 seconds.

In this case the system power was balanced, but the corridors controlled by the AGC's exceeded their limits when the disturbance occurred. Hence, some aFRR had to be activated in order to regain control of the power flow. Figure 5.53 shows how the power production changed in situation 3 when the load change happened. In NO5 and NO2 the power generation was reduced as a consequence of the congestions, while the power in SE2 was increased to compensate for the lost power initially being transferred from Norway.

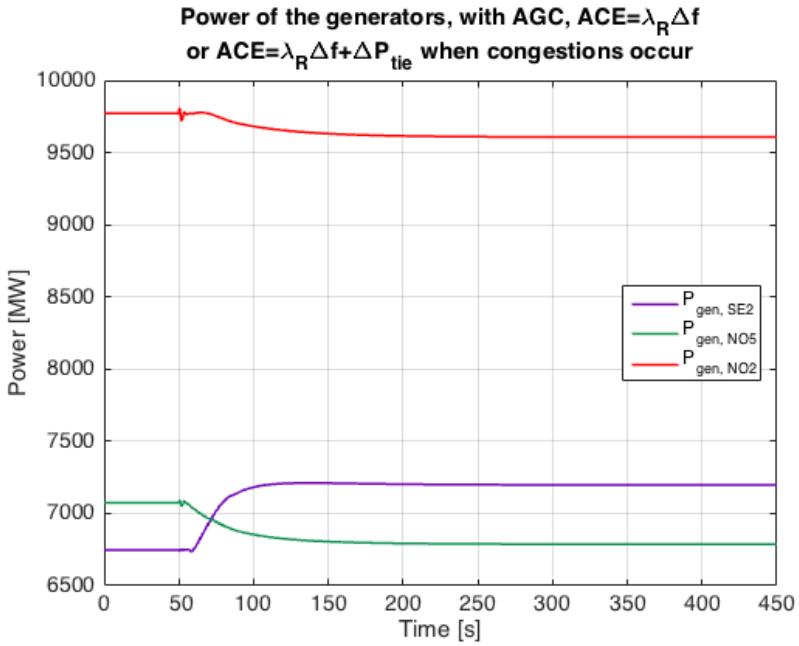

Figure 5.53: Power production of the generators in the areas where aFRR were activated in case 6. The load increase happened after 50 seconds.

Figure 5.54 shows an overview of how the power flow changed in situation 3, case 6. The power production in NO5 decreased as a consequence of the load step down in NO2, leading to a decrease in flow in the NO5-NO1 corridor. For the same reason the power production in NO2 was reduced and the power transmission from NO2 to NO1 increased. The flow in transmission corridor NO1-SE3 increased due to greater availability of power supply in NO2. The power generation increased in SE2, causing the flow in the SE2-SE3 corridor to increase. The power flow from SE3 to SE4 was increased by 800 MW in order to compensate for the load step up.

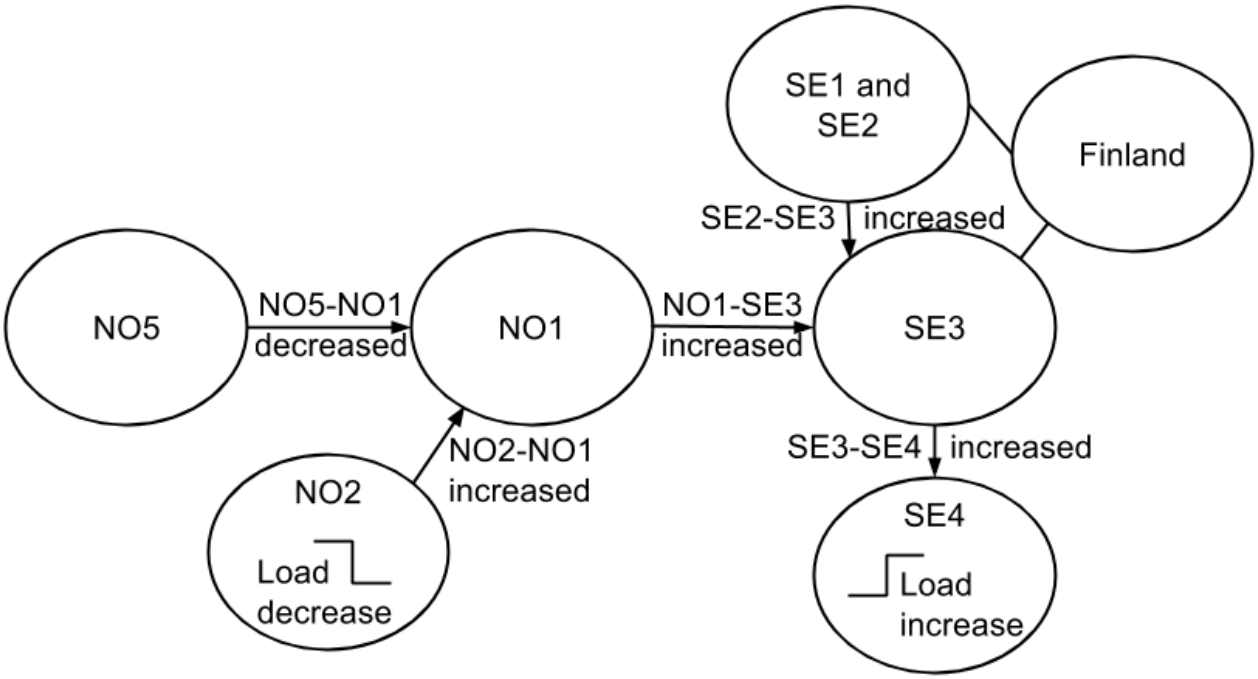

Figure 5.54: Overview of the power flow in situation 3, case 6.

All the ACE's reflected the system's response to the load disturbance. Figures 5.55, 5.56, and 5.57 show the ACE's of the AGC's in NO2, NO5, and Sweden, respectively. All the ACE's reacted to the frequency deviation and then the excess of the tie line reference values. The ACE's stabilized after a few hundred seconds, in accordance with the frequency. This is clearer in figure 5.55 than the following two figures, as the ACE changed less in NO2 than the other areas.

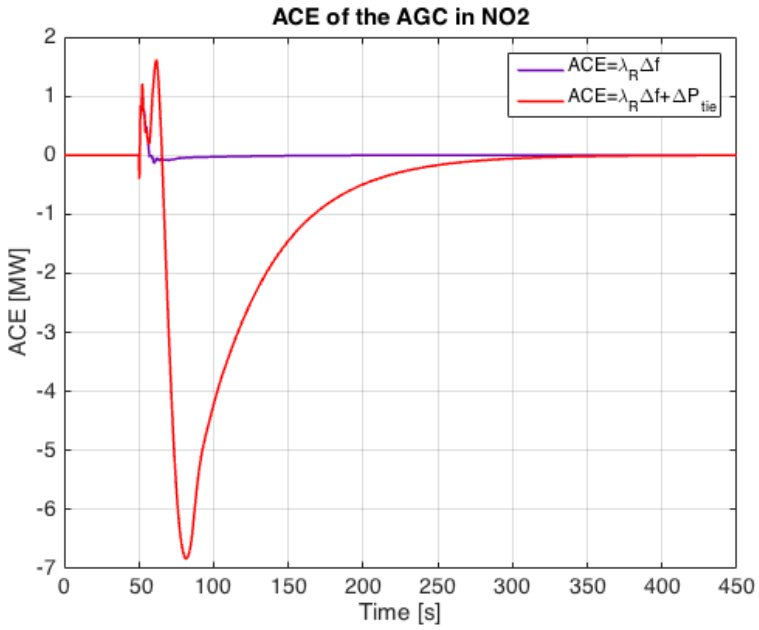

Figure 5.55: ACE of the AGC in NO2 in case 6. The load increase happened after 50 seconds.

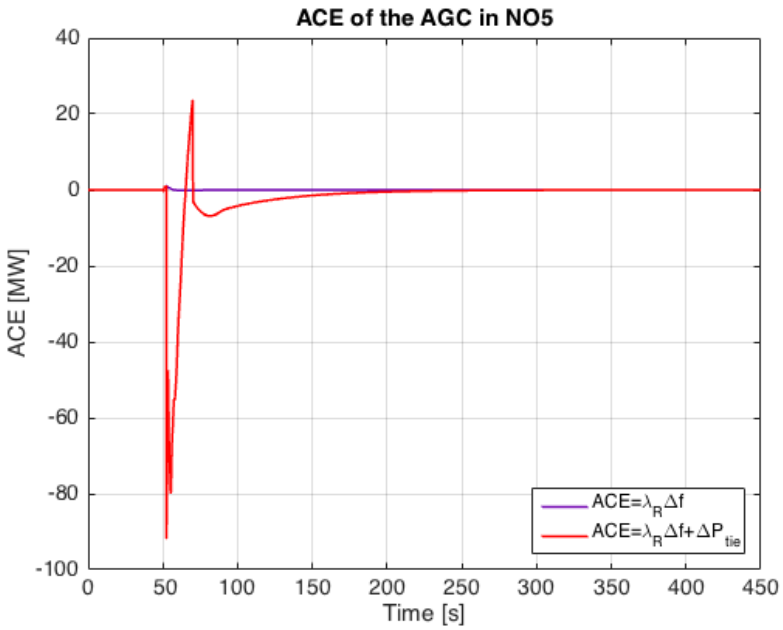

Figure 5.56: ACE of the AGC in NO5 in case 6. The load increase happened after 50 seconds.

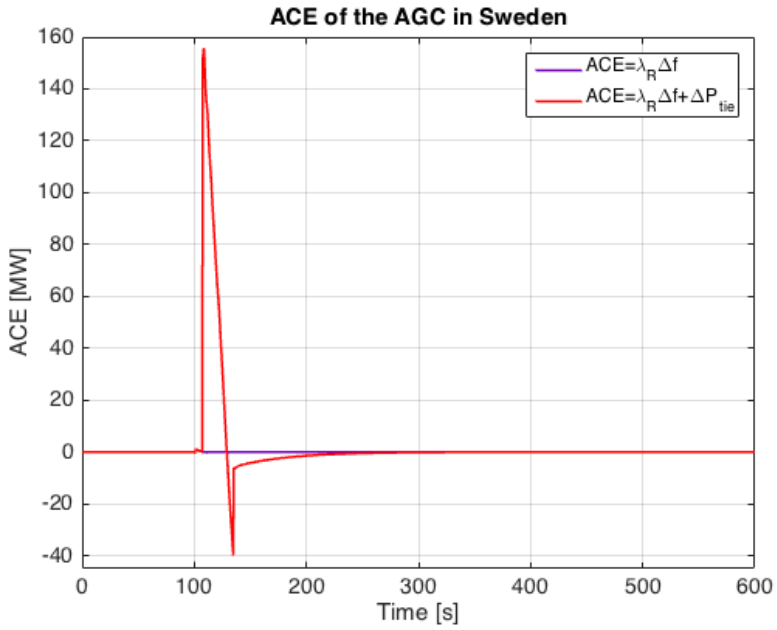

Figure 5.57: ACE of the AGC in Sweden in case 6. The load increase happened after 50 seconds.

5.8 Case 7: Load Increase in SE4, Simultaneous Load Increase in NO2

Case 7 is a load increase in SE4 of 450 MW and a simultaneous and equal load increase in NO2. The aFRR that were supposed to be activated per area and the participation factors of the AGC's in this case are listed in table 5.7.

Table 5.7: aFRR activation per area and participation factors of the AGC's, case 7.

Area	aFRR per area [MW]	Participation factor	Participation factor value [-]
NO2	295	α_{NO2}	1.0
NO5	290	α_{NO5}	1.0
SE1	160	α_{SE1}	0.51
SE2	70	α_{SE2}	0.22
SE3	75	α_{SE1}	0.24
FI	10	α_{SE2}	0.03

Figure 5.58 shows the frequency deviation. The frequency dropped but was

increased shortly after by the primary frequency control. Without AGC's, the frequency was stabilized 0.093825 Hz below the initial value, resulting in a system frequency response of 9592 MW/Hz. When AGC's were installed, the frequency restored to 50.00 Hz after a few hundred seconds; somewhat slower in situation 3 than in situation 2.

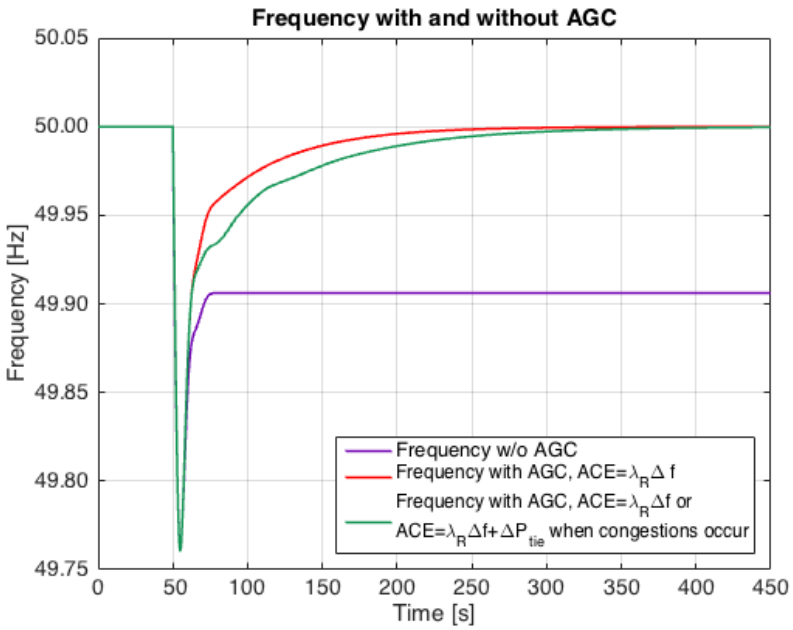

Figure 5.58: Frequency of the system in case 7. The load increase happened after 50 seconds.

The power flow in the NO5-NO1 corridor, seen in figure 5.59, increased in all situations, but as it exceeded the reference value, the flow was stabilized at 3900 MW in situation 3. The flow in the NO2-NO1 corridor, shown in figure 5.60, decreased in situation 1 and 2, while it increased from the initial value in situation 3. The latter was due to the decrease in power from NO5 to NO1. The power flow in the NO1-SE3 corridor, see figure 5.61, shows how the power transmission dropped when there were no AGC's, but the flow increased when they were included. The reason was the increased power in the NO2-NO1 and NO5-NO1 corridors. Of the tie lines controlled by the AGC's there was congestion only in the NO5-NO1 corridor in this case.

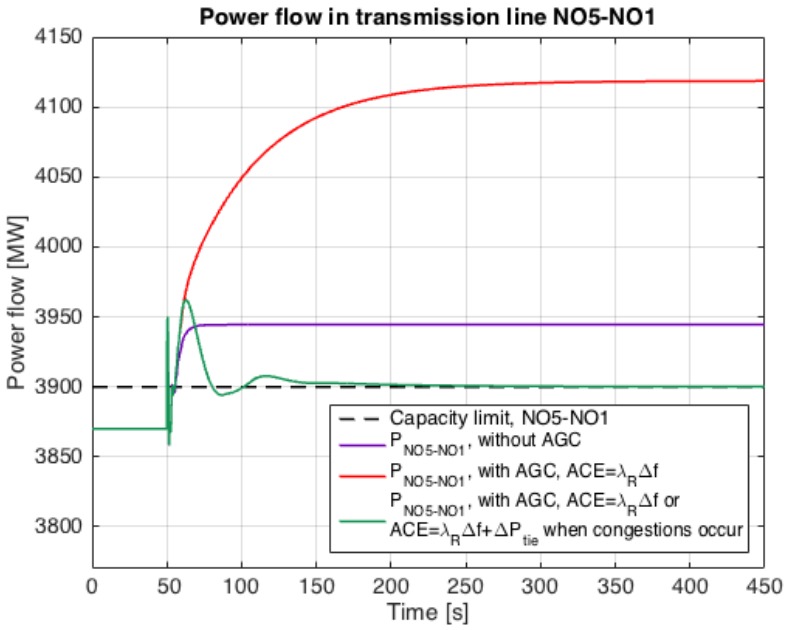

Figure 5.59: Power flow in the NO5-NO1 corridor in case 7. The load increase happened after 50 seconds.

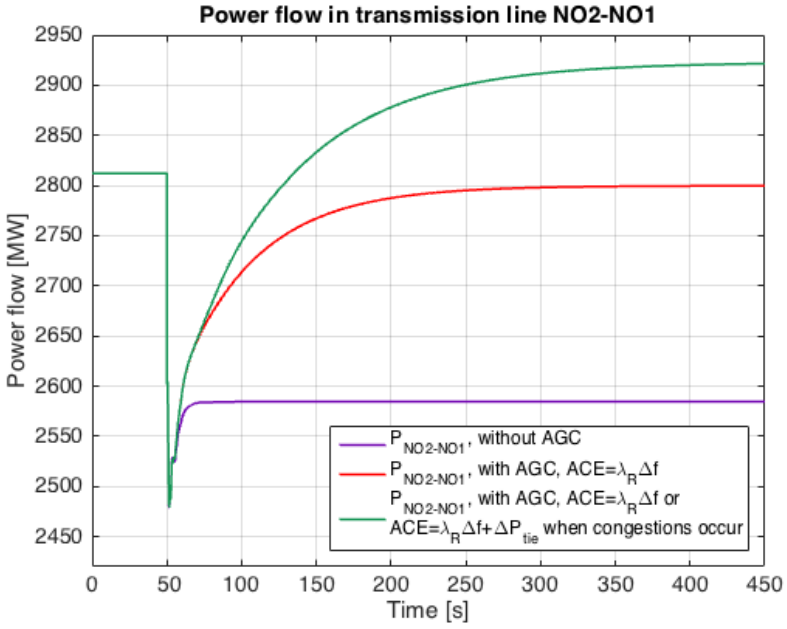

Figure 5.60: Power flow in the NO2-NO1 corridor in case 7. The load increase happened after 50 seconds.

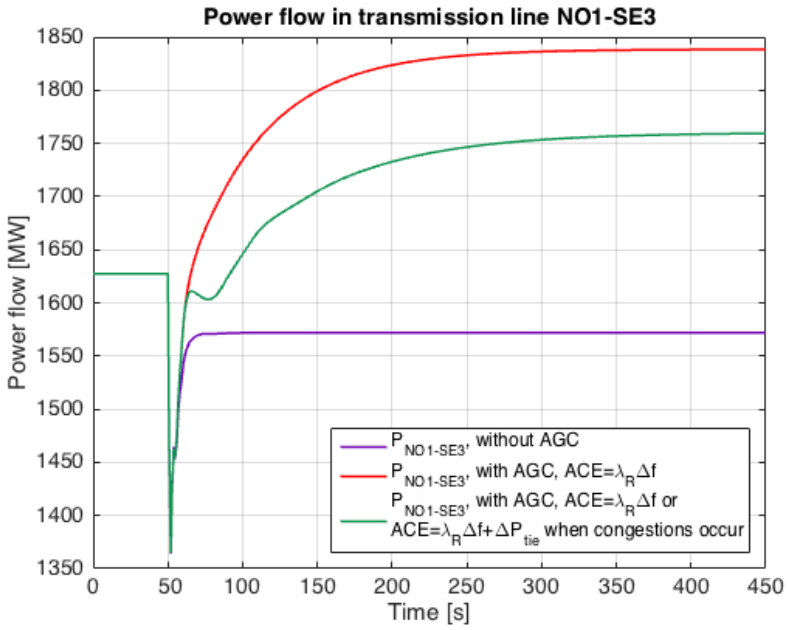

Figure 5.61: Power flow in the NO1-SE3 corridor in case 7. The load increase happened after 50 seconds.

The flow from SE2 to SE3 increased to transfer the aFRR activated in SE1, SE2, SE3, and FI. The power flow in the SE3-SE4 corridor increased by 450 MW. Figures 5.62 and 5.63 illustrate the results.

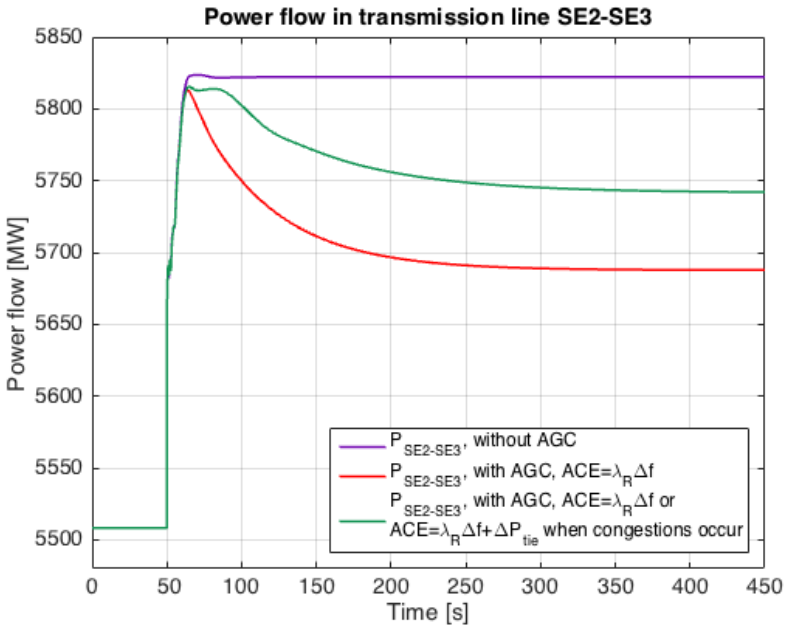

Figure 5.62: Power flow in the SE2-SE3 corridor in case 7. The load increase happened after 50 seconds.

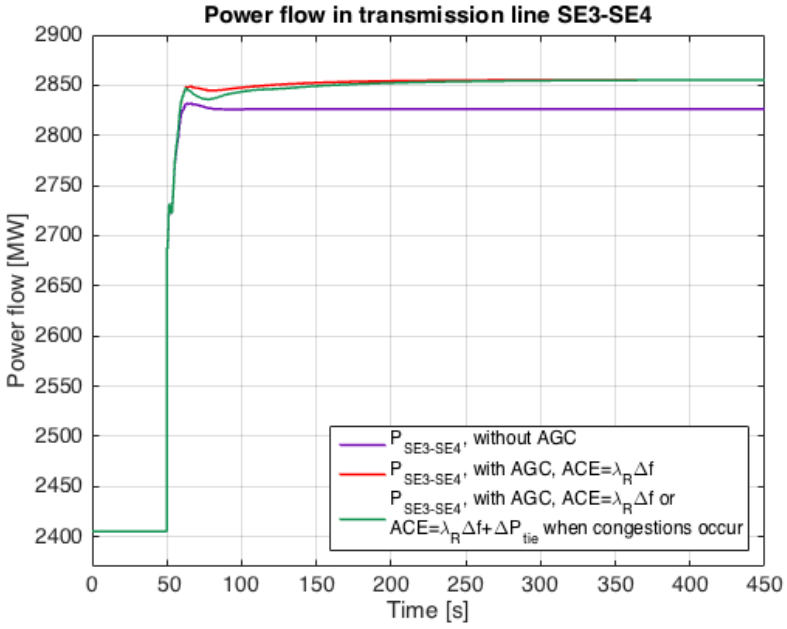

Figure 5.63: Power flow in the SE3-SE4 corridor in case 7. The load increase happened after 50 seconds.

Figure 5.64 shows the power production in the six areas where aFRR were activated in situation 3. In NO5 the power was only slightly increased due to the congestion in the NO5-NO1 corridor. SE3 did not offer much aFRR and thus had only a small increase in production. The power in SE2 increased by almost 100 MW, while it in SE1 increased by approximately 150 MW. The power increase in FI was minimal, while approximately 560 MW of aFRR were activated in NO2. The aFRR activation was equal to the total load increase of 900 MW.

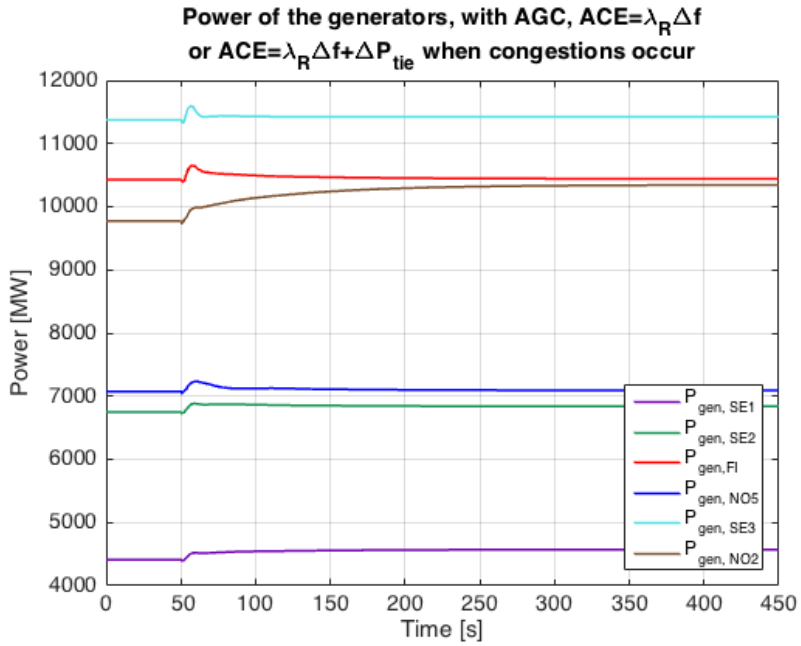

Figure 5.64: Power production of the generators in the areas where aFRR were activated in case 7. The load increase happened after 50 seconds.

Figure 5.65 shows an overview of how the power flow changed in situation 3, case 7. The power flow in corridor NO5-NO1 increased to the capacity limit, while the power flow in corridors NO2-NO1 and NO1-SE3 increased in order to deliver aFRR to SE4. The power flow increased also in corridors SE2-SE3 and SE3-SE4 such that the aFRR activated in SE1, SE2, SE3, and FI could be transferred to SE4.

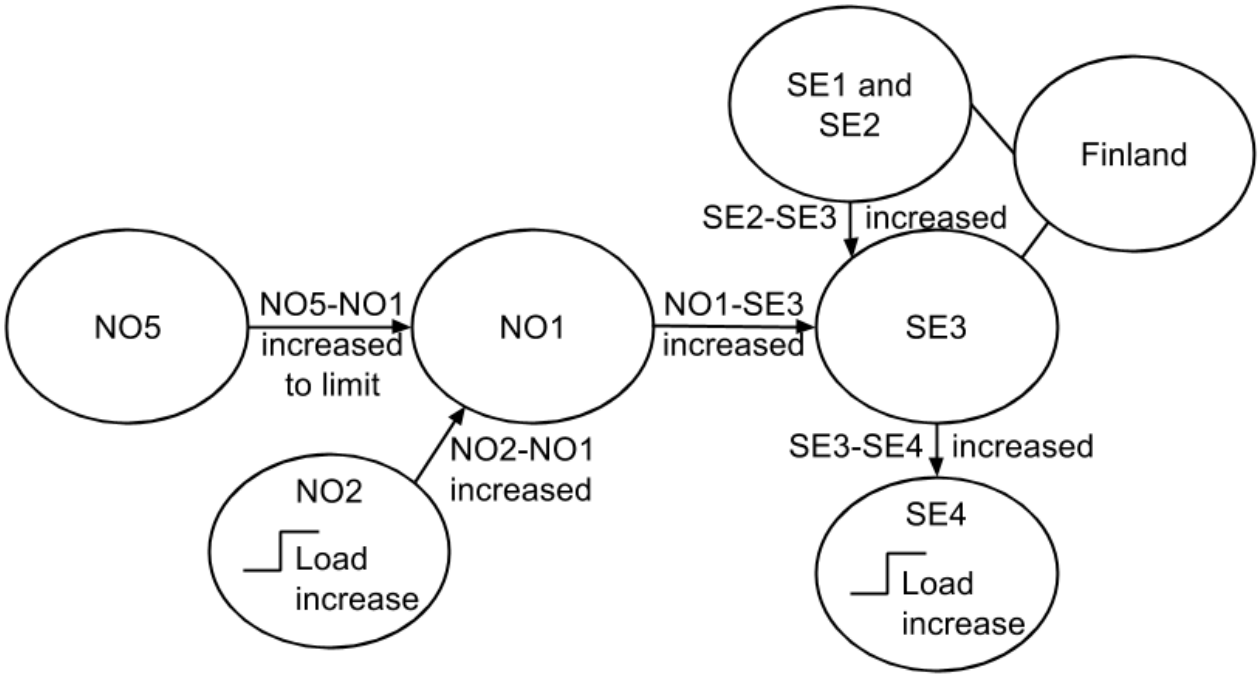

Figure 5.65: Overview of the power flow in situation 3, case 7.

Figures 5.66 and 5.67 show the ACE's in the AGC's of NO2 and Sweden, which were similar, and NO5, respectively. In NO2 and Sweden the ACE stepped up when the disturbances happened, and was restored to zero in accordance with the restoration of the frequency. The ACE in NO5 increased before rapidly decreasing as a consequence of the congestion in the NO5-NO1 corridor. The ACE stabilized at zero after a few hundred seconds in conformity with the restored frequency and the stabilization of the power transmission in NO5-NO1.

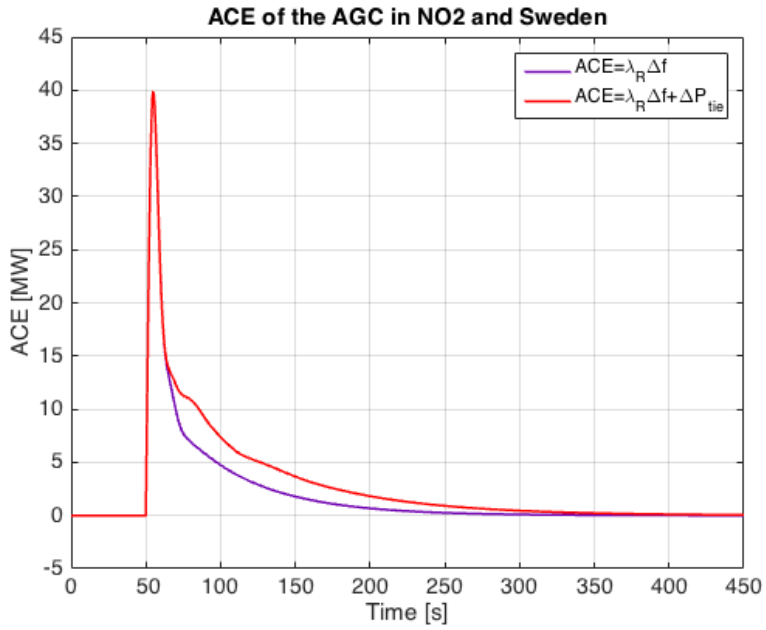

Figure 5.66: ACE of the AGC's in NO2 and Sweden in case 7. The load increase happened after 50 seconds.

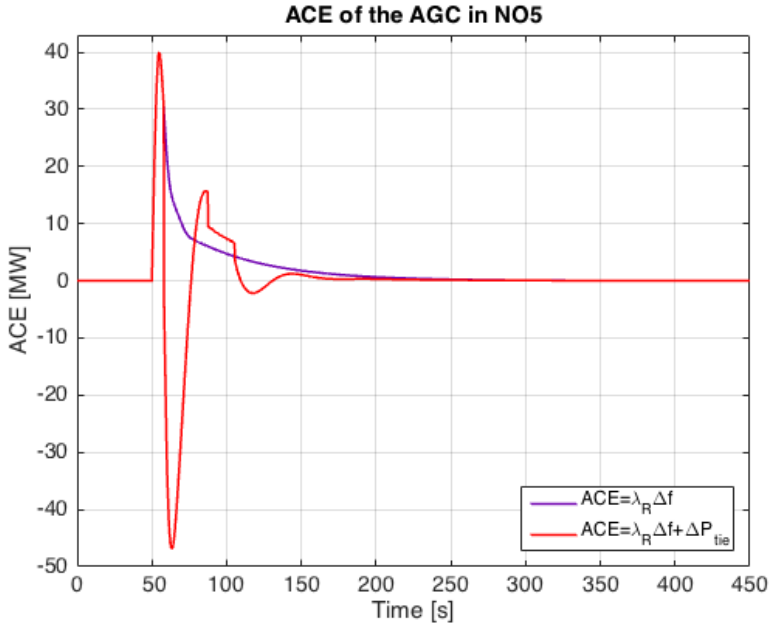

Figure 5.67: ACE of the AGC in NO5 in case 7. The load increase happened after 50 seconds.

5.9 Case 8: Hour Shift

The final case presented in this thesis uses data from the actual hour shift in the Nordic countries from 19:00–20:00 to 20:00–21:00 January 6, 2016. The loads in the areas changed in accordance with the data in table A.1 in appendix A.2, giving a net load change of -60 MW. The loads were again modeled as step blocks, and as the load values before and after the disturbance were in accordance with the planned flow for the specific hours, the disturbance was minimal. The power supply usually has the largest change around an hour shift, while the power demand changes throughout the hour. Instead of modeling the loads as step blocks in direct accordance with the power supply increase, an uneven load increase causing an imbalance could have been done instead. This would have better illustrated the secondary frequency control. However, this case still illustrates the flow change as result of the load changes and how the AGC's regulated a small decrease in net load.

For the -60 MW net load change only aFRR in NO5, the cheapest area, needed to be activated. The aFRR that were supposed to be activated and the participation factor of the AGC in this case are listed in table 5.8.

Table 5.8: aFRR activation per area and participation factors of the AGC's, case 8.

Area	**aFRR per area [MW]**	**Participation factor**	**Participation factor value [-]**
NO5	60	α_{NO5}	1.0

In this case there were no congestions, meaning that situation 2 and 3 gave equal results. Figure 5.68 shows how the frequency increased as the net load step down occurred, and how it dropped due to the primary frequency control. Without AGC's in the system the frequency stabilized 0.006255 Hz above the initial value of 50.00 Hz, giving a system frequency response of 9592 MW/Hz. When AGC's were included, the frequency was regulated back to 50.00 Hz after a few hundred seconds.

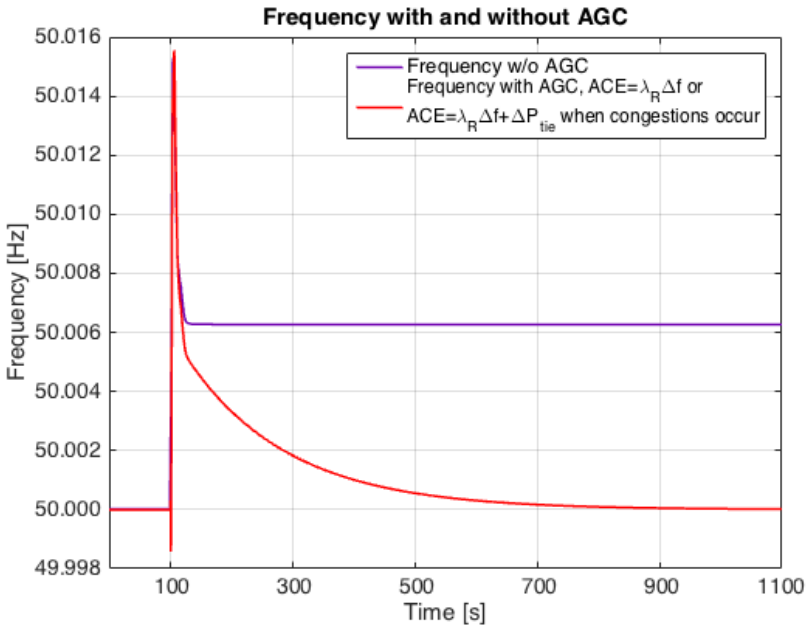

Figure 5.68: Frequency of the system in case 8. The load increase happened after 50 seconds.

Although the net load change was only -60 MW, the system power flow was different after the hour shift. In situation 1 the flow in the NO5-NO1 corridor, see figure 5.69, increased, while it dropped in order to restore the frequency at 50.00 Hz in situation 2 and 3. In the NO2-NO1 and NO1-SE3 corridors the transmission increased in all cases. The results are shown in figures 5.70 and 5.71. The power flow was increased slightly differently in situation 2 and 3 in order to restore the frequency.

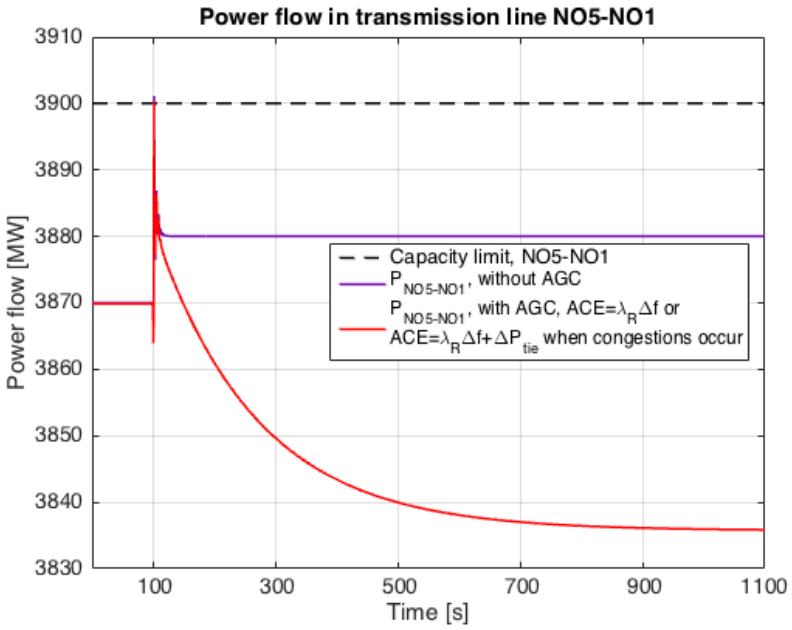

Figure 5.69: Power flow in the NO5-NO1 corridor in case 8. The load increase happened after 50 seconds.

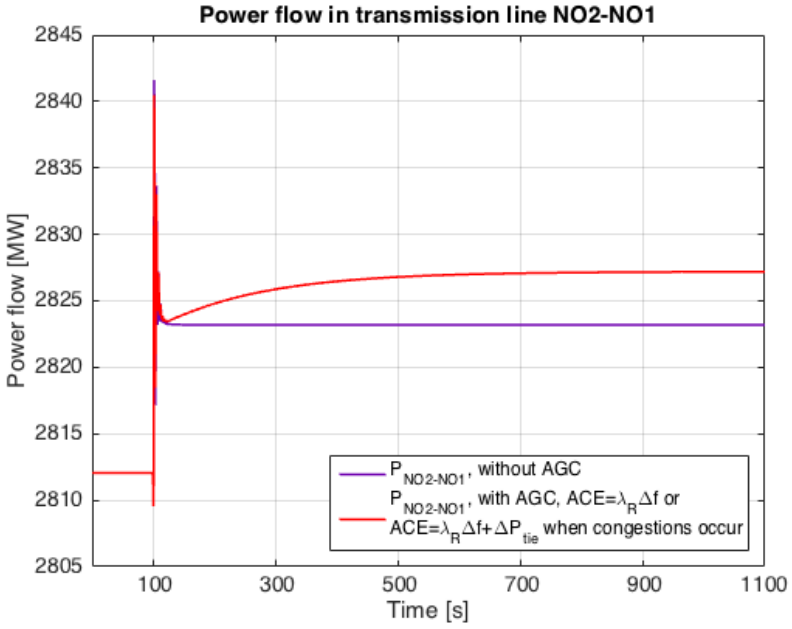

Figure 5.70: Power flow in the NO2-NO1 corridor in case 8. The load increase happened after 50 seconds.

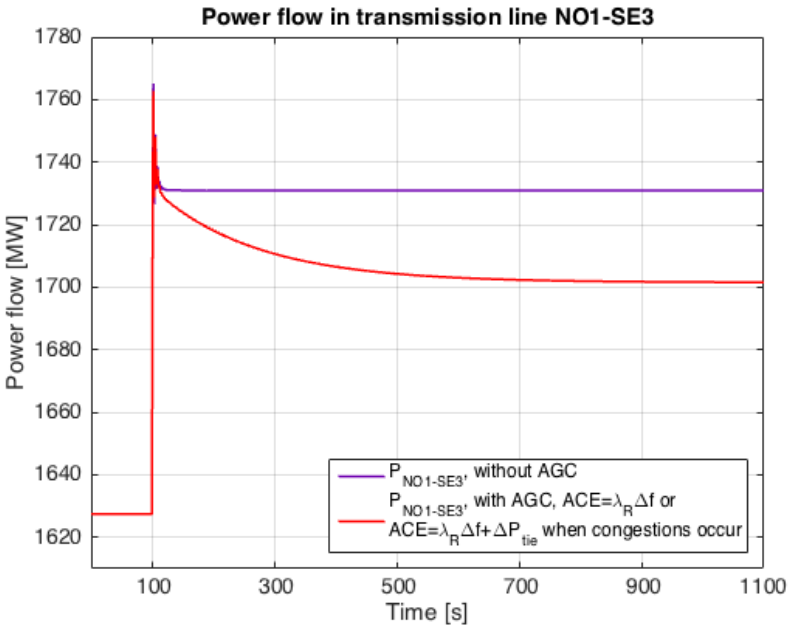

Figure 5.71: Power flow in the NO1-SE3 corridor in case 8. The load increase happened after 50 seconds.

Figure 5.72 shows the aFRR activated in situation 3 in this case. NO5 had the cheapest aFRR; hence only the AGC in this area was activated. The power decreased 60 MW in order to compensate for the net load drop.

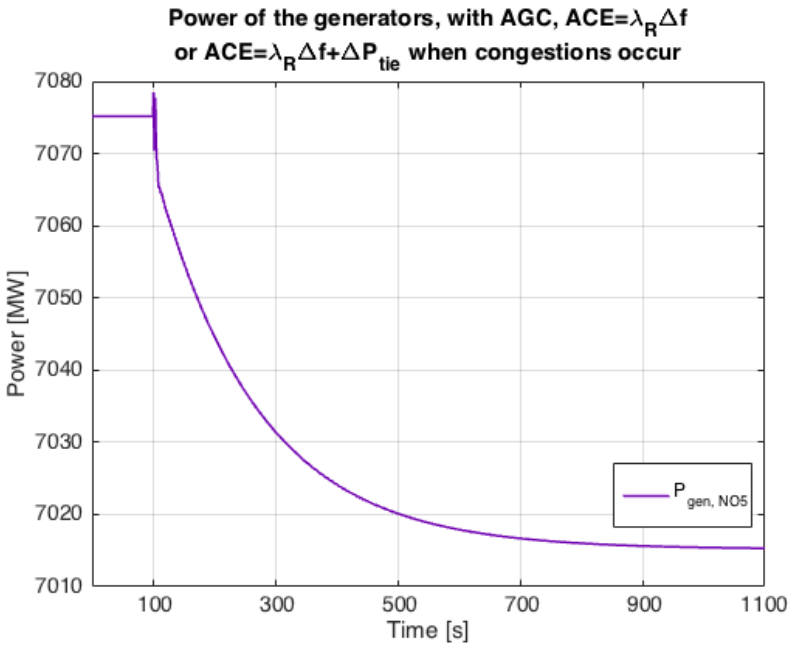

Figure 5.72: Power production of the generator in the area where aFRR were activated in case 8. The load increase happened after 50 seconds.

Figure 5.73 shows an overview of how the loads and power flow changed in situation 3, case 8. There was a mix of minor and major load changes in the areas, and power flow between the areas. In total, there was a net power decrease of 60 MW.

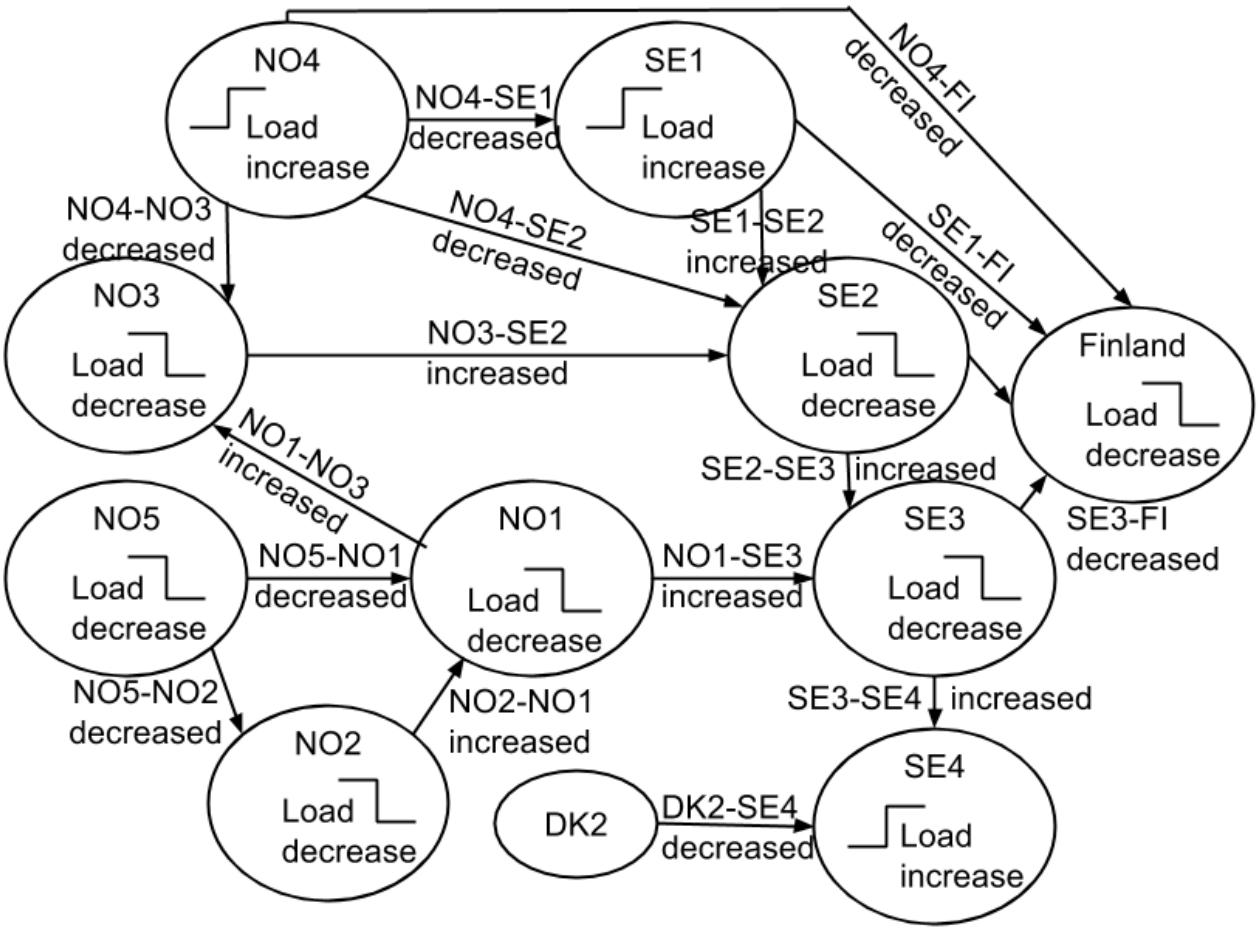

Figure 5.73: Overview of the power flow in situation 3, case 8.

The ACE's for this case are shown in figure 5.74. There were no congestions so the ACE was only dependent on the frequency, and equal for all three AGC's. The ACE dropped as the net load dropped, and stabilized at zero at the same time as the frequency was restored to the initial value.

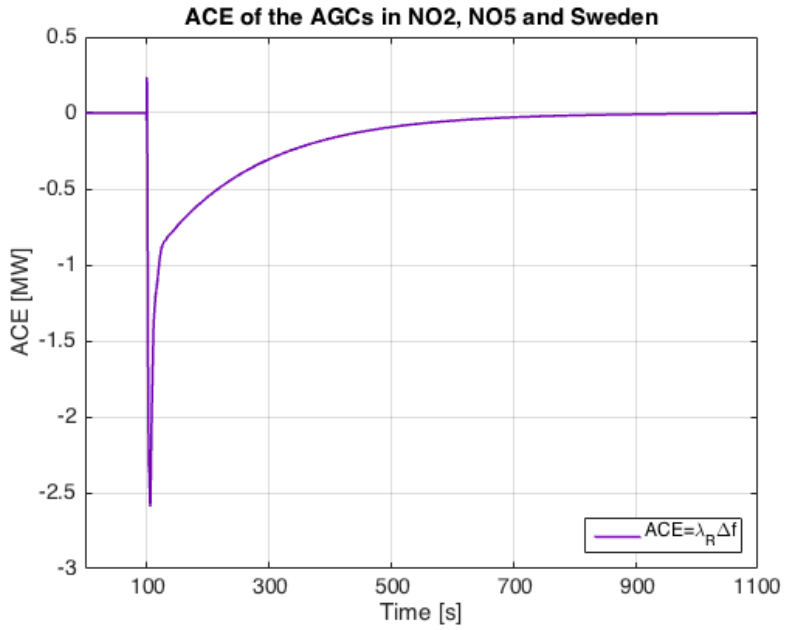

Figure 5.74: ACE of the AGC in NO2, NO5, and Sweden in case 8. The load increase happened after 50 seconds.

5.10 Discussion of Other Topics

As explained in section 2.1, the Nordic power system is operated as one price area as long as there are no congestions in the system. Whenever congestions occur, the system is divided into several price areas. In other words, the Nordic countries are regarded as one area unless grid capacities force smaller areas. This manner applies to the day ahead market, Elspot. There is currently little use of the secondary frequency control in the Nordic countries. In the rest of Europe aFRR is more prevalent and is used instead of mFRR. Each country regulates in accordance with their own ACE; the net import and export between countries is watched closely, and each country controls their own supply and demand. When discussing the structure of AGC implementation in the Nordic power system, one proposal is to combine the already existing congestion handling methodology in the Nordic power system with the European handling of the secondary frequency control. The suggestion is to include AGC's in all bidding zones in the Nordic countries, where tie lines to neighbouring areas are being controlled. As long as the capacity limits are not exceeded, the entire system would have a common ACE. If congestions occur the system would be divided into smaller areas, such that areas requesting aFRR would have to purchase aFRR from areas on the corresponding side of the congestion.

The various simulation results described in this chapter show that it is possible; the ACE's in the three control areas were equal when there were no congestions in the system, but varied when any of the tie lines congested. A challenge could perhaps be to control every tie line between all the areas. This must be considered when designing the control structure of the AGC's.

The proposal seems suitable also from a regulatory point of view. Although the Nordic countries have a well functioning collaboration when it comes to frequency control, the Nordic synchronous system still consists of four different countries with four different budgets. The current secondary frequency controller used in the Nordic system is common for the entire system. The secondary frequency control is relatively new in the Nordic power system, and currently all TSO's pay for the operation of the AGC. As the frequency is common in the Nordic synchronous system, it is hard to know which areas cause frequency instabilities. Implementation of AGC's in several or all bidding zones would mean that the area where an irregularity happens would be the area paying for restoration of power balance by purchasing aFRR from the cheapest available reserve.

As mentioned in section 2.6, the use of PTDF's is an alternative approach to DC PF when performing power flow calculations. In this context, the PTDF display is a convenient tool in congestion handling and could be implemented in an algorithm for the secondary frequency control. In the model presented in this thesis, a suitable choice of nodes could be each of the areas comprising a generator and a load. When experiencing congestions, the PTDF values would be ideal to decide in which nodes to e.g. generate enough power in order to fix the congestion.

Chapter 6

Conclusion

A simplified version of the Nordic synchronous system was represented in a model with eleven areas. The areas comprised one generator in accordance with the installed power generation per area, and one load equal to the value during an actual high load hour. Three AGC's were included in the system for the secondary frequency control. The inputs to the controllers were the frequency deviation and change in tie line power flow, while the output was the change in power production. The AGC's were modeled as classical AGC's with some modifications; the most important one being that the tie line power flow was only taken into account whenever the power flow in the tie lines exceeded the capacity limits. In other words, the ACE only regarded the frequency and was common for the entire system as long as no tie line congestions existed. Whenever congestions occurred in the controlled tie lines, the system was split into two or more areas operating with individual ACE's.

The activation of the secondary frequency control was based on a merit order list comprising available volumes and prices of the aFRR in each bidding zone. Hence, the control structure made sure that when disturbances occurred, the cheapest aFRR available was activated. The activation depended on whether there were any line congestions. Whenever the power transfer in any of the tie lines exceeded the capacity limits, aFRR were instead activated in areas where the congested line was not a hindrance.

As the secondary frequency control is relatively new in the Nordic power system, it is currently paid for by all the Nordic TSO's. By implementing AGC's in all the bidding zones, the areas experiencing disturbances would be the ones actually paying to restore the frequency by purchasing the cheapest aFRR available to the aforementioned areas. The Nordic countries and areas would be able to cooperate by buying and selling aFRR, in addition to being in control of the ACE in their own area.

One of the simulated cases in this thesis showed that AGC control of only three

areas were not enough as lines other than the controlled ones were congested. If the proposed solution is to be implemented in the Nordic power system, an important challenge in the control structure would be to control as many tie lines as possible in order to make sure that no grid capacities are exceeded.

Chapter 7

Further Work

A suggestion of further work is to put AGC's in all bidding areas. With several AGC's, more tie lines can be controlled and the capacity limits not exceeded.

The merit order lists for aFRR used in this thesis are simplified and only used as guidance for activation of aFRR. All the aFRR per area have the same price, such that all aFRR in the cheapest areas providing the requested amount of aFRR are activated simultaneously. In reality, the aFRR within an area would have different prices, i.e. the first 5 MW of up regulation in an area would be cheaper than the last 5 MW available. Making the merit order lists more realistic is a good proposal for further work.

The amount of aFRR activated in each area is in this thesis set by choosing the participation factors before doing the simulations. A suggestion for further work is to include the merit order lists in an algorithm within the model. The algorithm should follow more realistic merit order lists such that aFRR at all times are activated in the areas providing the cheapest bids, until congestions occur. This would also make sure that the AGC's do not activate more aFRR than what is available in each area.

Chapter 8

Bibliography

[1] Statnett. *Statnetts mediapakker* (Norwegian) [*Statnett's media packages*]. URL: `http://www.statnett.no/Media/Pressesenter/Mediapakke/`. Accessed June 7, 2016.

[2] Katrine G. Andersen. *Area Based Frequency Control in the Nordic Power System*. Project report, Norwegian University of Science and Technology, December 2015.

[3] Statnett. *Nordisk prosjekt for frekvensforbedring* (Norwegian) [*Nordic project for frequency enhancement*]. URL: `http://www.statnett.no/Kundeportal/Kundeinformasjon/Nordisk-prosjekt-for-frekvensforbedring/`. Accessed November 24, 2015.

[4] Statnett. *Systemansvaret (fos)* (Norwegian) [*The system responsibility*]. URL: `http://www.statnett.no/Drift-og-marked/Systemansvaret/`. Accessed November 24, 2015.

[5] Nord Pool Spot. *About us*. URL: `http://www.nordpoolspot.com/About-us/`. Accessed December 17, 2015.

[6] Statnett. *Kraftsystemet akkurat nå* (Norwegian) [*The power system right now*]. URL: `http://www.statnett.no/Drift-og-marked/Data-fra-kraftsystemet/Nordisk-kraftflyt/`. Accessed November 24, 2015.

[7] Eivind Lindeberg. Graduate engineer, Statnett SF. E-mail conversations in the fall of 2015 and the spring of 2016.

[8] Statnett. *Sekundærreserver (FRR-A)* (Norwegian) [*Secondary reserves (FRR-A)*]. URL: `http://www.statnett.no/Drift-og-marked/Markedsinformasjon/sekundarreserver/`. Accessed November 24, 2015.

[9] Statkraft. *Vannkraft* (Norwegian) [*Hydro power*]. URL: http://www.statkraft.no/Energikilder/Vannkraft/. Accessed May 28, 2016.

[10] Store Norske Leksikon. *Sverige – energi* (Norwegian) [*Sweden - energy*]. URL: https://snl.no/Sverige%2Fenergi. Accessed May 15, 2016.

[11] Store Norske Leksikon. *Finland*. URL: https://snl.no/Finland. Accessed May 15, 2016.

[12] Store Norske Leksikon. *Økonomi og næringsliv i Danmark* (Norwegian) [*Economy and business in Denmark*]. URL: https://snl.no/ÃŸkonomi_og_nÃęringsliv_i_Danmark. Accessed May 15, 2016.

[13] Nord Pool. *Historical Market Data*. URL: http://www.nordpoolspot.com/historical-market-data/. Accessed January 14, 2016.

[14] Statnett. *Kraftrekord* (Norwegian) [*Power record*]. URL: http://www.statnett.no/Media/Nyheter/Nyhetsarkiv-2016/Kraftrekord/. Accessed January 18, 2016.

[15] Bjørn H. Bakken and Kjetil Uhlen. *Market Based AGC with Online Bidding of Regulating Reserves. Power Engineering Society Summer Meeting, 2001*, Volume 2:848–853, 2001.

[16] Nord Pool. *Day-ahead market Elspot*. URL: http://www.nordpoolspot.com/TAS/Day-ahead-market-Elspot/. Accessed May 23, 2016.

[17] Nord Pool. *Price calculation*. URL: http://www.nordpoolspot.com/TAS/Day-ahead-market-Elspot/Price-calculation/. Accessed May 28, 2016.

[18] Ivar Wangensteen. *Power System Economics – the Nordic Electricity Market*. tapir academic press, Trondheim, Norway, 2nd edition, 2012.

[19] Jan Machowski, Janusz W. Bialek, and James R. Bumby. *Power System Dynamics: Stability and Control*. Wiley, 2011.

[20] Kjetil Uhlen and Olav B. Fosso. *Power system operation and Frequency control*. Lecture notes for the course TET4180 Electric Power System Stability, Norwegian University of Science and Technology, 2015.

[21] Statnett. *Om reservemarkeder* (Norwegian) [*About reserve markets*]. URL: http://www.statnett.no/Drift-og-marked/Markedsinformasjon/. Accessed December 3, 2015.

[22] Statnett. *Primærreserver (FCR)* (Norwegian) [*Primary reserves (FCR)*]. URL: http://www.statnett.no/Drift-og-marked/Markedsinformasjon/Primarreserver/. Accessed November 24, 2015.

[23] NVE. *Driften av Kraftsystemet 2013* (Norwegian) [*The operation of the power system 2013*]. URL: http://webby.nve.no/publikasjoner/rapport/2014/rapport2014_38.pdf. Accessed May 15, 2016.

[24] Eivind Lindeberg and David Whitley. *Appendix 1: Technical Product Specification For delivery of Frequency Restoration Reserves to Statnett*. URL: http://www.statnett.no/PageFiles/2581/LFC\%20Technical\%20Product\%20Specification.pdf. Accessed September 24, 2015.

[25] Statnett. *Tertiærreserve (FRR-M)* (Norwegian) [*Tertiary reserves (FRR-M)*]. URL: http://www.statnett.no/Drift-og-marked/Markedsinformasjon/RKOM1/. Accessed November 24, 2015.

[26] Jens G. Balchen, Bjarne A. Foss, and Trond Andresen. *Reguleringsteknikk*. Institutt for teknisk kybernetikk, Norges teknisk-naturvitenskapelige universitet, Trondheim, Norway, 5th edition, 2003.

[27] Bjørn H. Bakken. *Technical and economic aspects of operation of thermal and hydro power systems*. PhD thesis, Norwegian University of Science and Technology, Department of Electric Power Engineering, 1997.

[28] Kjetil Uhlen. *DC Power Flow and DC OPF*. Lecture notes for the course TET4115 Power System Analysis, Norwegian University of Science and Technology, November 2010.

[29] Power World Corporation. *Power Transfer Distribution Factors*. URL: http://www.powerworld.com/WebHelp/Content/MainDocumentation_HTML/Power_Transfer_Distribution_Factors.htm. Accessed April 26, 2016.

[30] Energinet.dk, Svenska Kraftnät, Fingrid, and Statnett. *Methodology and concepts for the Nordic Flow-Based Market Coupling Approach*. URL: http://www.fingrid.fi/fi/asiakkaat/asiakasliitteet/SÃđhkÃűmarkkinat%20ja%20edunvalvonta/Methodology%20and%20concepts%20for%20the%20Nordic%20Flow-Based%20Market%20Coupling%20Approach.pdf. Accessed May 31, 2016.

[31] Open Electrical. *Per-unit System*. URL: http://www.openelectrical.org/wiki/index.php?title=Per-unit_System. Accessed May 14, 2016.

[32] MathWorks. *The Language of Technical Computing.* URL: http://se.mathworks.com/products/matlab/. Accessed December 4, 2015.

[33] MathWorks. *Simulation and Model-Based Design.* URL: http://se.mathworks.com/products/simulink/. Accessed December 4, 2015.

[34] Nord Pool. *Elspot capacities.* URL: http://www.nordpoolspot.com/Market-data1/Elspot/Capacities1/Capacities/KEY/Norway/?view=table. Accessed January 14, 2016.

Appendix A

Block Diagrams and Parameter Values of the Model

This appendix comprises the block diagrams of the entire model, and tables listing all the parameter values used in the model.

A.1 Block Diagrams of the Model

Figure A.1 shows the entire block diagram of the model from chapter 4. The model was made using Simulink®. In figure A.1, the generators and AGC's are shown as subsystems in order to get a more lucid presentation of the model. The pink blocks are the normalized inertia constants of the generators, H_i, the system admittance matrix, Y, and the line flow matrix, Y_{lines}. The loads are modeled as simple step blocks, but in case 2 the load in NO1 is modeled as a ramp by using a Lookup Table block in Simulink, see figure A.2. Figure A.3 shows the block diagram of the generator, turbine, and turbine governor of area NO4. The other generators are similar but with parameter values in accordance with the specific areas. Figures A.4, A.5, and A.6 show the block diagrams of the modeled AGC's. In this thesis the AGC's in areas NO2 and NO5 activate aFRR only in NO2 and NO5. However, participation factors for areas NO1, NO3, and NO4 are included in the AGC's in the model even though aFRR are not activated in these areas.

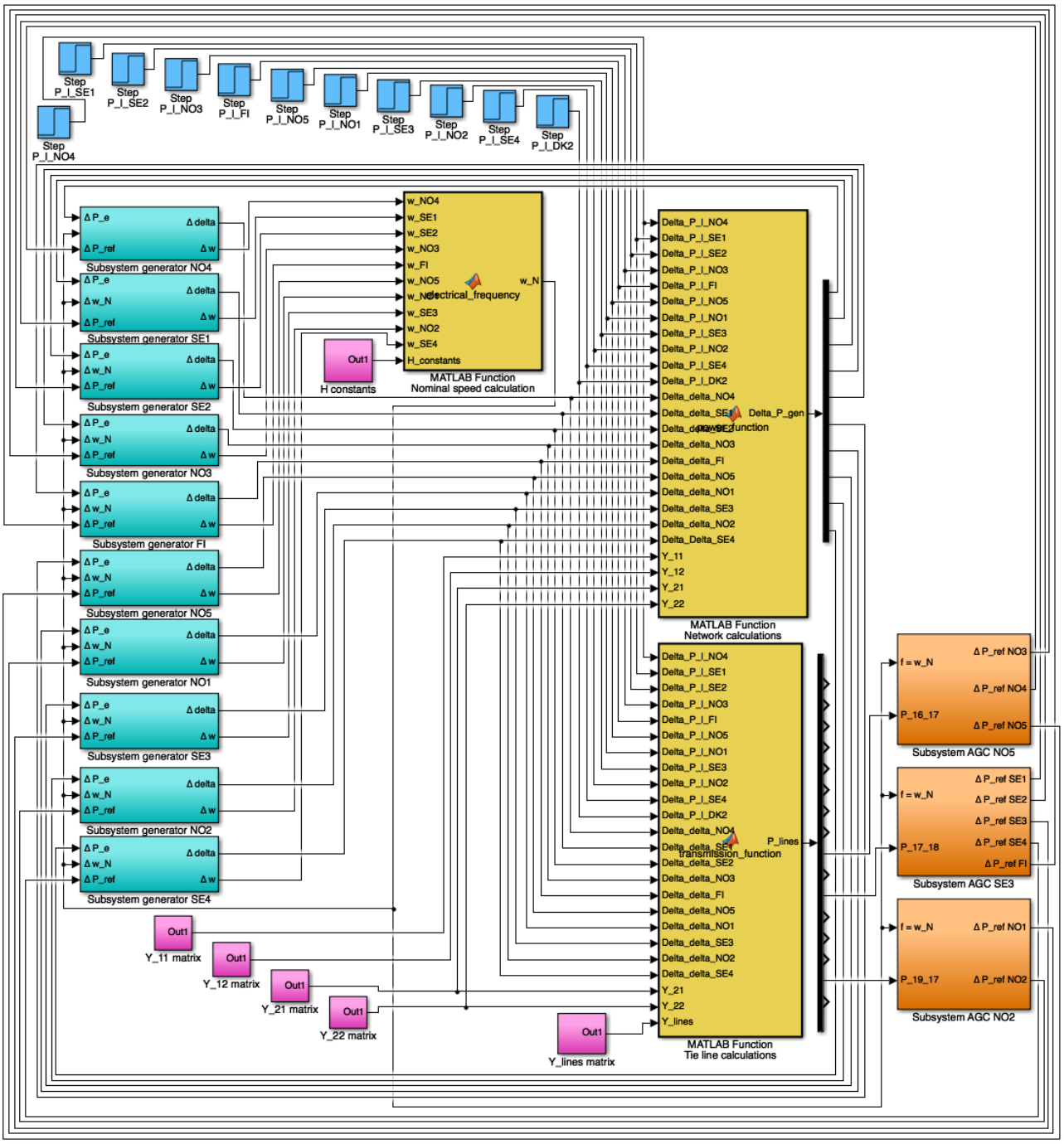

Figure A.1: The block diagram of the model made in Simulink®. The model comprises eleven areas, where all areas except for DK2 are modeled with a generator and a load. Three AGC's are modeled. The MATLAB® Function block called *Network calculations* calculates the change in electrical power for the generators. The block named *Nominal speed calculation* calculates the nominal speed of the system. The H_i constants are taken as input to this block. The block called *Tie line calculations* calculates the flow in the lines in order to get the tie line power flow, which is used as input to the AGC's. The *Network calculations* and the *Tie line calculations* block take the admittance matrix, Y, as input, while also the line flow matrix, Y_{lines}, is used as input to the *Tie line calculations* block.

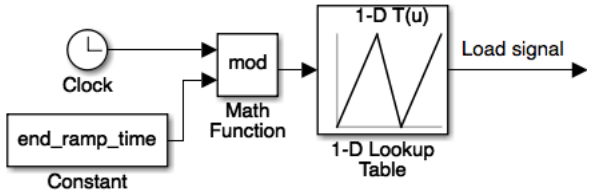

Figure A.2: The block diagram of the ramped load in NO1 in case 2. The 'end_ramp_time' indicates when the ramping in the model should end.

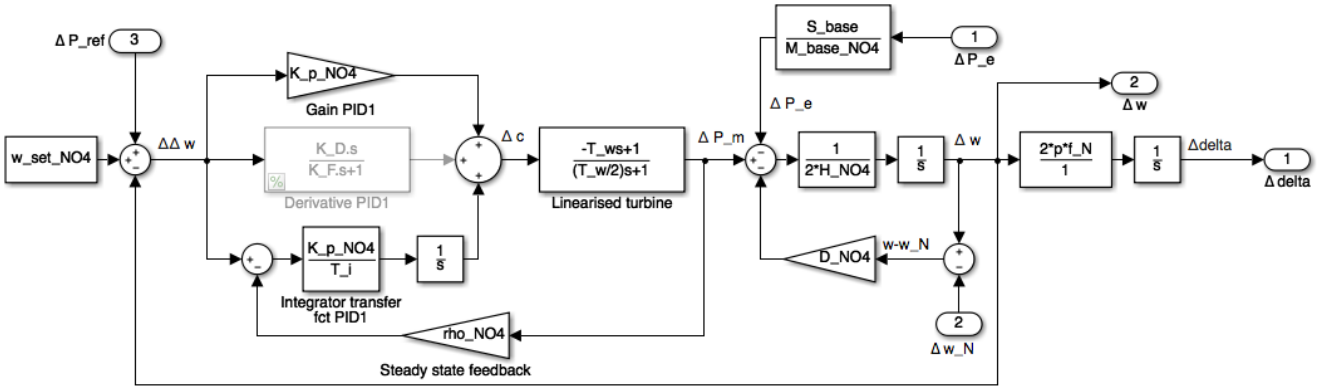

Figure A.3: The block diagram of the turbine, turbine governor, and the generator in area NO4. The other nine generator subsystems are similar, but with parameter values in accordance with the specific areas.

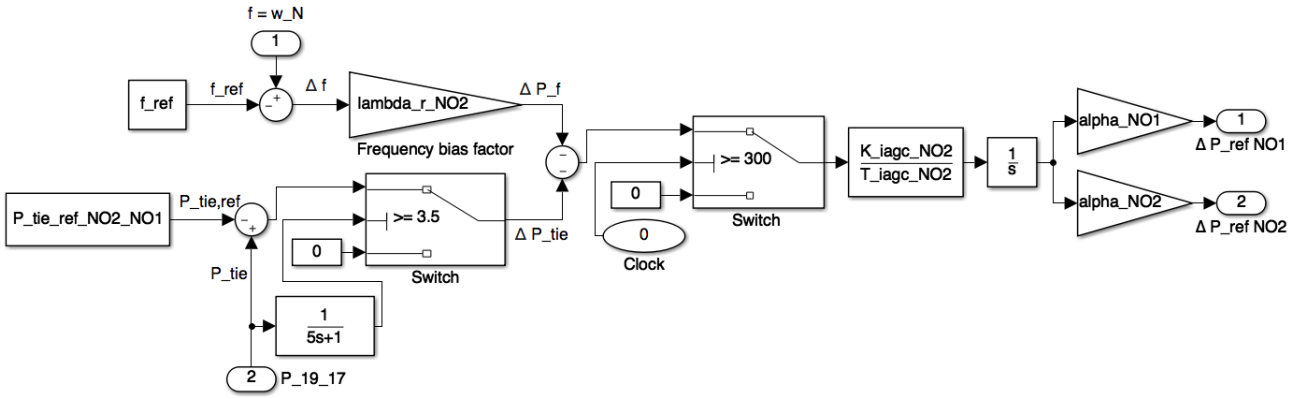

Figure A.4: The block diagram of the AGC in NO2.

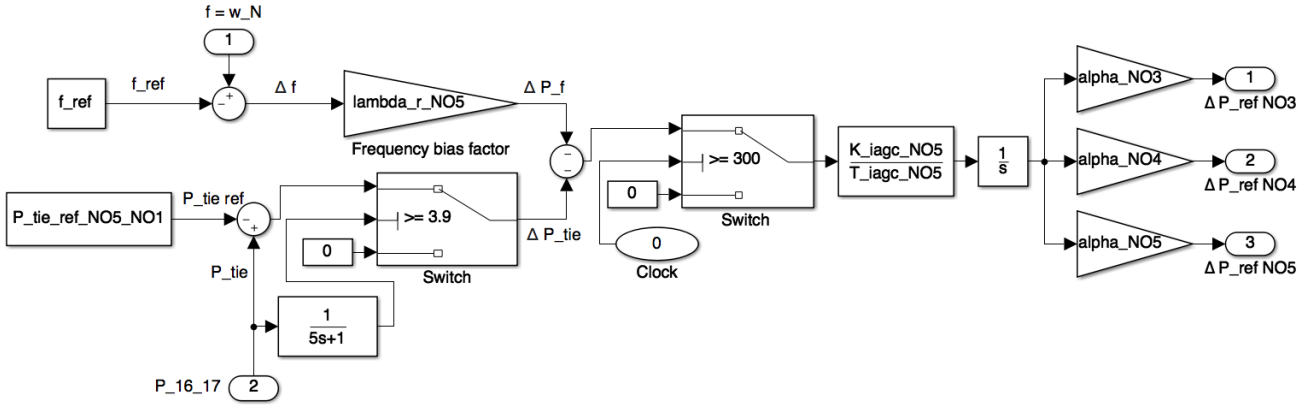

Figure A.5: The block diagram of the AGC in NO5.

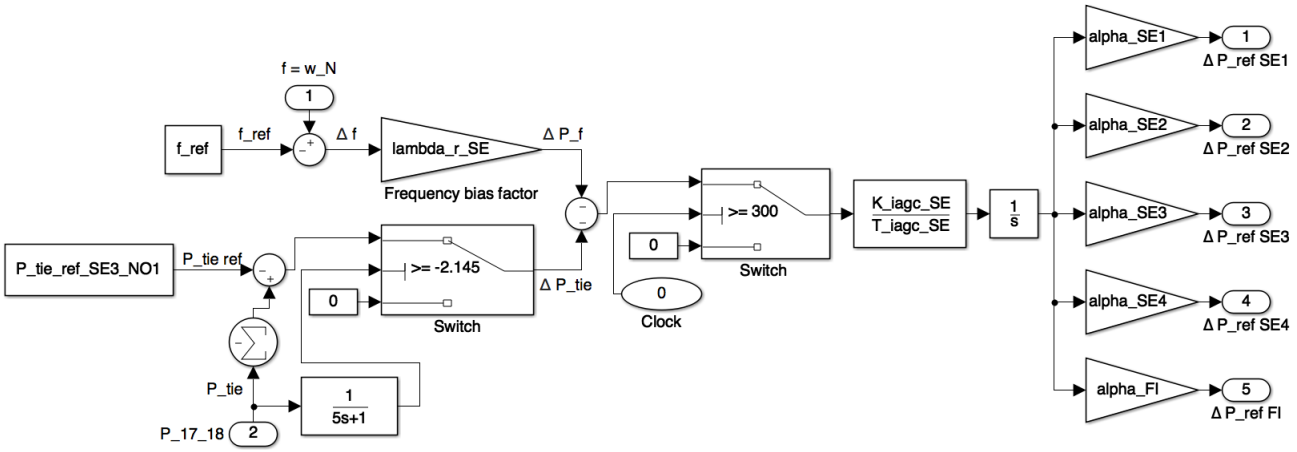

Figure A.6: The block diagram of the AGC in Sweden.

A.2 Parameter Values

This section lists the parameter values used in the modeled system.

Table A.1: Power production and demand in the areas during hours 19:00–20:00 and 20:00–21:00, January 6, 2016. As DK2 was modeled as a constant value equal to the power flow in the corridor connecting SE4 to DK2, the load was negative as the power flowed from DK2 to SE4 during these specific hours. The data was gathered from reference [13] and somewhat modified to get a suitable power flow.

Area	**Power production [MW], 19:00–20:00**	**Demand [MW], 19:00–20:00**	**Demand [MW], 20:00–21:00**
NO1	2608	7620	7520
NO2	9942	7072	7049
NO3	2813	3512	3509
NO4	4202	2838	2871
NO5	7200	3092	3074
SE1	4506	1652	1694
SE2	6871	3002	2931
SE3	11432	15091	14826
SE4	1489	4416	4838
FI	10539	12960	12573
DK2	-	-551	-241

Table A.2: Maximum transfer capacities in the lines of the modeled system. The data was gathered from reference [34].

Line	Value [MW]	Value [p.u.]
11-12 (NO4-SE1)	700	0.7
11-13 (NO4-SE2)	300	0.3
11-14 (NO4-NO3)	1000	1.0
11-15 (NO4-FI)	100	0.1
12-13 (SE1-SE2)	3300	3.3
12-15 (SE1-FI)	1500	1.5
13-14 (SE2-NO3)	1000	1.0
13-18 (SE2-SE3)	7300	7.3
14-17 (NO3-NO1)	500	0.5
15-18 (FI-SE3)	1200	1.2
16-17 (NO5-NO1)	3900	3.9
16-19 (NO5-NO2)	600	0.6
17-18 (NO1-SE3)	2145	2.145
17-19 (NO1-NO2)	3500	3.5
18-20 (SE3-SE4)	5300	5.3
20-21 (SE4-DK2)	1700	1.7

Table A.3: Transient direct axis reactances of the generators in the modeled system. The values were chosen in order to get satisfactory generator swings.

Parameter	Value [p.u.]
x'_{d1}	0.7
x'_{d2}	0.8
x'_{d3}	0.7
x'_{d4}	0.9
x'_{d5}	0.64
x'_{d6}	0.6
x'_{d7}	0.6
x'_{d8}	0.8
x'_{d9}	0.7
x'_{d10}	0.74

Table A.4: Line reactances in the modeled system. The reactances are the inverses of the maximum transfer capacities listed in table A.2. The reactances $x_{11,15}$ and $x_{12,15}$ were somewhat adjusted in order to get an appropriate power flow.

Parameter	**Value [p.u.]**
$x_{11,12}$	$\frac{1}{0,7}$
$x_{11,13}$	$\frac{1}{0,3}$
$x_{11,14}$	$\frac{1}{1,0}$
$x_{11,15}$	$\frac{1}{0,03}$
$x_{12,13}$	$\frac{1}{3,3}$
$x_{12,15}$	$\frac{1}{0,7}$
$x_{13,14}$	$\frac{1}{1,0}$
$x_{13,18}$	$\frac{1}{7,3}$
$x_{14,17}$	$\frac{1}{0,5}$
$x_{15,18}$	$\frac{1}{1,2}$
$x_{16,17}$	$\frac{1}{3,9}$
$x_{16,19}$	$\frac{1}{0,6}$
$x_{17,18}$	$\frac{1}{2.145}$
$x_{17,19}$	$\frac{1}{3,5}$
$x_{18,20}$	$\frac{1}{5,3}$
$x_{20,21}$	$\frac{1}{1,7}$

The speeds, ω_i, listed in table A.5, were calculated based on the following equation:

$$\omega_i = \rho_i \frac{P_i}{M_{base,i}} \tag{A.1}$$

ρ_i is the droop of the turbine governor per area listed in table A.5. P_i is the power production per area listed in table A.1. $M_{base,i}$ is the local base value of the power per area listed in table 4.1 in chapter 4.

Table A.5: Values used for the parameters in the modeled system. The values were chosen in order to get a suitable model for the purpose of this thesis. Some of the parameter values were alike in all areas comprising generators. These are noted by the subscript $_{NO1...FI}$.

Parameter	Value	Unit	Parameter	Value	Unit
$\omega_{set,NO1}$	0.11622	p.u.	p	π	-
$\omega_{set,NO2}$	0.10659	p.u.	$K_{p,NO1...FI}$	2.0	-
$\omega_{set,NO3}$	0.07484	p.u.	$K_{D,NO1...FI}$	0.0	-
$\omega_{set,NO4}$	0.09898	p.u.	$K_{F,NO1...FI}$	1.0	-
$\omega_{set,NO5}$	0.10613	p.u.	$T_{i,NO1...FI}$	5.0	s
$\omega_{set,SE1}$	0.08825	p.u.	T_w	1.5	s
$\omega_{set,SE2}$	0.10119	p.u.	f_N	50.00	Hz
$\omega_{set,SE3}$	0.37172	p.u.	f_{ref}	0.00	p.u.
$\omega_{set,SE4}$	0.09357	p.u.	$P_{tie,ref,NO1-SE3}$	2.145	p.u.
$\omega_{set,FI}$	0.17981	p.u.	$P_{tie,ref,NO2-NO1}$	3.5	p.u.
H_{NO1}	3.494	s	$P_{tie,ref,NO5-NO1}$	3.9	p.u.
H_{NO2}	3.370	s	$\lambda_{r,NO2}$	$\frac{1}{0.12}$	-
H_{NO3}	3.558	s	$\lambda_{r,NO5}$	$\frac{1}{0.12}$	-
H_{NO4}	3.592	s	$\lambda_{r,SE}$	$\frac{1}{0.12}$	-
H_{NO5}	3.500	s	$K_{i,agc,NO2}$	1.0	-
H_{SE1}	4.602	s	$K_{i,agc,NO5}$	1.0	-
H_{SE2}	3.300	s	$K_{i,agc,SE}$	1.0	-
H_{SE3}	5.403	s	$T_{i,agc,NO2}$	200	s
H_{SE4}	7.000	s	$T_{i,agc,NO5}$	200	s
H_{FI}	4.925	s	$T_{i,agc,SE}$	200	s
ρ_{NO1} (rho)	0.12	-	α_{NO1} $(alpha)$	0.0	-
ρ_{NO2} (rho)	0.12	-	α_{NO2} $(alpha)$	1.0	-
ρ_{NO3} (rho)	0.12	-	α_{NO3} $(alpha)$	0.04–0.28	-
ρ_{NO4} (rho)	0.12	-	α_{NO4} $(alpha)$	0.18–0.26	-
ρ_{NO5} (rho)	0.12	-	α_{NO5} $(alpha)$	0.53–1.0	-
ρ_{SE1} (rho)	0.12	-	α_{SE1} $(alpha)$	0.43–0.73	-
ρ_{SE2} (rho)	0.12	-	α_{SE2} $(alpha)$	0.16–0.35	-
ρ_{SE3} (rho)	0.50	-	α_{SE3} $(alpha)$	0.18–0.23	-
ρ_{SE4} (rho)	0.50	-	α_{SE4} $(alpha)$	0.0	-
ρ_{FI} (rho)	0.25	-	α_{FI} $(alpha)$	0.0–0.24	-
$D_{NO1...FI}$	10.0	p.u. power/ p.u. speed			

Appendix B

Calculation of System Frequency Response

Calculation of the system frequency response is based on the following expression:

$$\frac{\Delta f}{f_N} = \rho \frac{\Delta P}{P_N} \tag{B.1}$$

Rearranging gives:

$$\frac{\Delta P}{\Delta f} = \frac{P_N}{\rho f_N} = R \tag{B.2}$$

ρ [%] and $f_N = 50$ Hz gives:

$$\frac{P_N}{\rho 50} 100\% = \frac{2P_N}{\rho} = R_{permachine} \tag{B.3}$$

The total system frequency response is:

$$R_{system} = \sum R_{permachine} \tag{B.4}$$

Table B.1 shows the system frequency response of each generator and for the whole system. P_N for each area are the $M_{base,i}$ values listed in table 4.1 in chapter 4; the droops per area, ρ_i, are listed in table A.5 in appendix A.2.

Table B.1: System frequency response of the system.

Area	**System frequency response [MW/Hz]**
NO1	442
NO2	1833
NO3	733
NO4	833
NO5	1333
SE1	1000
SE2	1333
SE3	612
SE4	312
FI	1160
System in total	9592

When studying the frequency deviation from the initial value when a power change happens, the system frequency response can be recognized. By dividing the power change [MW] by the frequency deviation [Hz], the system frequency response is found.

Appendix C

System Admittance Matrix

Not all the busbars in the modeled system are connected, hence many of the admittance matrix elements are zero. Using the decomposing of the admittance matrix as in equation 3.2 in chapter 3 together with the reactances of the system, the admittance matrix can be expressed as:

$$Y_{11} = \begin{bmatrix} \frac{1}{x'_{d1}} & 0 & 0 & 0 & 0 & 0 & 0 & 0 & 0 & 0 \\ 0 & \frac{1}{x'_{d2}} & 0 & 0 & 0 & 0 & 0 & 0 & 0 & 0 \\ 0 & 0 & \frac{1}{x'_{d3}} & 0 & 0 & 0 & 0 & 0 & 0 & 0 \\ 0 & 0 & 0 & \frac{1}{x'_{d4}} & 0 & 0 & 0 & 0 & 0 & 0 \\ 0 & 0 & 0 & 0 & \frac{1}{x'_{d5}} & 0 & 0 & 0 & 0 & 0 \\ 0 & 0 & 0 & 0 & 0 & \frac{1}{x'_{d6}} & 0 & 0 & 0 & 0 \\ 0 & 0 & 0 & 0 & 0 & 0 & \frac{1}{x'_{d7}} & 0 & 0 & 0 \\ 0 & 0 & 0 & 0 & 0 & 0 & 0 & \frac{1}{x'_{d8}} & 0 & 0 \\ 0 & 0 & 0 & 0 & 0 & 0 & 0 & 0 & \frac{1}{x'_{d9}} & 0 \\ 0 & 0 & 0 & 0 & 0 & 0 & 0 & 0 & 0 & \frac{1}{x'_{d10}} \end{bmatrix} \tag{C.1}$$

$$Y_{12} = \begin{bmatrix} -\frac{1}{x'_{d1}} & 0 & 0 & 0 & 0 & 0 & 0 & 0 & 0 & 0 & 0 \\ 0 & -\frac{1}{x'_{d2}} & 0 & 0 & 0 & 0 & 0 & 0 & 0 & 0 & 0 \\ 0 & 0 & -\frac{1}{x'_{d3}} & 0 & 0 & 0 & 0 & 0 & 0 & 0 & 0 \\ 0 & 0 & 0 & -\frac{1}{x'_{d4}} & 0 & 0 & 0 & 0 & 0 & 0 & 0 \\ 0 & 0 & 0 & 0 & -\frac{1}{x'_{d5}} & 0 & 0 & 0 & 0 & 0 & 0 \\ 0 & 0 & 0 & 0 & 0 & -\frac{1}{x'_{d6}} & 0 & 0 & 0 & 0 & 0 \\ 0 & 0 & 0 & 0 & 0 & 0 & -\frac{1}{x'_{d7}} & 0 & 0 & 0 & 0 \\ 0 & 0 & 0 & 0 & 0 & 0 & 0 & -\frac{1}{x'_{d8}} & 0 & 0 & 0 \\ 0 & 0 & 0 & 0 & 0 & 0 & 0 & 0 & -\frac{1}{x'_{d9}} & 0 & 0 \\ 0 & 0 & 0 & 0 & 0 & 0 & 0 & 0 & 0 & -\frac{1}{x'_{d10}} & 0 \end{bmatrix} \tag{C.2}$$

$$Y_{21} = \begin{bmatrix} -\frac{1}{x'_{d1}} & 0 & 0 & 0 & 0 & 0 & 0 & 0 & 0 & 0 \\ 0 & -\frac{1}{x'_{d2}} & 0 & 0 & 0 & 0 & 0 & 0 & 0 & 0 \\ 0 & 0 & -\frac{1}{x'_{d3}} & 0 & 0 & 0 & 0 & 0 & 0 & 0 \\ 0 & 0 & 0 & -\frac{1}{x'_{d4}} & 0 & 0 & 0 & 0 & 0 & 0 \\ 0 & 0 & 0 & 0 & -\frac{1}{x'_{d5}} & 0 & 0 & 0 & 0 & 0 \\ 0 & 0 & 0 & 0 & 0 & -\frac{1}{x'_{d6}} & 0 & 0 & 0 & 0 \\ 0 & 0 & 0 & 0 & 0 & 0 & -\frac{1}{x'_{d7}} & 0 & 0 & 0 \\ 0 & 0 & 0 & 0 & 0 & 0 & 0 & -\frac{1}{x'_{d8}} & 0 & 0 \\ 0 & 0 & 0 & 0 & 0 & 0 & 0 & 0 & -\frac{1}{x'_{d9}} & 0 \\ 0 & 0 & 0 & 0 & 0 & 0 & 0 & 0 & 0 & -\frac{1}{x'_{d10}} \\ 0 & 0 & 0 & 0 & 0 & 0 & 0 & 0 & 0 & 0 \end{bmatrix} \tag{C.3}$$

$$\mathrm{Y}_{22} = \begin{bmatrix} y_{11,11} & -\frac{1}{x_{11,12}} & -\frac{1}{x_{11,13}} & -\frac{1}{x_{11,14}} & -\frac{1}{x_{11,15}} & 0 & 0 & 0 & 0 & 0 & 0 \\ -\frac{1}{x_{11,12}} & y_{12,12} & -\frac{1}{x_{12,13}} & 0 & -\frac{1}{x_{12,15}} & 0 & 0 & 0 & 0 & 0 & 0 \\ -\frac{1}{x_{11,13}} & -\frac{1}{x_{12,13}} & y_{13,13} & -\frac{1}{x_{13,14}} & 0 & 0 & 0 & -\frac{1}{x_{13,18}} & 0 & 0 & 0 \\ -\frac{1}{x_{11,14}} & 0 & -\frac{1}{x_{13,14}} & y_{14,14} & 0 & 0 & -\frac{1}{x_{14,17}} & 0 & 0 & 0 & 0 \\ -\frac{1}{x_{11,15}} & -\frac{1}{x_{12,15}} & 0 & 0 & y_{15,15} & 0 & 0 & -\frac{1}{x_{15,18}} & 0 & 0 & 0 \\ 0 & 0 & 0 & 0 & 0 & y_{16.16} & -\frac{1}{x_{16,17}} & 0 & 0 & -\frac{1}{x_{16,19}} & 0 \\ 0 & 0 & 0 & -\frac{1}{x_{14,17}} & 0 & -\frac{1}{x_{16,17}} & y_{17,17} & -\frac{1}{x_{17,18}} & -\frac{1}{x_{17,19}} & 0 & 0 \\ 0 & 0 & -\frac{1}{x_{13,18}} & 0 & -\frac{1}{x_{15,18}} & 0 & -\frac{1}{x_{17,18}} & y_{18,18} & 0 & -\frac{1}{x_{18,20}} & 0 \\ 0 & 0 & 0 & 0 & 0 & -\frac{1}{x_{16,19}} & -\frac{1}{x_{17,19}} & 0 & y_{19,19} & 0 & 0 \\ 0 & 0 & 0 & 0 & 0 & 0 & 0 & -\frac{1}{x_{18,20}} & 0 & y_{20,20} & -\frac{1}{x_{20,21}} \\ 0 & 0 & 0 & 0 & 0 & 0 & 0 & 0 & 0 & -\frac{1}{x_{20,21}} & y_{21,21} \end{bmatrix} \tag{C.4}$$

The diagonal elements of the Y_{22} matrix are listed below:

$$\begin{aligned}
y_{11,11} &= \frac{1}{x'_{d1}} + \frac{1}{x_{11,12}} + \frac{1}{x_{11,13}} + \frac{1}{x_{11,14}} + \frac{1}{x_{11,15}} \\
y_{12,12} &= \frac{1}{x'_{d2}} + \frac{1}{x_{11,12}} + \frac{1}{x_{12,13}} + \frac{1}{x_{12,15}} \\
y_{13,13} &= \frac{1}{x'_{d3}} + \frac{1}{x_{11,13}} + \frac{1}{x_{12,13}} + \frac{1}{x_{13,14}} + \frac{1}{x_{13,18}} \\
y_{14,14} &= \frac{1}{x'_{d4}} + \frac{1}{x_{11,14}} + \frac{1}{x_{13,14}} + \frac{1}{x_{14,17}} \\
y_{15,15} &= \frac{1}{x'_{d5}} + \frac{1}{x_{11,15}} + \frac{1}{x_{12,15}} + \frac{1}{x_{15,18}} \\
y_{16,16} &= \frac{1}{x'_{d6}} + \frac{1}{x_{16,17}} + \frac{1}{x_{16,19}} \\
y_{17,17} &= \frac{1}{x'_{d7}} + \frac{1}{x_{14,17}} + \frac{1}{x_{16,17}} + \frac{1}{x_{17,18}} + \frac{1}{x_{17,19}} \\
y_{18,18} &= \frac{1}{x'_{d8}} + \frac{1}{x_{13,18}} + \frac{1}{x_{15,18}} + \frac{1}{x_{17,18}} + \frac{1}{x_{18,20}} \\
y_{19,19} &= \frac{1}{x'_{d9}} + \frac{1}{x_{16,19}} + \frac{1}{x_{17,19}} \\
y_{20,20} &= \frac{1}{x'_{d10}} + \frac{1}{x_{18,20}} + \frac{1}{x_{20,21}} \\
y_{21,21} &= \frac{1}{x_{20,21}}
\end{aligned}$$

Appendix D

Line Flow Matrix

Below is the line flow matrix of the modeled system. The negative signs are placed in order to get positive flows.

$$
\mathrm{Y}_{lines} = \begin{bmatrix}
y_{11,13} & 0 & -y_{11,13} & 0 & 0 & 0 & 0 & 0 & 0 & 0 & 0 \\
y_{11,14} & 0 & 0 & -y_{11,14} & 0 & 0 & 0 & 0 & 0 & 0 & 0 \\
y_{11,15} & 0 & 0 & 0 & -y_{11,15} & 0 & 0 & 0 & 0 & 0 & 0 \\
-y_{11,12} & y_{11,12} & 0 & 0 & 0 & 0 & 0 & 0 & 0 & 0 & 0 \\
0 & y_{12,13} & -y_{12,13} & 0 & 0 & 0 & 0 & 0 & 0 & 0 & 0 \\
0 & y_{12,15} & 0 & 0 & -y_{12,15} & 0 & 0 & 0 & 0 & 0 & 0 \\
0 & 0 & y_{13,14} & -y_{13,14} & 0 & 0 & 0 & 0 & 0 & 0 & 0 \\
0 & 0 & y_{13,18} & 0 & 0 & 0 & 0 & -y_{13,18} & 0 & 0 & 0 \\
0 & 0 & 0 & 0 & 0 & y_{16,17} & -y_{16,17} & 0 & 0 & 0 & 0 \\
0 & 0 & 0 & -y_{14,17} & 0 & 0 & y_{14,17} & 0 & 0 & 0 & 0 \\
0 & 0 & 0 & 0 & 0 & 0 & y_{17,18} & -y_{17,18} & 0 & 0 & 0 \\
0 & 0 & 0 & 0 & -y_{15,18} & 0 & 0 & y_{15,18} & 0 & 0 & 0 \\
0 & 0 & 0 & 0 & 0 & 0 & 0 & y_{18,20} & 0 & -y_{18,20} & 0 \\
0 & 0 & 0 & 0 & 0 & -y_{16,19} & 0 & 0 & y_{16,19} & 0 & 0 \\
0 & 0 & 0 & 0 & 0 & 0 & -y_{17,19} & 0 & y_{17,19} & 0 & 0 \\
0 & 0 & 0 & 0 & 0 & 0 & 0 & 0 & 0 & -y_{20,21} & y_{20,21}
\end{bmatrix} \tag{D.1}
$$

Appendix E

MATLAB® Scripts

This appendix contains the MATLAB® scripts of the three MATLAB® function blocks in the model seen in figure A.1 in appendix A.1.

Network Calculations Script

```
function Delta_P_gen = power_function(Delta_P_l_NO4,...
    Delta_P_l_SE1,Delta_P_l_SE2,Delta_P_l_NO3,Delta_P_l_FI,...
    Delta_P_l_NO5,Delta_P_l_NO1,Delta_P_l_SE3,Delta_P_l_NO2,...
    Delta_P_l_SE4,Delta_P_l_DK2,Delta_delta_NO4,Delta_delta_SE1,...
    Delta_delta_SE2,Delta_delta_NO3,Delta_delta_FI,...
    Delta_delta_NO5,Delta_delta_NO1,Delta_delta_SE3,...
    Delta_delta_NO2,Delta_delta_SE4,Y_11,Y_12,Y_21,Y_22)

Delta_P_load = [-Delta_P_l_NO4 ; -Delta_P_l_SE1 ;...
    -Delta_P_l_SE2 ; -Delta_P_l_NO3 ; -Delta_P_l_FI ;...
    -Delta_P_l_NO5 ; -Delta_P_l_NO1 ; -Delta_P_l_SE3 ;...
    -Delta_P_l_NO2 ; -Delta_P_l_SE4 ; -Delta_P_l_DK2];

Delta_delta_gen = [Delta_delta_NO4 ; Delta_delta_SE1 ;...
    Delta_delta_SE2 ; Delta_delta_NO3 ; Delta_delta_FI ;...
    Delta_delta_NO5 ; Delta_delta_NO1 ; Delta_delta_SE3 ;...
    Delta_delta_NO2 ; Delta_delta_SE4];

Delta_delta_load = Y_22\(Delta_P_load - (Y_21 * Delta_delta_gen));
    % The \ symbol implies the inverse
```

```
Delta_P_gen = Y_11 * Delta_delta_gen + Y_12 * Delta_delta_load;
end
```

Tie Line Calculations Script

```
function P_lines = transmission_function(Delta_P_l_NO4,...
    Delta_P_l_SE1,Delta_P_l_SE2,Delta_P_l_NO3,Delta_P_l_FI,...
    Delta_P_l_NO5,Delta_P_l_NO1,Delta_P_l_SE3,Delta_P_l_NO2,...
    Delta_P_l_SE4,Delta_P_l_DK2,Delta_delta_NO4,...
    Delta_delta_SE1,Delta_delta_SE2,Delta_delta_NO3,...
    Delta_delta_FI,Delta_delta_NO5,Delta_delta_NO1,...
    Delta_delta_SE3,Delta_delta_NO2,Delta_delta_SE4,...
    Y_21,Y_22,Y_lines)

Delta_P_load = [-Delta_P_l_NO4 ; -Delta_P_l_SE1 ;...
    -Delta_P_l_SE2 ; -Delta_P_l_NO3 ; -Delta_P_l_FI ;...
    -Delta_P_l_NO5 ; -Delta_P_l_NO1 ; -Delta_P_l_SE3 ;...
    -Delta_P_l_NO2 ; -Delta_P_l_SE4 ; -Delta_P_l_DK2];

Delta_delta_gen = [Delta_delta_NO4 ; Delta_delta_SE1 ;...
Delta_delta_SE2 ; Delta_delta_NO3 ; Delta_delta_FI ;...
Delta_delta_NO5 ; Delta_delta_NO1 ; Delta_delta_SE3 ;...
Delta_delta_NO2 ; Delta_delta_SE4];

Delta_delta_load = Y_22\(Delta_P_load - (Y_21 * Delta_delta_gen));
    % The \ symbol implies the inverse

P_lines = Y_lines * Delta_delta_load;
    % multiplying the Y_lines matrix with the delta vector
    % to get the flow in the lines
end
```

Nominal Speed Calculation Script

```
function w_N = electrical_frequency(w_NO4,w_SE1,w_SE2,w_NO3,...
    w_FI,w_NO5,w_NO1,w_SE3,w_NO2,w_SE4,H_constants)
```

```
H_NO4 = H_constants(1);
H_SE1 = H_constants(2);
H_SE2 = H_constants(3);
H_NO3 = H_constants(4);
H_FI  = H_constants(5);
H_NO5 = H_constants(6);
H_NO1 = H_constants(7);
H_SE3 = H_constants(8);
H_NO2 = H_constants(9);
H_SE4 = H_constants(10);

numerator = ((H_NO4 * w_NO4) + (H_SE1 * w_SE1) +...
    (H_SE2 * w_SE2) + (H_NO3 * w_NO3) + (H_FI * w_FI) +...
    (H_NO5 * w_NO5) + (H_NO1 * w_NO1) + (H_SE3 * w_SE3) +...
    (H_NO2 * w_NO2) + (H_SE4 * w_SE4));

denominator = (H_NO4 + H_SE1 + H_SE2 + H_NO3 + H_FI +...
    H_NO5 + H_NO1 + H_SE3 + H_NO2 + H_SE4);

w_N = numerator/denominator;

end
```